RESEARCH REPORT

Thermal and Mechanical Finite Element Modeling of Wood-Floor Assemblies Subjected to Furnace Exposure

As part of the Investigation into the

Structural Stability of Engineered Lumber in Fire Conditions

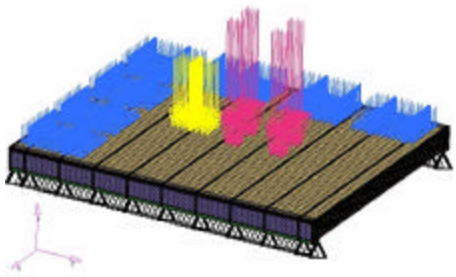

Project Number: 07CA42520
File Number: NC9140

December 31, 2008

Prepared by:

Mahmood Tabaddor, PhD
Corporate Research

Reviewed by:

Pravinray D. Gandhi, PhD, PE
Director
Corporate Research

Robert Backstrom
Senior Engineer
Corporate Research

Information conveyed by this Report applies only to the specimens actually involved in these tests. Underwriters Laboratories Inc. (UL) has not established a factory Follow-Up Service Program to determine the conformance of subsequently produced material, nor has any provision been made to apply any registered mark of UL to such material.

The issuance of this Report in no way implies Listing, Classification or Recognition by UL and does not authorize the use of UL Listing, Classification or Recognition Marks or other reference to UL on or in connection with the product or system.

UL, its trustees, employees, sponsors, and contractors, make no warranties, express or implied, nor assume and expressly disclaim any legal liability or responsibility to any person for any loss or damage arising out of or in connection with the interpretation, application, or use of or inability to use, any information, data, apparatus, product, or process disclosed in this Report. This Report cannot be modified or reproduced, in part, without the prior written permission of Underwriters Laboratories Inc.

ACKNOWLEDGMENTS

In carrying out this investigation, UL partnered with Michigan State University (MSU) to help review the literature on wood properties and generate some material properties for the wood components of assemblies 1 and 2, which are necessary inputs for the computational modeling analysis. These objectives were very well realized under the direction of Dr. Venkatesh Kodur, professor in the Civil and Environmental Engineering department at MSU. Dr. Kodur has conducted many years of research at the National Research Council of Canada and now at MSU on the fire performance of structures. The work of Dr. Kodur and his students for this project have been integrated into various sections of the report and will be highlighted as such.

The authors very gratefully acknowledge the insights and experience of the members of the Chicago Fire Department (CFD) and the International Association of Fire Chiefs (IAFC). The authors would like to give special recognition to James M. Dalton, Coordinator of Research of CFD for his comments and technical direction.

For support on ANSYS modeling and meshing, UL partnered with Mindware Engineering headquartered in Novi, Michigan.

This work was supported by a fire research and education grant sponsored by the Fire Prevention and Safety Grants under the direction of the Department of Homeland Security/Federal Emergency Management Agency/Assistance to Firefighters Grants.

EXECUTIVE SUMMARY

This report is part of an investigation into the structural stability of engineered wood-based products. The prevalence of these products in the construction industry is driven by their high stiffness to weight ratio allowing for the use of lightweight assemblies and innovative designs. However, field experience suggests that the fire performance of these engineered wood products is inferior to traditional timber.

One part of this investigation involved the fire testing of several different floor assemblies. The test data provided a wealth of information on the relative performance of various materials and designs. In these tests, assemblies were exposed to fire in a large-scale horizontal furnace following the standard time-temperature curve of the ASTM E119 test. The assemblies were loaded on the periphery to represent the more realistic non-uniformity of loading in residences. In addition, two 300 lbs mannequins representing fully loaded fire fighters were placed on the floors.

The next phase of the project involved the application of computational modeling tools, such as finite element analysis (FEA), to simulate and predict the fire performance of these wood-based floor assemblies. This report details the outcome of modeling two specific unprotected floor assemblies: one construction consisting of dimensional lumber supports, and the second, a floor assembly with engineered wood I-joist supports. The unprotected engineered lumber support floor assembly represents the basement of houses.

Models for each assembly required information on the heat source, mechanical loads, thermal and mechanical boundary conditions, construction details, and material properties. In modeling wood-based products in fire, several challenges exist. The first challenge is that wood burns unlike other common construction materials such as masonry, concrete and steel. The burning of wood is an exothermic reaction whose byproducts are char and smoke. Second, in the typical fire environment, construction elements are exposed to a very wide temperature range. Over this wide range, wood degrades and decomposes significantly changing material properties such as thermal conductivity, modulus of elasticity and others. Third, wood is a complex product whose properties vary with orientation and position. In building a model to simulate the complex process of a structure in fire, the analyst must develop clear and transparent assumptions that will lead to a tractable yet consequential model.

For this project, the following assumptions guided the development of the finite element models:

- Wood properties were isotropic and homogeneous.
- The process of moisture evaporation and diffusion within wood was modeled through effective thermal properties.
- The temperature distribution with the floor assembly was independent of the structural response.
- The heat source in the furnace was modeled as a point source with a radiation view factor of 1.0.
- All joining details of floor, sub-floor and supports were assumed to be ideal leading to perfect heat transfer and perfect mechanical contact.

Thermal results were computed using a transient thermal analysis including radiation, convection and conduction modes of heat transfer. For the structural results, a nonlinear, quasi-static analysis was performed at select points in time, transferring the temperature data into the structural model to calculate material properties. For both analyses, the commercial general-purpose FEA code ANSYS was employed. The use of a single multi-physics code lessened the challenges associated with data transfer from one analysis type to another.

For the thermal model, it was apparent that an accurate measure of the heat input from the furnace was not available. The data taken from the furnace thermocouples - which typically follow the standard time-temperature curve – deviated substantially from the standard time-temperature curve being much lower during the early stages of the test. This lack of an accurate measure of the heat input naturally affected the expected results of the model. Furthermore, it was found that it would be necessary to model the internal heat generation of wood combustion within the model. The model results for temperature and burning rate also pointed to the need for more extensive measurements on the properties of charred wood.

For the structural model, the deflection results did not match well with the test data. The main challenge for the structural model was capturing the reduction of cross section as the wood chars. This loss of cross section leads to lower loading bearing capacity. In this study, very small elastic modulus values were assigned to elements whose temperatures exceeded 570 ^{0}F (300 ^{0}C) as a means of representing this loss of structural stiffness. During fire exposure, the modulus would reach extremely small values as wood is converted to char. However, as the elastic modulus was reduced, convergence of a solution became problematic. As the modulus could not be reduced to very low values, the results must be interpreted with care. At this point, without further improvements to the model, the actual deflection numbers could not be explored with confidence but some qualitative assessments were still worthwhile. In this case, as the temperatures within the members exceeded the ignition temperature of wood, the results from the models showed that assembly 2, the unprotected floor

assembly with engineered lumber I-joists, had a greater increase in the rate of downward deflection than assembly 1, unprotected floor assembly with standard timber.

Despite the shortfall of the first order model in predicting the actual deflections of the wood floor assemblies, the central challenges and the path forward in improving computational models of burning structures have been identified and reported. With validated models, sensitivity studies can more easily be carried out to assess the effect of various types of loads, dimensional and geometric changes.

One important lesson from this modeling project was that with the regular fire testing, which is carried out in the field of fire safety engineering and certification, design of the fire test should consider the requirements for model validation. This will advance the use of modeling tools to help supplement fire testing in developing new safety guidelines, building codes, and firefighting tactics.

TABLE OF CONTENTS

LIST OF FIGURES

LIST OF TABLES

INTRODUCTION

The work described in this report is part of a broader effort to better understand and predict the fire performance of various types of wood-based assemblies employed in the construction of buildings and residential dwellings and to compile data to further discussions and advancements on safety guidelines, building codes, and firefighting tactics for new wood-based products.

The first part of this project[1] involved large-scale fire testing of nine different assemblies identified in Table 1 according to the ASTM E119 standard[2]. Assembly 2 was an unprotected floor constructed using an engineered I-Joist as the supporting member (Figure 1). The floor assembly was non-traditionally loaded and placed in a furnace, subjected to the fire endurance test of ASTM E119 standard. This floor collapsed at approximately 6 minutes into the test versus 18 minutes for Assembly 1, an unprotected floor supported by 2 x 10 in. dimensional lumber.

Figure 1 - Picture of standard dimensional lumber (l) and Engineered I-Joist (r)

According to a 2007 Engineered Wood Association newsletter, pre-fabricated wood I-joists comprise 50% of new wood-frame construction[3]. The main driver for the introduction of these products is the increase in stiffness to weight ratio. The benefits of cost savings from using lightweight constructions and efficiencies in installation have increased the preference for these types of wood-based products. However, over the years, the data on firefighter fatalities and injuries have led to concerns[4] captured by headlines such as 'Common Building Material Poses Deadly Threat to Firefighters – Wood I-Joists Burn Quickly, Floor Fails' dated November 12, 2008[5], which reports

[1] The second part of this project produced a web-based educational program available at www.ul.com/fire/structural.html.
[2] Report on Structural Stability of Engineered Lumber in Fire Conditions, UL Report, September 30, 2008.
[3] Technical Topics, Form TT-015 C, APA Engineered Wood Association, November 2007.
[4] J. Kirsch, Silent Floors, Silent Killers?, Fire Engineering, April 2007.
[5] http://www.wisn.com/news/17968429/detail.html

two firefighters falling through floors made of manufactured wood. Though lightweight constructions may have superior structural performance under 'normal' conditions, this trend may reverse in a fire environment.

Table 1 - Summary of assemblies built and tested

Test Assembly No.	Supports	Ceiling	Floor or Roof
1	2 by 10s @ 16 inch centers	None	1 by 6 subfloor & 1 by 4 finish floor
2	12 inch deep "I" joist @ 24 inch centers	None	23/32 inch OSB subfloor, carpet padding & carpet
3	2 by 10s @ 16 inch centers	1/2 inch regular gypsum wallboard	1 by 6 subfloor & 1 by 4 finish floor
4	12 inch deep "I" joist @ 24 inch centers	1/2 inch regular gypsum wallboard	23/32 inch OSB subfloor, carpet padding & carpet
5	Parallel chord truss with steel gusset plate connections, 14 inch deep @ 24 inch centers	1/2 inch regular gypsum wallboard	23/32 inch OSB subfloor, carpet padding & carpet
6	Parallel chord truss with glued connections, 14 inch deep @ 24 inch centers	1/2 inch regular gypsum wallboard	23/32 inch OSB subfloor, carpet padding & carpet
7	2 by 6s @ 16 inch centers with 2/12 pitch	1/2 inch regular gypsum wallboard	1 by 6 roof deck covered with asphalt shingles
8	2 by 10s @ 16 inch centers	3/4 inch plaster	1 by 6 subfloor & 1 by 4 finish floor
9	Roof truss with steel gusset plate connections @ 24 inch centers with 2/12 pitch	1/2 inch regular gypsum wallboard	7/16 inch OSB covered with asphalt shingles

To understand and predict the behavior of wood-based products and constructions, testing can provide some answers. However, fire testing in isolation will only lead to incremental additions to a fundamental understanding that is necessary to effectively develop safety and design guidelines. Complementing testing with computer-based engineering analysis tools such as finite element analysis (FEA) methods can provide greater insight and larger data sets for more effective decision-making. In this report,

the application and outcome of using FEA methods to predict the fire performance of wood-based floor assemblies are discussed.

Scope of Computational Modeling

The initial role of computational modeling in Structural Stability of Engineered Lumber in Fire Conditions project was limited to providing some suggestions on a suitable instrumentation scheme for the testing phase. However, this role was enlarged substantially to further the progress and validation of computational modeling tools in predicting the fire performance of wood-based constructions. As such, the scope for this portion of the project is to identify the challenges and, if possible, validate the output of FEA-based models (ANSYS). Specifically, models were built and analyzed to calculate the thermal and structural responses of assemblies 1 and 2 to the high temperatures seen during the fire endurance test of ASTM E119. The model boundaries and loads were set to match the conditions and setup of the tests as described in the UL test report issued on September 30, 2008.

Computational Modeling Deliverables

With the enhanced role of computational modeling for this grant, the deliverables for this project were revised and are listed below:

- Transient thermal finite element analysis of Assembly 1
    - Comparison of predicted temperatures with test data
- Structural nonlinear finite element analysis of Assembly 1 using temperature data from thermal model
    - Comparison of predicted floor deflections with test data
- Transient thermal finite element analysis of Assembly 2
    - Comparison of predicted temperatures with test data
- Structural nonlinear finite element analysis of Assembly 2 using temperature data from thermal model
    - Comparison of predicted floor deflections with test data
- Evaluation and assessment of modeling approach
- Recommendations for future research

SURVEY OF RESEARCH[6]

There are several challenges in the predicting the response of wood-based structures to fires. First and foremost, the fire environment leads to very high temperatures [1]. To predict the thermal and structural responses of wood-based components and structures to these high temperatures, material properties over a wide temperature range are required. Next, unlike steel and concrete, wood burns leading to material degradation and decomposition through pyrolysis (Figure 2). The combustion of wood and, its subsequent charring, lead to heat generation, flame spread, and dramatic changes in material properties [2, 12]. Another complication is that wood is a complex composite of natural polymers and is generally anisotropic, heterogeneous and porous. For example, Young's modulus depends upon grain orientation. As if this were not enough, the properties of wood are also affected by moisture content [3]. In a fire environment, any moisture contained within wood will evaporate and diffuse altering material properties. Finally the failure mode of a wood-based building component would depend upon details of the construction, material imperfections, connections, etc.

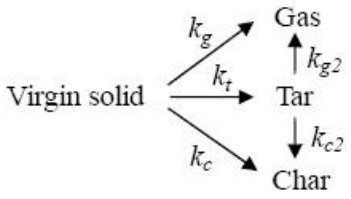

Figure 2 - Kinetics model of wood pyrolysis

All this very quickly suggests that a model that fully accounts for all the physics of combustion, material degradation, moisture transport, micro-scale structure, and failure modes of wood will be very challenging. So to meet this challenge, the engineer must pick and choose components and the level of complexity of the model that are most relevant to the objectives of the particular analysis. Data-driven and transparent assumptions must guide the model building and analysis so that practical results can be obtained without too much difficulty and in reasonable time periods allowing for stage-by-stage validation. Quite often a great deal of benefit can be gained from the qualitative predictions of modeling in assessing the relative impact and trends of different materials and designs.

[6] This is a brief survey of the technical literature in the English language using the Google search engine and the Compendex technical article database.

As mentioned above, what separates wood from other common materials used in construction such as steel, masonry, and concrete is that wood burns and chars. The burning of solids in air by external heating requires that surface temperatures reach critical levels known as the ignition temperature [4]. The high temperature of the solid surface leads to pyrolysis or decomposition of the surface materials and the release of gaseous volatiles. Some of these volatiles are flammable so that in a very hot air environment, a self-sustaining exothermic reaction may initiate [1]. For lignocellulosic materials such as wood, pyrolysis also leads to the formation of a carbonaceous char layer on the surface [5]. As the temperatures continue to increase from the external heat source and the flaming of the wood, the process persists as deeper layers and unburned surfaces of the wood dry, decompose and char. This is a simplification of a very complex process whose outcome depends on many variables such as heat flux, oxygen concentration, airflow, wood composition, and moisture conditions [13].

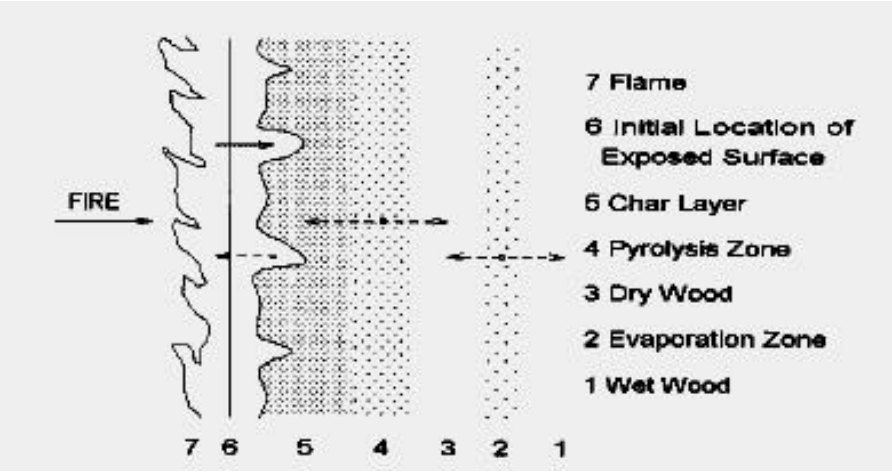

Figure 3 – Schematic of pyrolysis within a wood slab [6]

Measuring and tracking the char layer has been one element to determining the fire resistance of wood-based components and structures. The char layer replaces wood with structurally weak material and so effectively reduces the load-bearing cross-section of the component. In addition to mechanical properties, the char layer has thermal properties that are different from the original wood. The thermal properties of char tend to improve fire resistance of wood. The pyrolysis zone in Figure 3 suggests that a layer exists whose properties lie between those of dry wood and char. For wood temperatures around 280 ^{0}C to 300 ^{0}C are generally prescribed as the start of pyrolysis [6]. In this area, a great deal of work has been carried out to experimentally measure and predict the charring rate of different types of wood

[6,7,8]. A large number of experiments [9] suggest a nonlinear correlation between time and char depth[7].

For building components in a fire environment, the combined thermal and mechanical loadings lead to concerns regarding the stability of the component or structure. To predict the structural response of a building component first requires knowledge of the temperatures throughout the component and connections (Figure 4). In this area, most of the work for wood in high temperatures has concentrated on modeling and predicting the thermal behavior of wood under drying conditions such as kiln-drying [10]. The temperatures within the wood for these applications do not exceed 100 ^{0}C, which is much lower than the temperatures seen during fires [11].

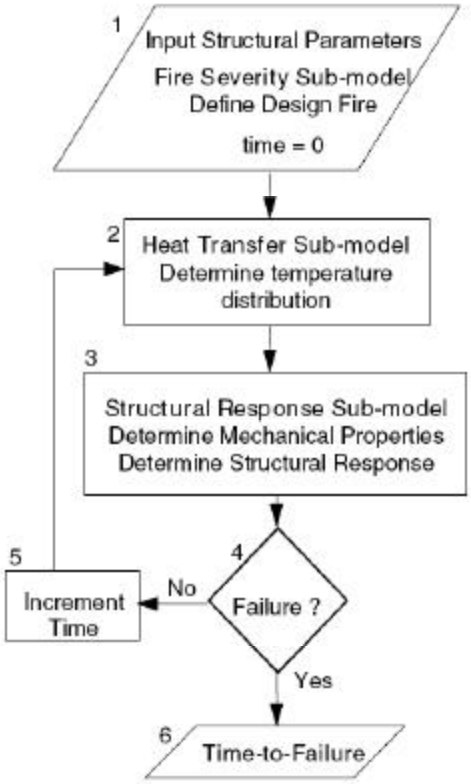

Figure 4 - Schematic for thermal and structural modeling of structures in fire [19]

A thermal model requires measured thermal properties as input over the wide temperature range seen during a fire [14, 15,20]. Typical measured thermal properties such as thermal conductivity and specific heat are 'effective' properties in that they implicitly include other processes such as moisture evaporation and diffusion [16].

[7] More detail provided in the Thermal Materials Properties section of this report.

In modeling the heat transfer from a fire source, radiation heat transfer [17] is the main mechanism for surface heating of exposed wood (Figure 5). The fire radiates heat to the structural elements where the intervening gases and products of combustion may play a role in the altering the heat flow [18]. With wood, the micro-scale structure consists of pores and grains. Heat transfer through the wood generally consists of conduction, convection and radiation. However, typically, in measuring thermal conductivity of wood samples, the data represents properties on a macro-scale as it includes the combined effect of all forms of heat transfer within the wood. The composition of wood also leads to thermal properties that are generally anisotropic.

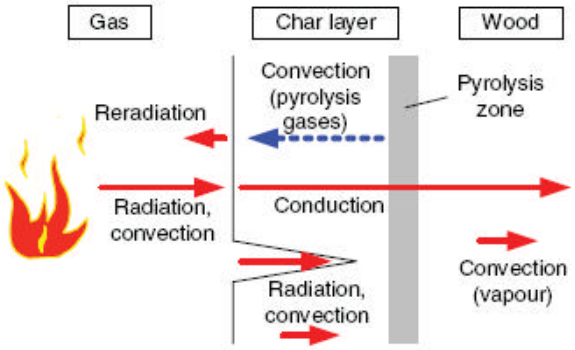

Figure 5 - Heat flux in wood from fire source [16]

Once a thermal model is built and verified, then there is need for test data for model validation. According to ASTM E1355 [21], verification implies that the solution of the equations is properly executed while validation is defined as 'the degree to which a calculation method is an accurate representation of the real world …'. Many such data sets are available - or could be made available with improvements in the instrumentation scheme - for model validation. These tests are the fire resistant tests carried out regularly according to standards such as ASTM E119 [26]. Fire resistance is assigned by exposing building components to standard fire tests that receive heat from a furnace. The fire rating is assessed based on temperature and stability criteria. A number of papers detail the test setup and results for the fire resistance testing of various wood-based floor assemblies [22, 23, 24, 25, 54].

To simplify the overall analysis, it was generally assumed that the thermal results do not depend upon the structural response of the building component. In other words, if the floor bends, the heat flux reaching the underside of the floor and the heat distribution within the components are not significantly altered. This allows the solution of the thermal model to be run and validated separate from the structural analysis [27].

The structural modeling of wood encompasses all the issues confronted in the thermal model such as temperature dependence, water phase change and anisotropy of material properties plus some additional challenges such as the charring of wood, connection details, bonding behavior of adhesives, creep, plasticity, buckling, and fracture.

Research in using FEA methods to predict the mechanical response of wood under 'normal' conditions has been carried out with a focus on modeling orthotropic material properties [32], wood fracture and failure [33, 34], effect of joining methods [35], effect of openings in webs [36], influence of adhesives [38] and more sophisticated constitutive modeling to account for creep and hygroexpansion strains in high temperature environments [37].

Though codes [41] do provide some guidance through design rules for wood in the 'abnormal' conditions of fire, computational modeling tools such as FEA will enhance the possibilities of performance-based fire safety design. Such tools will never replace testing entirely but instead will require more functional test data for model inputs and validation. For instance, the combined effect of high temperature and moisture requires careful correlation between material properties measured from small-scale tests and the large-scale fire tests. Clancy [38] suggested that the measured elastic modulus can be affected by the fast loading rate and quicker drying of typical material property tests which may lead to artificially higher values than that of the material in a real fire situation where creep may play an important role. Furthermore, high temperatures appear to adversely degrade compressive modulus or strength at a greater rate than the tensile modulus or strength for light-timber [39].

These challenges will remain as new wood-based engineered products [50] enter the market. The design of fire safe buildings requires a system approach so that the interaction of components and connections is critical [52]. In a real building fire, there is also concern for safety after the extinction of the fire and so the response of structures and the behavior of materials during the cooling period must be investigated.

Overall, the performance of a building component or an entire structure in fire involves a great deal of uncertainty related to fuel loads, material properties, etc. and so a hybrid approach joining FE tools (or other numerical techniques) and probabilistic modeling will plausibly be the best path forward [19].

MATERIAL PROPERTIES

There has been much work on measuring the properties of the wide variety of wood types leading to a very wide range of values. Unlike steel and cement, there is still no established database for 'typical' wood properties. Therefore, for this project, the thermal and mechanical properties of samples taken from the materials used to construct floor assemblies 1 and 2 were measured.

The entirety of material properties includes thermal and mechanical properties for the different wood components. The thermal properties consist of thermal conductivity, specific heat, thermal expansion, emissivity, and thermal diffusivity. The mechanical properties relevant to the analysis are strength, modulus of elasticity, and Poisson's ratio. Since the combustion process is not being modeled in detail, some criteria related to the initiation of charring, charring rate and the effect of charring on materials must be considered. This section provides information on the high temperature thermal, mechanical and charring properties of wood for use in fire resistance modeling of floor systems.

Thermal Material Properties[8]

There is limited information in the literature on the high temperature property relationships of wood. Further, these properties vary significantly among different species of wood and also on the test conditions of the specimen, such as moisture content and age. The source for the data is taken from various technical publications and tests[9] that were carried out on four components of assemblies 1 and 2, namely A, B, C and D. Sample A is conventional wood and sample B is engineered lumber used in the supports of floor assemblies 1 and 2, respectively. Samples C and D represent tongue and groove (T&G) wood and oriented-strand board (OSB) used as sub-floor in assemblies 1 and 2, respectively.

Density

Density of wood varies with species and in general the oven-dry density (ρ) of commercially important woods ranges from 300 kg·m^{-3} (white cedar) to 700 kg·m^{-3} (hickory, black locust). The density of Douglas fir varies from 430 to 480 kg·m^{-3}, and that of southern pine, from 510 to 580 kg·m^{-3}. The true density of the solid material that forms the walls of wood cells (α_t) is about 1500 kg·m^{-3} for most types of wood.

[8] The content of this section is from the Final report on the 'High Temperature Material Properties of Wood' by Dr. Kodur and dated November 25, 2008, as part of the partnering arrangement with MSU.

[9] Details on the testing conducted at MSU can be found in the Appendix D.

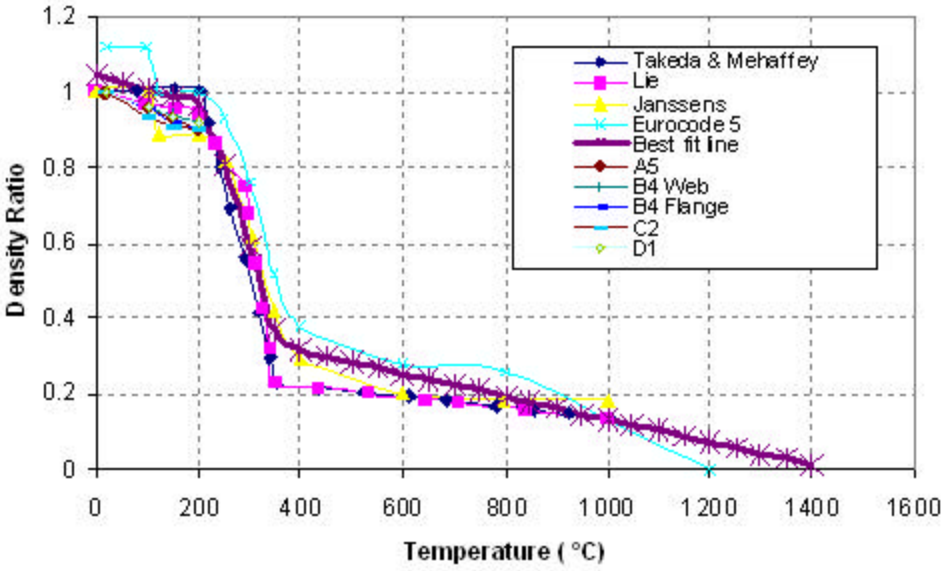

Figure 6 – Variation of density ratio with temperature for wood

The density of wood decreases with increasing temperature. A review of the literature shows that the density of wood varies slightly for temperatures below 200 ^{0}C. However, the decrease in density is rapid after 200 ^{0}C and until temperatures reach 350 ^{0}C. This can be attributed to significant evaporation of moisture (water) present in wood. After 350 ^{0}C density decreases at a slow rate due to occurrence of charring of wood. Figure 6 shows the variation of density ratio (defined as the ratio of density at elevated temperature to that at room temperature) with temperature. In general the density ratio drops to about 0.9 at 200 °C and then declines sharply to about 0.2 at about 350 °C. The source of data for Figure 6 comes from information presented in papers, reports, and codes [28, 29, 30, 31] and covers a wide range of species. Also, plotted in Figure 6 is the data obtained from thermal property tests on the four test samples (A, B, C and D). It can be seen from the Figure 6 that there is not a significant variation in the data from different sources for the temperature range of 20-300 ^{0}C.

The following equation that best fits the data for the variation of density ratio (DR) of wood with temperature (T) was generated for possible use in numerical models. Accordingly the density ratio can be expressed as:

$$
\begin{aligned}
DR &= 1.046-0.0004*T && 0\ ^oC = T = 200\ ^oC \\
&= 1.910-0.004*T && 200\ ^oC < T = 350\ ^oC \\
&= 0.435-0.0003*T && 350\ ^oC < T
\end{aligned}
$$

Thermal Conductivity

The thermal conductivity of wood varies with species type and is generally in the range of 0.1 to 0.8 $W \cdot m^{-1} \cdot K^{-1}$ at room temperature. In most species the thermal conductivity increases initially up to a temperature range of 150 to 200 °C, then decreases linearly until 350 °C, and finally increases again beyond 350 °C. Figure 7 shows the variation of thermal conductivity of wood with respect to temperature. The source of data for this figure comes from information presented in paper, reports and codes [28, 29, 30, 31] and covers a wide range of species. In addition, measured thermal conductivity values for the four test samples (A, B, C, and D) are also plotted in Figure 7.

It can be seen from Figure 7 that the variation of thermal conductivity for temperatures below 125 ^{0}C is almost linear, followed by an increasing trend for temperatures between 125 ^{0}C to 200 ^{o}C. For temperature range of 200 ^{o}C to 250 ^{0}C, thermal conductivity decreases and then follows an increasing trend for temperatures above 250 ^{o}C. The measured thermal conductivity values for engineered wood (Sample B) are much higher than that for conventional wood (Sample A).

The following equation that best fits the data for the variation of thermal conductivity (k) of wood (as well as OSB) with temperature (T) was generated for possible use in numerical models. Accordingly the thermal conductivity can be expressed as:

$$
\begin{aligned}
k &= 0.1075-(4*10^{-5})*T && 0\ ^0\text{C} = T = 125\ ^0\text{C} \\
&= 0.078+0.0002*T && 125\ ^o\text{C} < T = 200\ ^0\text{C} \\
&= 0.387-0.0013*T && 200\ ^o\text{C} < T = 250\ ^0\text{C} \\
&= 0.0007*T && 250\ ^o\text{C} < T
\end{aligned}
$$

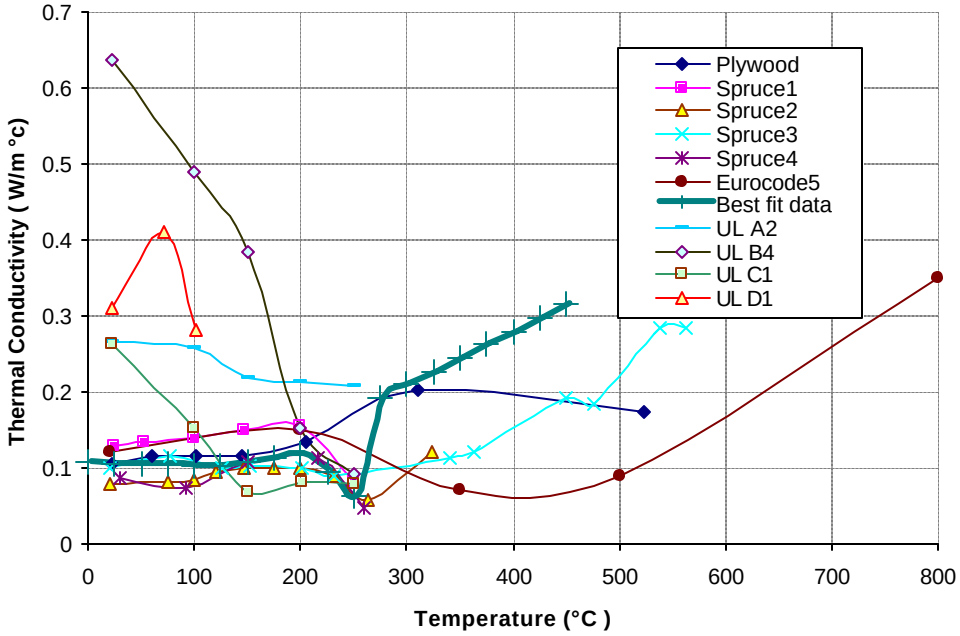

Figure 7 – Variation of thermal conductivity with temperature for wood

Specific Heat

The specific heat is highly influenced by the amount of moisture present in wood. The specific heat varies as a function of temperature and is usually measured by a differential scanning calorimeter (DSC). The variation of specific heat with temperature provides useful information on the nature of decomposition reactions that take place between 150 °C and 370 °C.

Figure 8 shows the variation of specific heat of wood with temperature. The source of data for this figure comes form information presented in papers, reports and codes [28, 29, 30, 31] and covers a wide range of species. Also plotted in Figure 8 is the measured data on the four test samples. It can be seen from Figure 8 that the variation of specific heat does not follow any specific trend. However, the Eurocode 5 relations [31] represent a more reliable trend as the specific heat value of wood peaks at 100 °C. This peak can be attributed to evaporation of moisture present in wood at about 100 °C, for which large amount of heat is required. This trend is commonly observed in other materials such as concrete, which have high moisture content. While the specific heat for samples fits with in the general range for other specimens, no specific conclusions can be made on the variation.

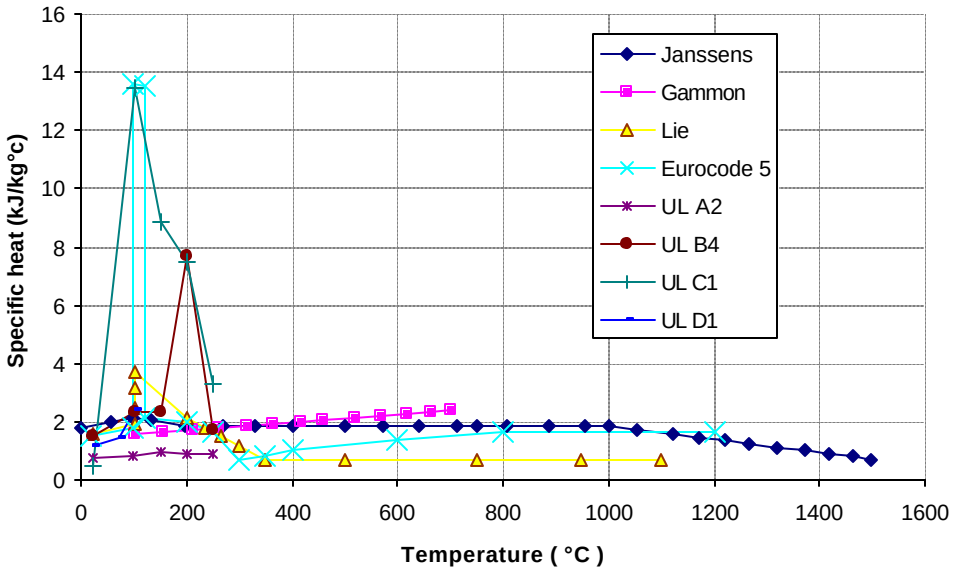

Figure 8 – Variation of specific heat with temperature for wood

The following values that best fits the data for the variation of specific heat (*c*) of wood with temperature (T) was generated for possible use in numerical models. Accordingly, the specific heat at different temperature ranges is given Table 2.

Table 2 – Specific heat of wood at various temperatures

Temperature (^{0}C)	Specific heat (kJ/kg^{0}C)
20 to 90	1.53
90	1.77
100	13.60
120	2.12
200	2.00
250	1.62
300	0.71

Thermal Expansion

The thermal expansion (or shrinkage) of wood is influenced by the orientation of the grain and also by the density of wood. The coefficient of linear thermal expansion (β) ranges from 3.2×10^{-6} to 4.6×10^{-6} $m \cdot m^{-1} \cdot K^{-1}$ along the grain, and from 21.6×10^{-6} to 39.4×10^{-6} $m \cdot m^{-1} \cdot K^{-1}$ across the grain. Malhotra [43] reported that wood expands up to a temperature of 80 ^{0}C, with an expansion coefficient of $3.5*10^{-6}$ /^{o}C.

Wood shrinks at temperatures above 100 °C, because of the reduction in moisture content. Lie [30] reported that the amount of shrinkage can be estimated as 8 percent in the radial direction, 12 percent in tangential direction, and an average of 0.1 to 0.2 percent in the longitudinal direction. Thomas [42] recomended a total longitudinal thermal expansion of 0.175% over a temperature range of 0 ^{o}C to 150 ^{o}C. Linear expansion coefficient across the grain can range from 5 to 10 times the parallel-to-grain expansion coefficient.

The following values (see Table 2) that best fits the data for the variation of thermal elongation of wood with temperature (T) was generated for possible use in numerical models.

Table 3 – Thermal Elongation of wood at various temperatures

Temperature (^{0}C)	Thermal deformation (m/m/^{0}C)
20	0.00008
50	0.0002
100	-0.0004
150	-0.0006
200	-0.0008
250	-0.001
300	-0.0012

Charring

Wood members derive much of their fire resistance property through the charring process. Thus charring is one of the main high-temperature properties associated with wood and should be considered in predicting performance under fire conditions. The rate of charring is influenced by the radiant heat flux or, alternatively, the fire severity. Generally, a constant transverse-to-grain char rate of 0.6 mm/min can be used for woods subjected to standard fire exposure. The charring rate parallel to the grain of wood is approximately twice the rate when it is transverse to the grain. These charring rates should be used only when attempting to model the performance of wood sections in the fire resistance furnace.

A number of parameters, the most important ones being density, moisture content, and contraction of wood influence charring. It is reasonable to modify the 0.6 mm/min to approximately 0.4 mm/min for moist dense wood, or to 0.8 mm/min for dry and lightwood. The fire retardants, often used to reduce flame spread in wood, may only slightly increase the time until ignition of wood.

Specific charring rates for different types of wood can be found in various references. Most national codes specify a constant charring rate of 0.60-0.75 mm for softwoods and about 0.5 mm per minute for hardwoods. Eurocode 5 [31] gives an expression for charring depth in a wood member exposed to standard fire as:

$$d_{char,0} = b_0 t$$

where $d_{char,0}$ = design charring depth for one-dimensional charring
$ß_0$ = one-dimensional design charring rate under standard fire exposure
t = time of fire exposure

Australian code [55] gives notional charring rate ß (mm/min) as

$$b = 0.4 + (\frac{280}{r_{12}})^2$$

where $?_{12}$ is wood density at 12% moisture content (kg/m^3).

In North America, the proposed charring rate, ß, based on White's model [9] is as follows:

$$b = 2.58 \frac{b_n}{t^{0.187}}$$

where $ß_n$ = notional charring rate obtained from char depth measured after 1 hr of fire exposure ($ß_n$ =0.635 mm per minute)
t = time in minutes

The resulting char layer thickness c (mm) at time t (minutes) can be calculated as:

$$c = ßt = 2.58\ ß_n\ t^{0.813}$$

Table 4 shows some of the experimentally derived charring rates in various studies. In modeling lightweight assemblies exposed to ASTM E-119 fire exposure, for conventional wood joists or T&G wood a charring rate of 0.7 mm/min for the first 15 minutes and a charring rate of 0.6 mm/min for the remaining time can be used. For the case of engineered lumber and OSB sub flooring a higher charring rate of 0.8 mm/min for the first 10 minutes and 0.7 mm/min for the remaining duration can be used.

Table 4 – Charring rate for different species of wood

Reference	Type of specimen	Timber type	Char rate (mm/min)
Wardle [47]	Beam	Spruce	0.5-0.6
		Douglas fir	0.6
		Baltic fir(laminated)	0.6
	Column	Fir	0.55
		Fir (Glulam)	0.66
Schaffer [44]	Panel	Douglas fir Southern pine White oak	0.68
Tenning [48]	Beam	Glulam	0.62
		Laminated pine	0.5-0.66
		Oak	0.4
		Teak	0.35
Odeen [49]	Beam	Fir	0.6-0.62
		Oak	0.4
		Teak	0.37
Fredlund [40]	Slab	Spruce	0.365
		Pine	0.339
		Chipboard	0.167
Rogowski [51]	Column	Hemlock	0.55(parallel) 0.67 (perpendicular)
		Fir	0.64 (parallel) 0.78 (perpendicular)
		Redwood	0.71 (parallel) 0.74 (perpendicular)
		Cedar	0.71 (parallel) 0.85 (perpendicular)

Mechanical Material Properties

The mechanical properties of wood that influence fire resistance are modulus of elasticity, tensile strength, compressive and bending strengths and Poisson's ratio. Modulus of elasticity is generally taken as the ratio of stress to strain. Poisson's ratio is one of the important properties of wood because of its heterogeneous nature and is defined as the ratio of transverse to axial strain. Since wood is an orthotropic material, the strength and stiffness in longitudinal and transverse directions are influenced by grain orientation. The mechanical properties of wood are affected by the temperature and are also influenced by moisture content, rate of charring, and grain orientation. A review of the literature indicates that parallel to grain properties are most widely available as they significantly influence the behavior of wood members in structures.

Modulus of Elasticity

The modulus of elasticity (MOE) of wood varies with the species and also is dependent on the orientation of grains. The MOE of air-dry, clear wood ranges from 5.5 x 10^3 to 15.0 x 10^3 MPa. The MOE parallel to grain decreases with temperature. A review of the literature shows that the MOE parallel to grain decreases slowly up to a temperature of 200 ^{0}C. After 200 ^{0}C the decrease in the MOE is more rapid. Figure 9 shows the variation of MOE ratio (ratio of modulus of elasticity at elevated temperature to that at room temperature) parallel to grain with respect to temperature. All the reported data is for MOE in tension, however, Thomas [42] reported values for both in tension and compression. It can be seen from Figure 9 that the modulus of elasticity parallel to grain in tension decreases gradually up to about 200 ^{0}C and then the rate of decrease is steeper. In the case of compression, (based on Thomas' data) MOE parallel to grain decreases at a slow rate up to about 50 ^{0}C and then the rate of decrease is steeper up to about 125 ^{0}C, following which it almost remains constant.

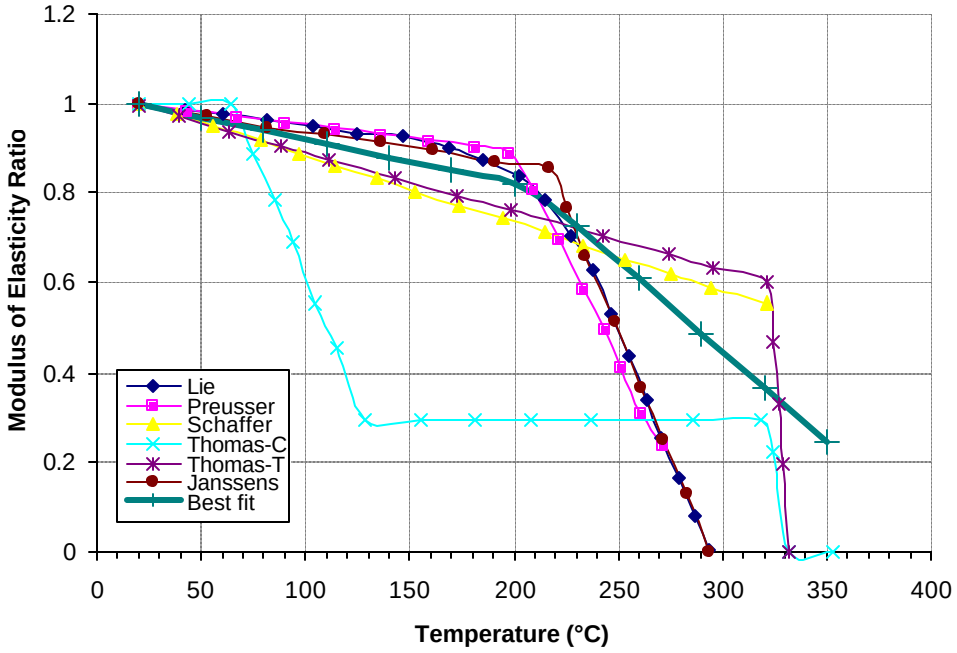

Figure 9 – Variation of MOE with temperature for wood

Based on the data available from literature, best-fit equations are presented below:

MOE ratio = -0.001*T + 1.019 20 °C = T = 200 ^{0}C
= -0.004*T + 1.647 200 °C < T = 350 ^{0}C

where T = temperature in ^{0}C.

Tensile Strength

The tensile strength of wood parallel to grain decreases with temperature. Figure 10 shows the variation of tensile strength ratio (ratio of tensile strength at a given temperature to that at room temperature) as a function of temperature. The tensile strength parallel to grain decreases slowly for temperatures up to 100 ^{0}C and then the rate of decrease is faster for temperatures up to 350 ^{0}C.

Data available from the literature has been used to arrive at a best-fit equation for the variation of tensile strength ratio with temperature.

$$\text{Tensile strength ratio} = -0.001*T + 1.02 \quad 20\ ^\circ\text{C} = T = 100\ ^0\text{C}$$
$$= -0.003*T + 1.216 \quad 100\ ^\circ\text{C} < T = 350\ ^0\text{C}$$

where T = temperature in ^{0}C.

Compressive Strength

Compressive strength of wood parallel to grain decreases linearly with an increase in temperature. A study of literature shows that compressive strength ratio (ratio of compressive strength at a given temperature to that at room temperature) decreases linearly except for data provided by Thomas [42]. Figure 11 shows the variation of compressive strength ratio (ratio of compressive strength at any temperature to that at room temperature) with temperature.

Based on the available data in literature, an expression has been arrived at for the variation of compressive strength ratio with temperature.

$$\text{Compressive strength ratio} = -0.003*T + 1.065 \quad 20\ ^\circ\text{C} = T = 350\ ^0\text{C}$$

where T = temperature in ^{0}C.

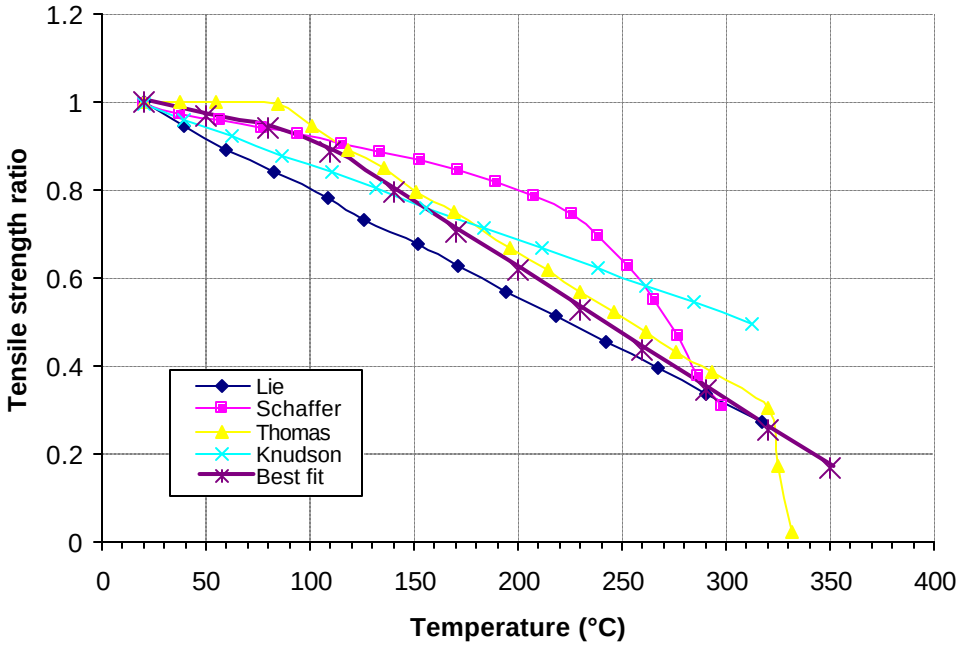

Figure 10 – Variation of tensile strength ratio with temperature for wood

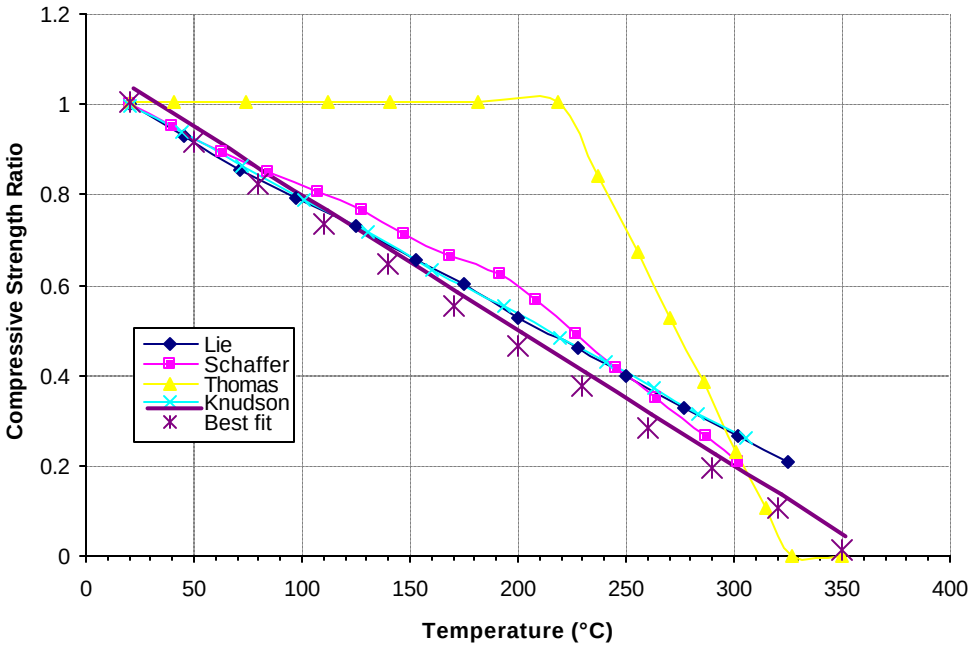

Figure 11 – Variation of compressive strength ratio with temperature for wood

Test Specimen Property Tests

Strength tests were carried out on wood samples A and B according to the applicable ASTM standards. Details of the test specimens along with the test apparatus, measured strength values are presented in Appendix D. Since joist elements (not sub flooring) perform load-bearing function only conventional wood (Specimen A in floor assembly 1) and engineered lumber (Specimen B in floor assembly 2) were considered for strength tests at room and high temperatures. Compressive and tensile tests were conducted on wood specimens, both parallel and perpendicular to grain. A summary of test results is provided in Appendix C. Values of compressive and tensile strength parallel to grain at room temperature are presented in Table 5.

Table 5 – Compressive and tensile strength parallel to grain for test specimens at room temperature

Specimen	Test data Stress (MPa)		Published data Stress range (MPa)	
	Compressive	Tensile	Compressive	Tensile
A	54.3	64.6	13.8-55.2	No reliable data available
B	46.7	49.7		

Data from tension strength tests, parallel to grain, was used to derive elastic modulus of specimens A and B at room temperature. The computed elastic modulus was found to be 10,563 MPa and 17,643 MPa for specimens A and B, respectively. From the literature review, it was found that the elastic modulus for conventional wood is in the ranges of 5.5×10^3 to 15.0×10^3 MPa. Thus the elastic modulus of Specimen A is within the range reported for wood, while engineered lumber (B), due to enhanced properties, has higher modulus.

It can be seen from the above table that the values of compressive strength parallel to grain at room temperature are within the range specified in the literature [45]. Hence the above expressions can be used to generate high temperature strength properties of wood. However, the test data presented in Table 5 and in Appendix C have to be used with care due to limited number of tests on the specimens. A large number of parameters influence the properties of the wood and to generate a reliable set of data, a larger sample of specimens should be tested. The accuracy of the proposed recommendations (test data and proposed relationships) can be improved through additional tests and analysis.

Poisson's Ratio

Poisson's ratio is defined as the ratio of transverse to axial strain. Values of Poisson's ratio vary within and between species of wood and are also affected by moisture content and specific gravity of wood. A review of literature indicate that Poisson's ratio vary from 0.019 to 0.641 for hardwoods and from 0.025 to 0.467 for softwoods [45].

Adhesives

In this research, the properties of any adhesives that were part of the construction of the engineered I-Joists were not considered.

FINITE ELEMENT ANALYSIS

The building and running of an FEA model requires detailed information on the boundary conditions, assembly geometry and construction, loadings, material properties, and expected failure modes. With this information, then the analyst must select the relevant elements and constitutive models along with proper numerical controls for convergence and stability. In this study, the commercial FEA code ANSYS [53] was selected for the thermal analysis and structural analysis.

Thermal FE Analysis

The predictions of the structural deflections of the floor assemblies subjected to a heat source first require knowledge the temperature distributions throughout the assembly. In this study, the thermal performance of two different unprotected floor assemblies[10] was calculated. These floor assemblies were tested in the UL large-scale horizontal furnace according to the standard time-temperature curve described in the ASTM E119 standard.

Modeling the Furnace Fire Exposure

In simulating a high temperature heat source, radiation will be the dominant heat transfer mode. In the furnace, it was assumed that the furnace walls did not re-radiate heat to the structure. The gases within the furnace were assumed to be transparent to any radiation heat. The view factor for radiation was set to 1.0. This implies that the entire underside of the floor assembly – except for some boundaries to be described later - is equally heated by the heat source. These assumptions allowed for the modeling of the furnace burners as a point heat source. Next it was assumed that this point source generates heat based on the temperatures from the furnace thermocouples (or any other representative source). To model radiation heat transfer in ANSYS, the entire exposed underside of the floor assembly was modeled using SURF152 elements. According to ASTM E119 [26], the furnace burner output should be controlled to deliver a specified temperature versus time as shown in Figure 12. The equation shown below provides an analytical representation of the standard time-temperature [56] curve for modeling purposes.

[10] Refer to test report for more details: Report on Structural Stability of Engineered Lumber in Fire Conditions, UL Report, Project 07CA42520, File Number NC9140, September 30, 2008.

$$T - T_0 = a[1 - \exp(-3.79553\sqrt{t})] + b\sqrt{t}$$

where
a = 750 for °C, 1350 for °F
b = 170.41 for °C, 306.74 for °F
t = time (hr)

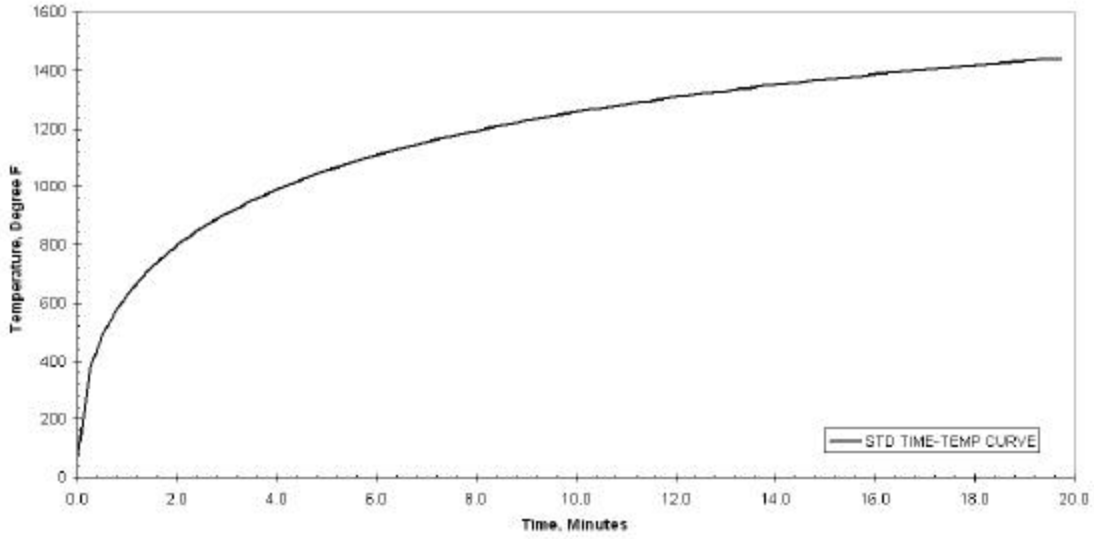

Figure 12 - Standard time-temperature curve from ASTM E119 for the first 20 minutes

The To in the analytical expression for the standard time-temperature curve was set to 20 ^{0}C (68 ^{0}F). The thermal analysis included convection heat transfer for both the top and bottom of the floor assemblies. The convective heat transfer to the bottom of the assembly was from the furnace and the convective heat transfer for the top of the assembly (unexposed surface) was to ambient with an assumed temperature of 26 ^{0}C (80 ^{0}F). The primary gas in the furnace was assumed to be air and the convection heat transfer coefficient for the top was set to 5 W/(m^2 ^{0}K) [0.88 BTU/(hr sq ft ^{0}F)] and for the underside, the convection heat transfer coefficient was set to 10 W/(m^2 ^{0}K) [1.76 BTU/(hr sq ft ^{0}F)]. An effective emissivity of 0.6 was set for radiation heat exchange. The effects of smoke and soot generation from the burning of the wood floor assemblies on heat transfer were considered unimportant for this level of analysis.

As the heat source is a function of time, this necessitated a transient thermal analysis. For such an analysis, initial conditions at the start of the analysis must be prescribed. All points in the assembly were set to an initial temperature of 70 ^{0}F.

Thermal Model Details for Assembly 1

For floor assembly 1, a full-scale 3-D FE model with overall dimensions of 17 feet 10 inches by 13 feet 10 inches as shown in Figure 13 was built. The dimensions were based on drawings shown in the Appendix A. The 2 x 10 in. support members are shown at 16 inches spacing. 1 x 3 in. wood members comprise the cross bridging. These components support a 1 x 6 in. T&G plywood sub floor and ¾ inch thick red oak T&G floor. The details of the T&G connectivity were ignored and the entire sub floor and floor were modeled as uniform. The contacts between all adjoining components were assumed to be continuous and perfect thereby ignoring any adhesive or other joining methods. For the heat transfer model, this implies that there is no heat loss at interfaces.

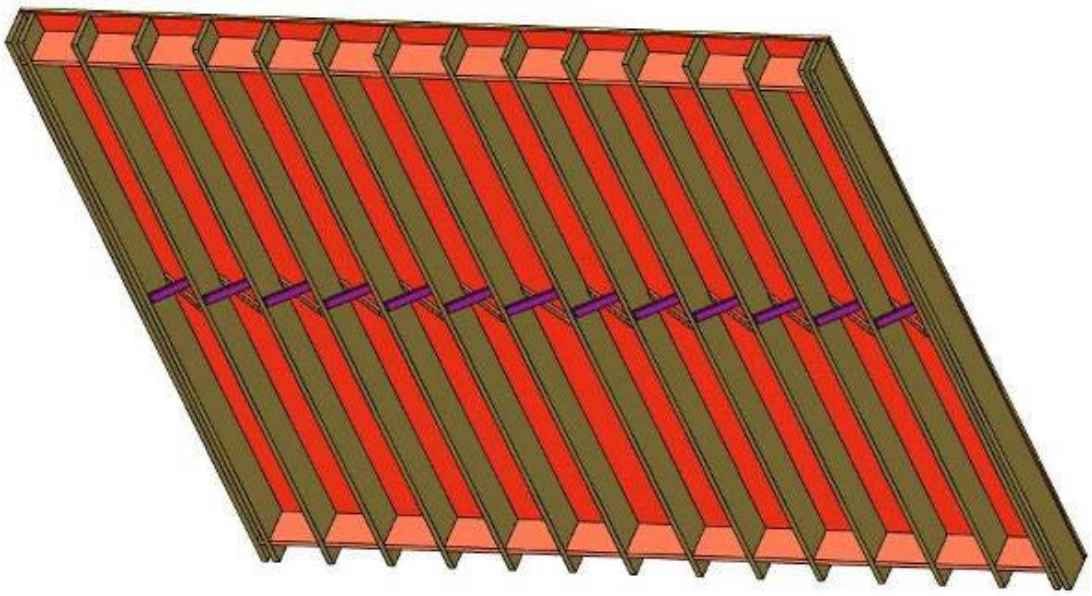

Figure 13 - FE model of Assembly 1

In addition to the wood-based components, there was a red rosin paper (0.01 inch thick), which was included in the thermal model. Any thermal influence from the objects providing mechanical loading such as the concrete blocks was ignored. The model was meshed using SOLID70 thermal elements. The FEA model for this assembly consisted of a total of 139,954 elements. Each full transient thermal analysis consumed approximately 4 hours of CPU time on a SGI Altix 3300 workstation.

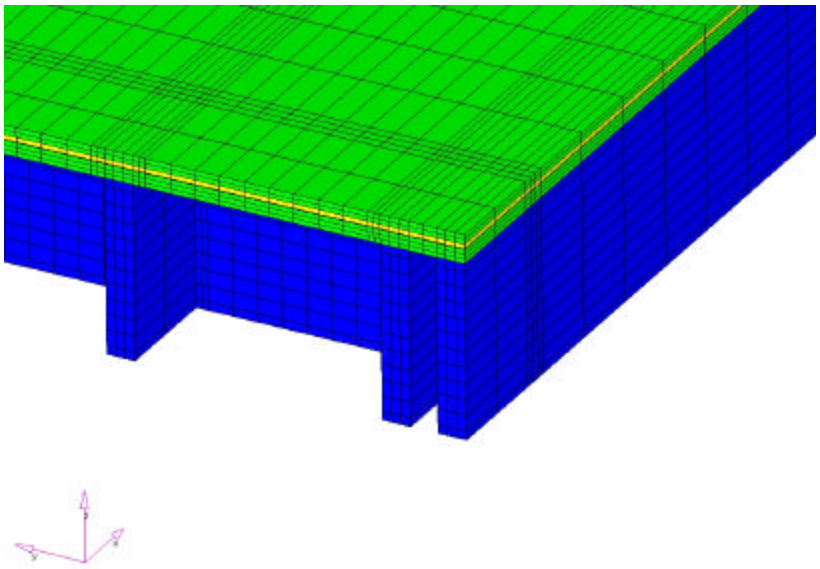

Figure 14 - Close up of FE mesh

Table 6 - Thermal property inputs for Assembly 1

Wood for sub-floor and finished floor

Thermal Conductivity				Specific Heat			
Temp C	Temp F	W/mC	BTU/hr-in-F	Temp C	Temp F	KJ/kg C	BTU/lb-F
20	68	0.28	1.349E-02	20	68	1.53	3.65E-01
100	212	0.13	6.265E-03	89	192.2	1.53	3.65E-01
150	302	0.07	3.373E-03	90	194	1.77	4.23E-01
200	392	0.085	4.096E-03	100	212	13.60	3.25E+00
250	482	0.085	4.096E-03	120	248	2.12	5.06E-01
300	572	0.17	8.193E-03	200	392	2.00	4.78E-01
				250	482	1.62	3.87E-01
				300	572	0.71	1.70E-01

Wood for Joists and cross-bridging

Thermal Conductivity				Specific Heat			
Temp C	Temp F	W/mC	BTU/hr-in-F	Temp C	Temp F	kJ/kg C	BTU/lb-F
20	68	0.28	1.349E-02	20	68	0.80	1.91E-01
100	212	0.26	1.253E-02	89	192.2	0.80	1.91E-01
150	302	0.23	1.108E-02	90	194	1.00	2.39E-01
200	392	0.22	1.060E-02	100	212	5.00	1.19E+00
250	482	0.21	1.012E-02	120	248	1.00	2.39E-01
300	572	0.25	1.205E-02	200	392	0.90	2.15E-01
				250	482	0.90	2.15E-01
				300	572	0.90	2.15E-01

Rosin Paper and Air

Thermal Conductivity			Specific Heat		
	W/mC	BTU/hr-in-F		kJ/kg C	BTU/lb-F
Rosin Paper	0.05	2.410E-03	Rosin Paper	1.70	4.06E-01
Air	0.02	9.638E-04	Air	1.00	2.39E-01

Table 7 - Density and density ratio for components of assembly 1

Density			
		kg/m^3	lb/in^3
Wood		500.00	1.8064E-02
Rosin Paper		470.00	1.6980E-02
Air		1.00	3.6128E-05
Wood Density			
Room Temp Density (kg/m^3)			*500*
Temp C	**Temp F**	**Density Ratio**	**Density (lb/in^3)**
20	68	1.0384	1.8757E-02
50	122	1.0264	1.8541E-02
100	212	1.0064	1.8179E-02
150	302	0.9864	1.7818E-02
200	392	0.9364	1.6915E-02
250	482	0.8106	1.4642E-02
300	572	0.7106	1.2836E-02

The outer edges of the floor were assumed to be adiabatic as they are in contact with vermiculite concrete and sealed with fire resistive caulk. Table 6 and Table 7 list all the thermal property inputs for the runs to be discussed next. For all analyses in this report, density was assumed constant[11].

Thermal Results for Assembly 1

Figure 15 shows the temperatures at various points in the floor assembly as a function of time. These points represent thermocouple measurements from test and model results at similar locations. A schematic of the instrumentation scheme is shown in Appendix A. For the test data, the temperature measurements represent an average of many thermocouples dispersed throughout the floor assembly. For the model, a single representative point – not close to the boundaries - was sufficient since the heat reaching the underside of the floor is uniform and so that the natural variations arising from material, construction, heat source and other non-uniformities are not present.

The model results (labeled 1b) shown in Figure 15 represent the case where the heat source follows the standard time-temperature curve. However, a comparison with the thermocouple measurements representing the furnace temperature (labeled Test: Furnace) shows that there is a significant difference between these two curves. In the early stages, the furnace thermocouples measure much lower temperatures than the standard time-temperature curve. The furnace thermocouples measure temperatures lower than the surface of the joists and bottom of sub-floor. So using the furnace

[11] Though not shown, thermal results including density ratio did not differ from the constant density case.

thermocouple measurements as the sole heat input to the model would lead to significant underestimation of heat flux reaching underside of the floor assembly.

Test notes indicate that the bottom of the 2 by 10 in. joists began to char at about 1 minute. So that very early into the test, wood is already burning and it is possible that air movement and soot generation affected the thermal feedback and measurements by the furnace thermocouples. This lack of an accurate measure of the heat input into the floor introduces a source of error for the predictions of the model.

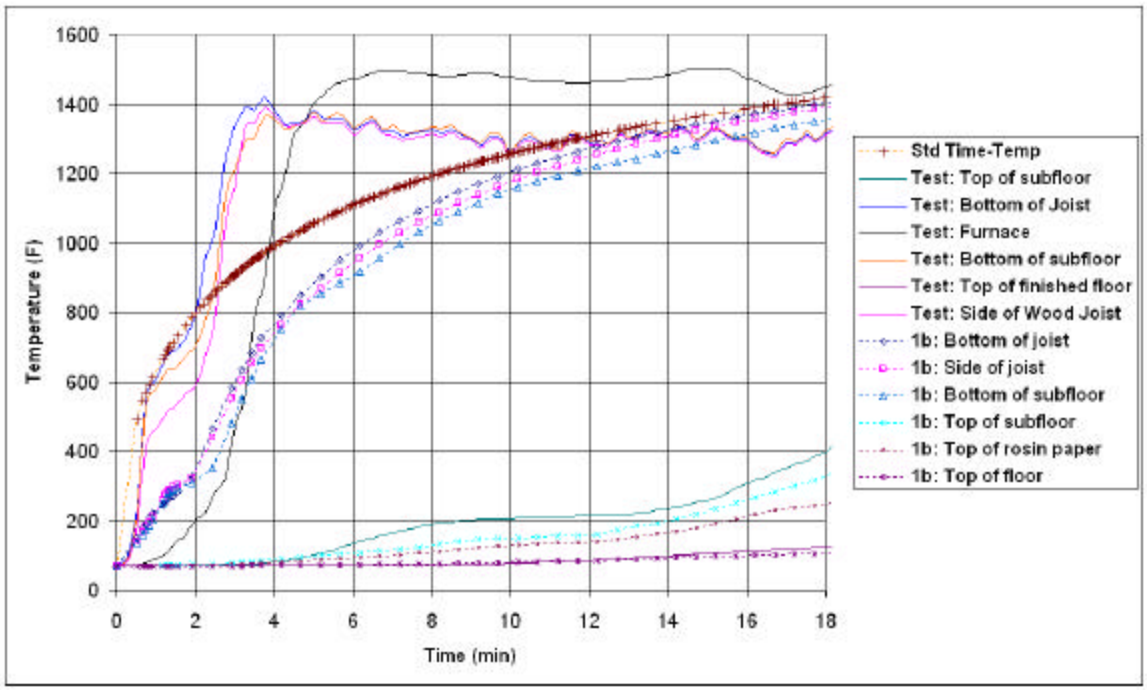

Figure 15 - Thermal results for model with standard time-temperature input

Nevertheless, it is still worthwhile to review the results. For the model, the standard time-temperature curve provides an upper limit to the temperatures that can be reached in the model. For both the test and model, the hottest temperatures occur at points measured underneath the floor assembly, which is exposed to the furnace burners. For both model and test, points representing the unexposed surface or the interface of the sub-floor and floor show much lower temperatures, below the ignition temperature of wood. The unexposed surfaces do not begin to heat up until at least 6 minutes from the start of the burners. There is a plateau region seen for the unexposed surface temperatures around 200 ^{0}F. At this temperature, free water trapped within the wood evaporates absorbing heat without any observable increase in temperature. For the model, the same plateau is seen in the sub-floor and floor interface. Recall that the peak in the specific heat mimics the moisture evaporation

within the wood. For the test, thermocouples were placed between the rosin paper and bottom of the floor. From the model, temperature readings from the bottom of the rosin paper and top of the sub-floor were added. This model underestimated the rapid temperature buildup in the underside of the floor for the first 8 minutes and so this model is not expected to provide a good basis for the structural analysis.

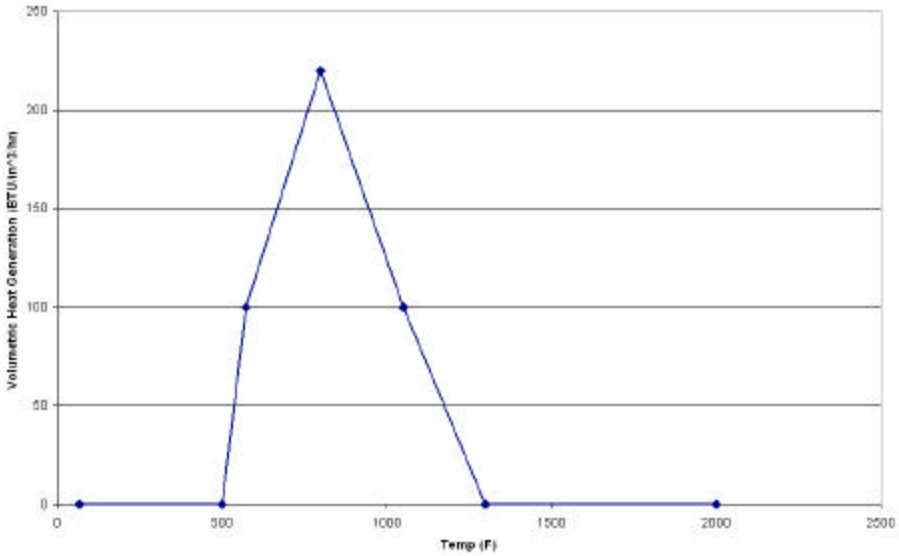

Figure 16 - Heat generation profile for wood components

One obvious shortcoming of the model is the exclusion of the exothermic heat generated by wood combustion. The model results (labeled 1e) shown in Figure 17 included a representative heat generation profile (Figure 16) in addition to the heat source following the standard time-temperature curve. This heat profile was initiated within an element volume once it reached an average temperature of 570 ^{0}F and ended by 1200 ^{0}F. In this case, a significant change in the temperature rise was predicted by the model for the underside of the floor more closely matching the sudden rise seen to occur after 2 minutes. However, the initial temperature rise during the first 3 minutes shows differences as large as 300 ^{0}F. Also now the sub-floor/floor interface and the unexposed surface are heating up much faster than the test.

This simple representation of the heat generation of the wood combustion process certainly requires further refinement. The higher temperatures of the unexposed surface suggest that the thermal properties especially as it relates to charring may also need modification. However, the results show that the inclusion of this heat generation term improved the predictions of the model.

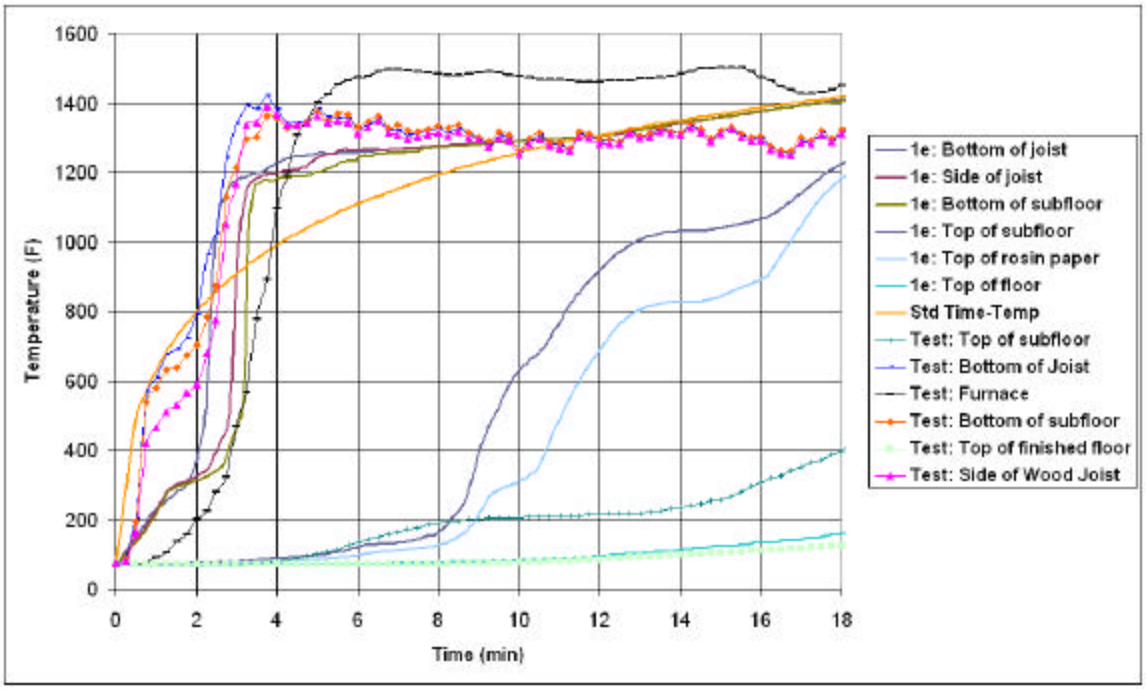

Figure 17 - Thermal results for model with heat generation and standard time-temperature input

In addition to the furnace thermocouples, another set of thermocouples, called interstitial thermocouples were placed near the bottom of the floor assembly in the cavity defined by the bottom of the sub-floor and the sides of adjoining joists (see Appendix A). A review of the thermocouple measurements from the interstitial spaces of assembly 1 (Figure 18) show that they provide much higher readings than that of the standard time-temperature curve and the readings of the furnace thermocouples. These interstitial thermocouples are located closer to the underside of the floor assemblies. This location would expose these thermocouples to the heat flux from the furnace burners and the thermal feedback from the nearby wood combustion. However, these readings are expected to provide a better representation of the heat input into the bottom of the floor than the furnace thermocouples. In setting the heat source to follow the time-temperature data from the interstitial thermocouples, excluding the heat generation term to avoid the possible double counting of heat reaching the underside of the floor assembly.

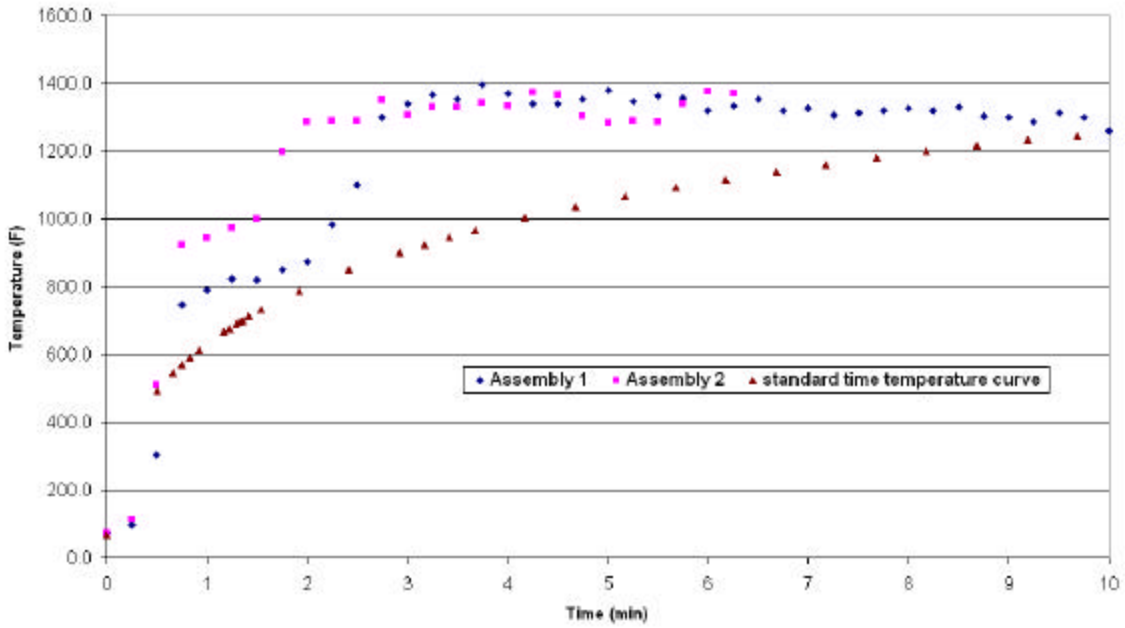

Figure 18 – Comparison of thermocouple measurements taken in the interstitial spaces of the floor assemblies

Figure 19 shows the model results for the case where the heat source was calculated based on the measurements of the interstitial thermocouples. In this case, the model results were substantially improved as compared to the case with only the heat input following the standard time-temperature curve despite the fact that heat generation was not included in the analysis.

However, there is still the issue of the large temperature discrepancy in the early part of the test for the underside of the floor. Resolving this discrepancy is important for improving the predictability of the structural analysis[12].

The explanation for the discrepancy is that the heat transfer to the underside of the floor is likely inadequate. This heat flux reaches the underside of the floor via radiation and convection. Typically, in the early stages of a furnace fire exposure, convection is dominant but as the temperature increases, radiation becomes more prominent due to its fourth power dependence on temperature.

[12] The run times for analyses with heat generation were 3-4 times longer than the cited run times of 4 hours for all the other analyses.

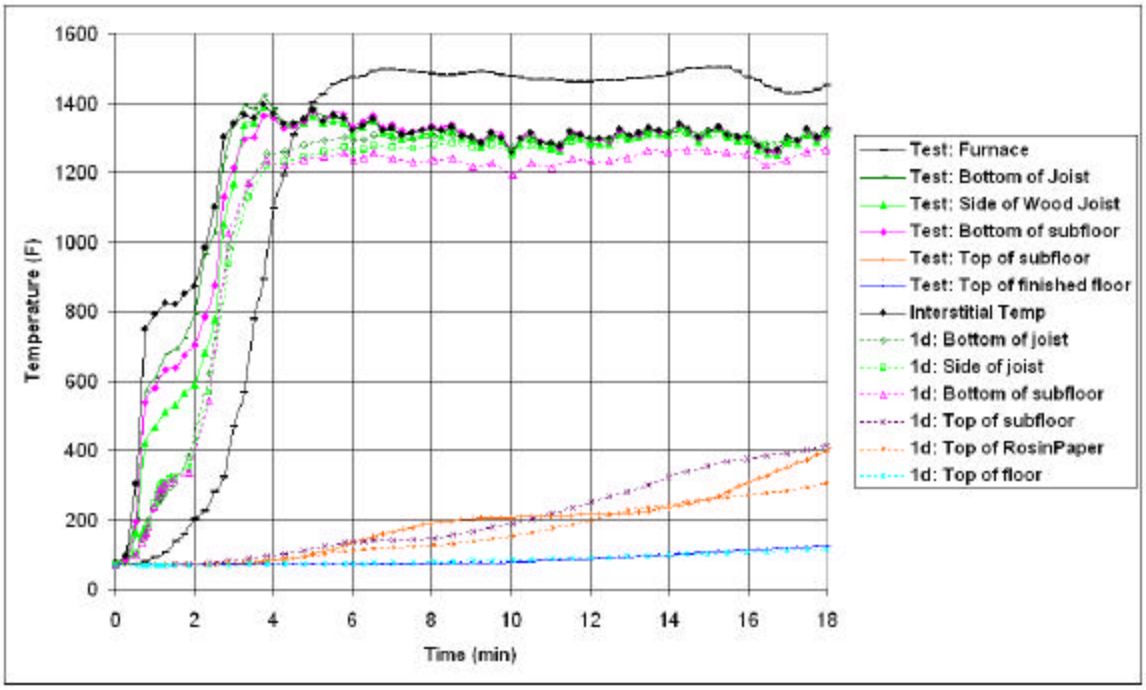

Figure 19 - Thermal results with heat input calculated based on temperatures of the interstitial thermocouples

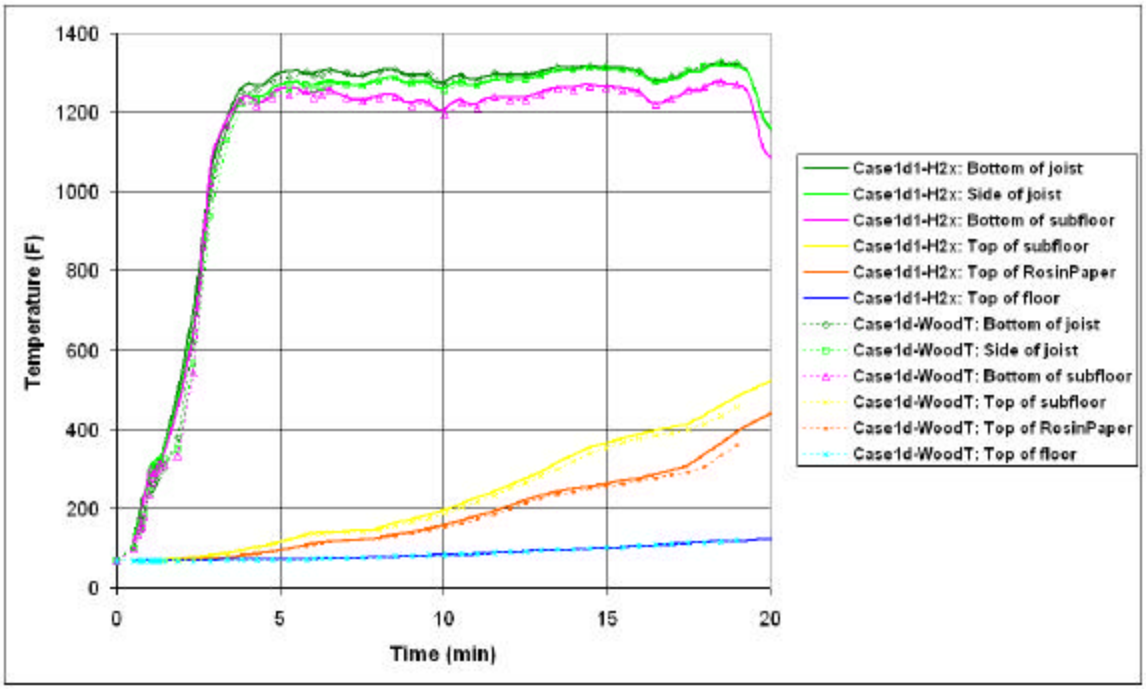

Figure 20 - Effect of doubling convection heat transfer coefficient

Figure 20 shows the effect of doubling the convection coefficient for the underside of the floor model. There is some increase in temperature between the baseline case (Case 1d) and the doubled convection coefficient case (Case 1d1-H2x) in the time range of 1-2 minutes. However, this change did not bring the results in line with the test data.

Figure 21 shows the sensitivity of the temperatures to an increase of the emissivity from 0.6 to 0.9. There are some regions between the baseline case (Case 1d) and the higher emissivity (Case 1d2-E0.9) where a temperature increase is noted. However, this change did not close the gap between the model temperatures and the thermocouple temperatures of the floor assembly underside during the early part of the test.

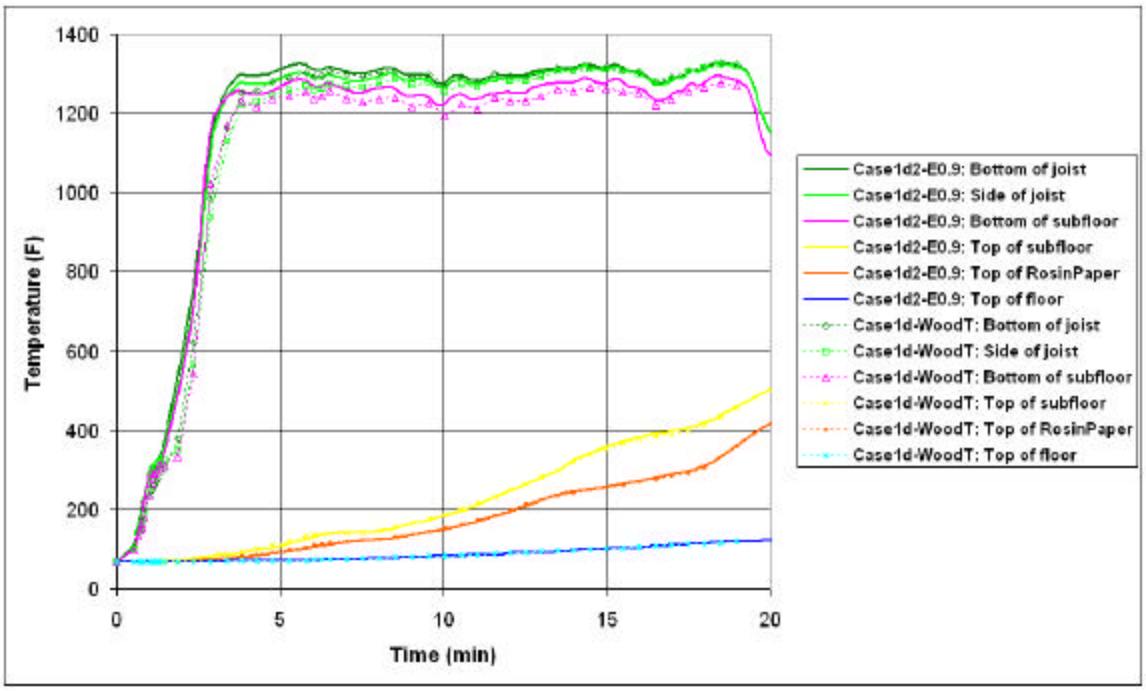

Figure 21 - Sensitivity to effective emissivity

The accuracy of the results from the structural analysis will greatly depend upon the predicted temperature distributions from the thermal analysis. Since temperatures in the early stages of the model are still below the test measurements, this error will carry into the structural results. Hence, the thermal model will be 'calibrated' to the measured temperatures of the underside of the floor assembly. To realize this, temperatures of the underside were set to follow the thermocouple measurements from the bottom of the sub-floor as shown in Figure 22. In addition, thermal conditions along the edges of the floor were defined (Figure 23) to better represent the thermal protection that is in the form of vermiculite concrete and other fillers

meant to protect the test frame. With these modifications, the thermal model results (Case 1g) for the bottom of the sub-floor, side of joists and bottom of joists overlay the test measurements on the bottom of the sub-floor as shown in Figure 22.

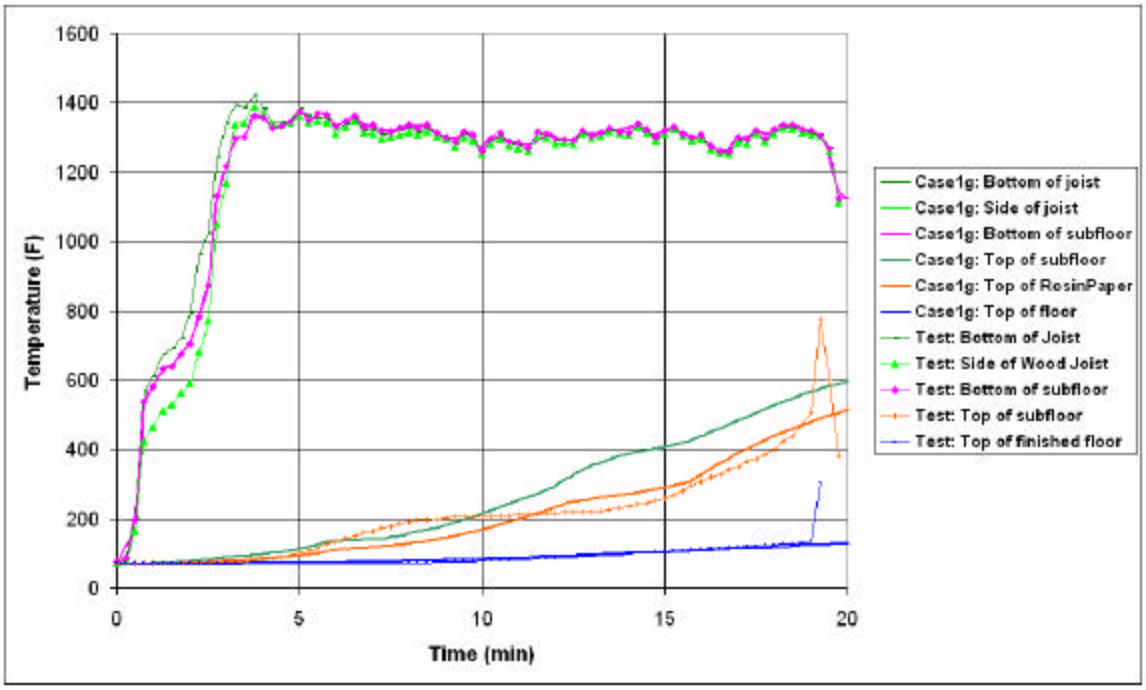

Figure 22 – Thermal model results for prescribed temperature for underside of floor assembly

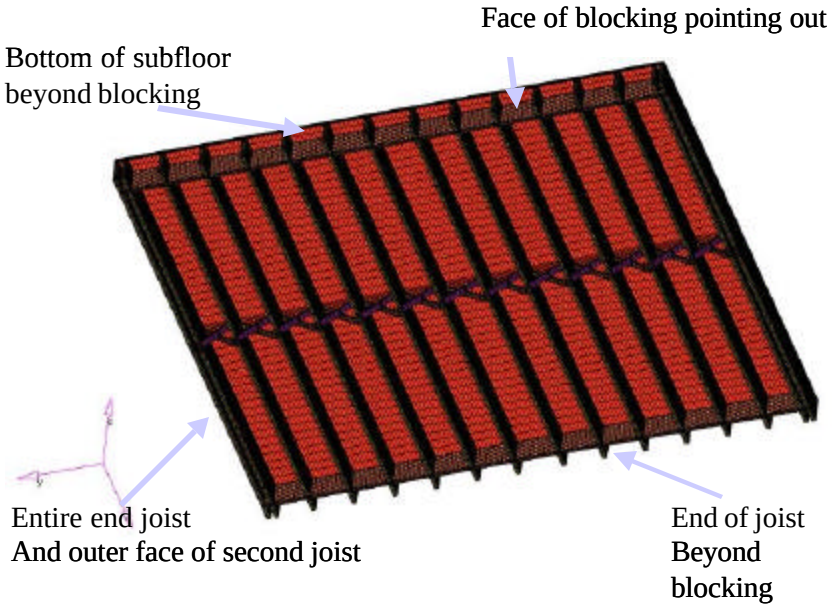

Figure 23 – Portions of assembly 1 underside not exposed directly to furnace

The next step was to calculate the burning rate and charring within the model based on the progression of temperature through a cross section of the assembly. Selecting the nodes that populate the thickness direction of the support joist and carrying out calculations based on the nodal distances and a temperature of 570 ^{0}F representing the start of combustion, the burning rate of the supports was approximately 4 mm/min, which is much higher than the 0.6-0.8 mm/min from tests and the open literature.

One of the key advantages of computational modeling is that detailed data is available throughout a component and its connections. For instance, examining the temperature contours can provide insight into the manner in which the supports are heating up. Figure 24 shows the temperatures contours in the supports at about 5 minutes into the simulation of the fire test. The rounding effect of the lower part of the support is apparent.

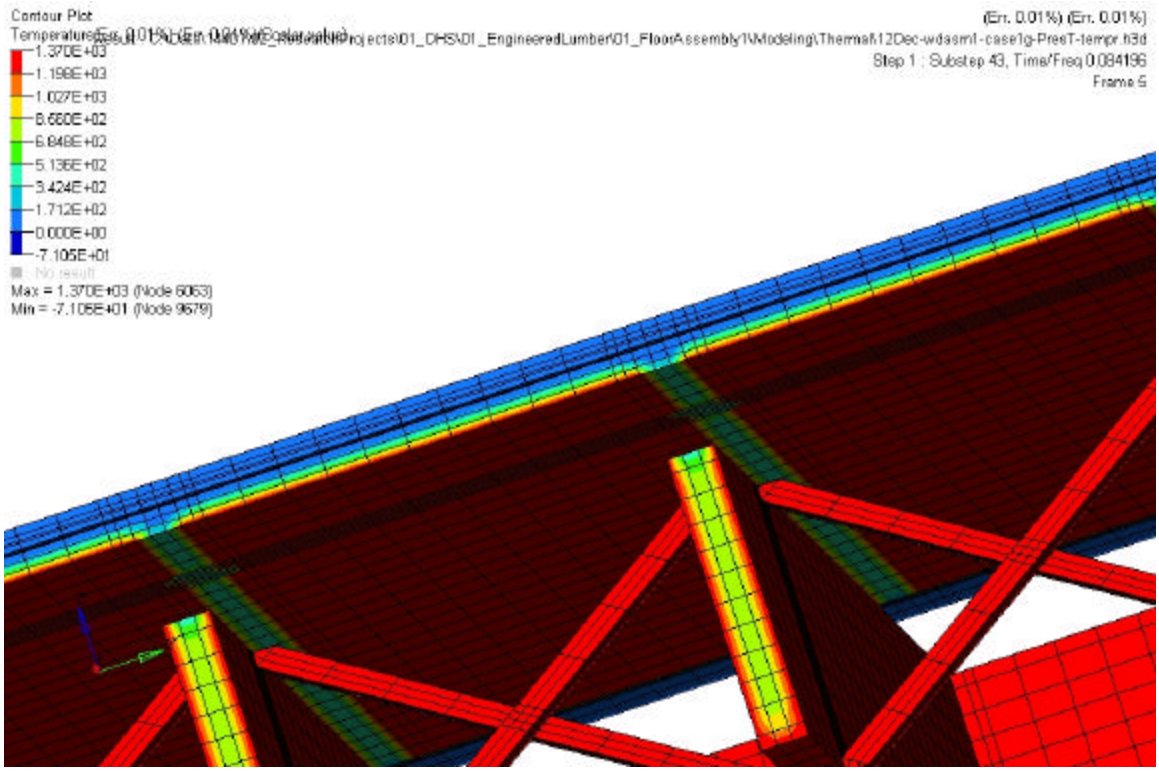

Figure 24 – Exploded view of thermal model displaying temperature contours at 5 minutes

Thermal Model Details for Assembly 2

For assembly 2, a full-scale 3-D FE model was built with overall dimensions of 17 feet 10 inches by 13 feet 10 inches as shown in Figure 25. The dimensions were based on drawings shown in the Appendix A. The supporting members are engineered lumber I-joists (Figure 26). The chords were constructed from laminated veneer lumber (LVL) while the web is oriented strand board (OSB). These I-joists provide integrity to a 23/32-inch thick OSB sub-floor. The exposed surface of the floor was covered with ½ inch thick carpet and 7/16 inch thick carpet padding. The contacts between all adjoining components were assumed to be continuous and perfect thereby ignoring any adhesive or other joining methods. For the heat transfer model, this implied that there is no heat loss at interfaces.

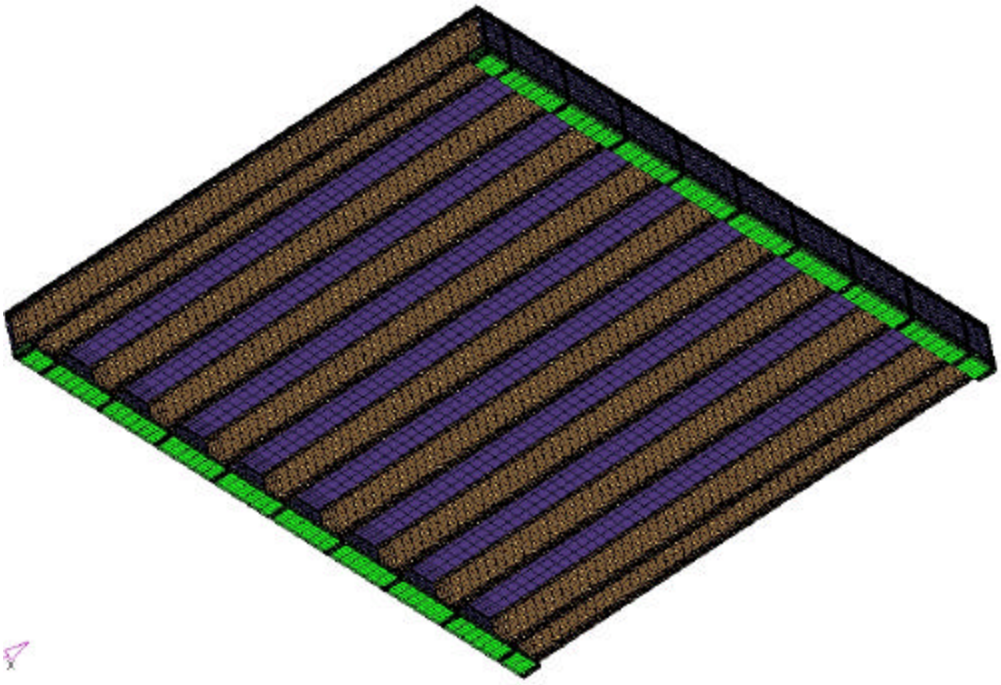

Figure 25 - FE model for assembly 2

Any thermal influence from the objects providing mechanical loading such as the concrete blocks was ignored. The model was meshed using SOLID70 thermal elements. There were a total of 103,328 elements. Though for the thermal models of assembly 1 and 2, computational advantage could have been gained through a quarter model, for the sake of ease of transfer of data from the thermal to the structural model (detailed in later sections), which has no such symmetry, the thermal analyses was performed with full models.

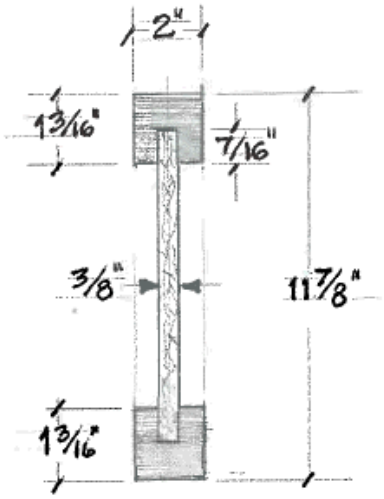

Figure 26 - Cross section of I-Joist

Figure 27 is a close up of the FE mesh and model near one corner. The details of the edge supports were included in the model.

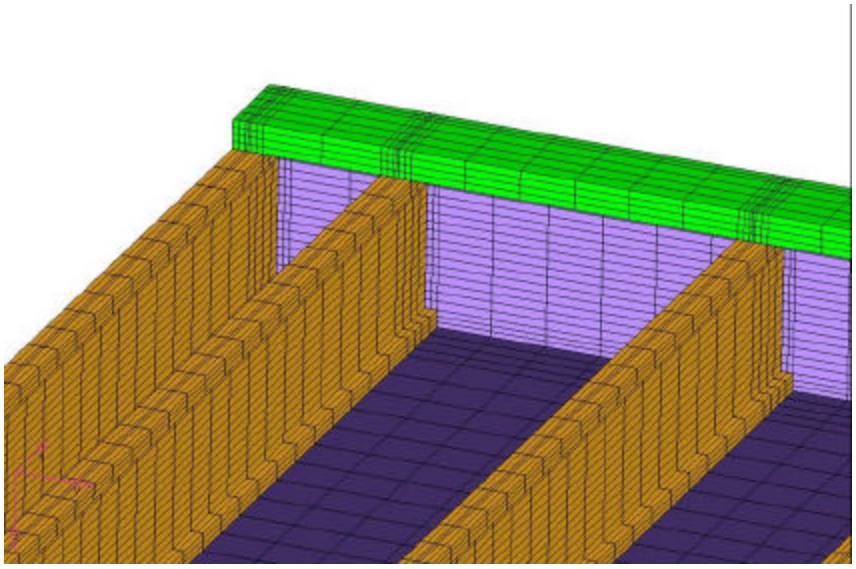

Figure 27 - Close up of FE mesh on the underside of floor assembly 2

The outer edges of the floor were assumed to be adiabatic as they are in contact with vermiculite concrete and sealed with fire resistive caulk. Table 8 and Table 9 list all the thermal property inputs for the runs to be discussed next. The density was assumed to be constant[13]. Generic properties for the carpet and carpet padding were found from the open literature and assumed constant.

[13] Though not shown, thermal results including density ratio did not differ from the constant density case.

For a transient analysis, initial conditions must be prescribed. In this case, all points in the assembly were set to an initial temperature of 70 ^{0}F.

Table 8 – Thermal property inputs for thermal model of assembly 2

Joist and boundary components

Thermal Conductivity				Specific Heat			
Temp C	Temp F	W/mC	BTU/hr-in-F	Temp C	Temp F	KJ/kg C	BTU/lb-F
20	68	0.6	2.892E-02	20	68	1.80	4.30E-01
100	212	0.5	2.410E-02	89	192.2	1.80	4.30E-01
150	302	0.38	1.831E-02	90	194	2.00	4.78E-01
200	392	0.15	7.229E-03	100	212	2.20	5.25E-01
250	482	0.09	4.337E-03	180	356	2.40	5.73E-01
300	572	0.12	5.783E-03	200	392	8.00	1.91E+00
1093	2000	0.12	5.783E-03	250	482	2.00	4.78E-01
				300	572	2.00	4.78E-01
				1093	2000	2.00	4.78E-01

Oriented Strand Board

Thermal Conductivity				Specific Heat			
Temp C	Temp F	W/mC	BTU/hr-in-F	Temp C	Temp F	kJ/kg C	BTU/lb-F
20	68	0.3	1.446E-02	20	68	1.53	3.65E-01
50	122	0.28	1.349E-02	89	192.2	1.53	3.65E-01
100	212	0.25	1.205E-02	90	194	1.77	4.23E-01
150	302	0.25	1.205E-02	100	212	2.50	5.97E-01
200	392	0.25	1.205E-02	120	248	2.12	5.06E-01
250	482	0.15	7.229E-03	200	392	2.00	4.78E-01
300	572	0.25	1.205E-02	250	482	1.62	3.87E-01
1093	2000	0.25	1.205E-02	300	572	0.71	1.70E-01
				1093	2000	0.71	1.70E-01

Padding and Carpeting

Thermal Conductivity				Specific Heat			
Temp C	Temp F	W/mC	BTU/hr-in-F	Temp C	Temp F	kJ/kg C	BTU/lb-F
		0.06	2.892E-03	20	68	1.40	3.34E-01

Table 9 - Density and density ratio for components of assembly 2

Joist and boundary components			
Density (kg/m^3)			**700**
Temp C	Temp F	Density Ratio*	Density (lb/in^3)
20	68	1.0384	2.626E-02
50	122	1.0264	2.596E-02
100	212	1.0064	2.545E-02
150	302	0.9864	2.495E-02
200	392	0.9364	2.368E-02
250	482	0.8106	2.050E-02
300	572	0.7106	1.797E-02
1093	2000	0.7106	1.797E-02
Oriented Strand Board			
Density (kg/m^3)			**570**
Temp C	Temp F	Density Ratio*	Density (lb/in^3)
20	68	1.0384	2.138E-02
50	122	1.0264	2.114E-02
100	212	1.0064	2.072E-02
150	302	0.9864	2.031E-02
200	392	0.9364	1.928E-02
250	482	0.8106	1.669E-02
300	572	0.7106	1.463E-02
1093	2000	0.7106	1.463E-02
Padding and Carpeting			
Density (lb/in^3)			4.63E-03

Thermal Results for Assembly 2

For the floor assembly, the primary heat source, especially prior to any wood burning, were the furnace burners. Typically these furnace burners are controlled to follow the standard time-temperature curve based on measurements from 16 furnace thermocouples. Figure 28 shows the difference in heating rates between the averaged measurements of the 16 furnace thermocouples and the standard time-temperature curve. In this instance, similar to assembly 1, the furnace thermocouples show much lower temperatures than the standard time-temperature curve with a different characteristic heating rate. Again, the combustibility of the wood floor assembly adversely affected the thermocouple measurements making them ineffectual as a measure of the heat input for the floor thermal model. For this reason, following the same methodology as for assembly 1, the heat source was set to follow the standard time-temperature curve as a first estimate.

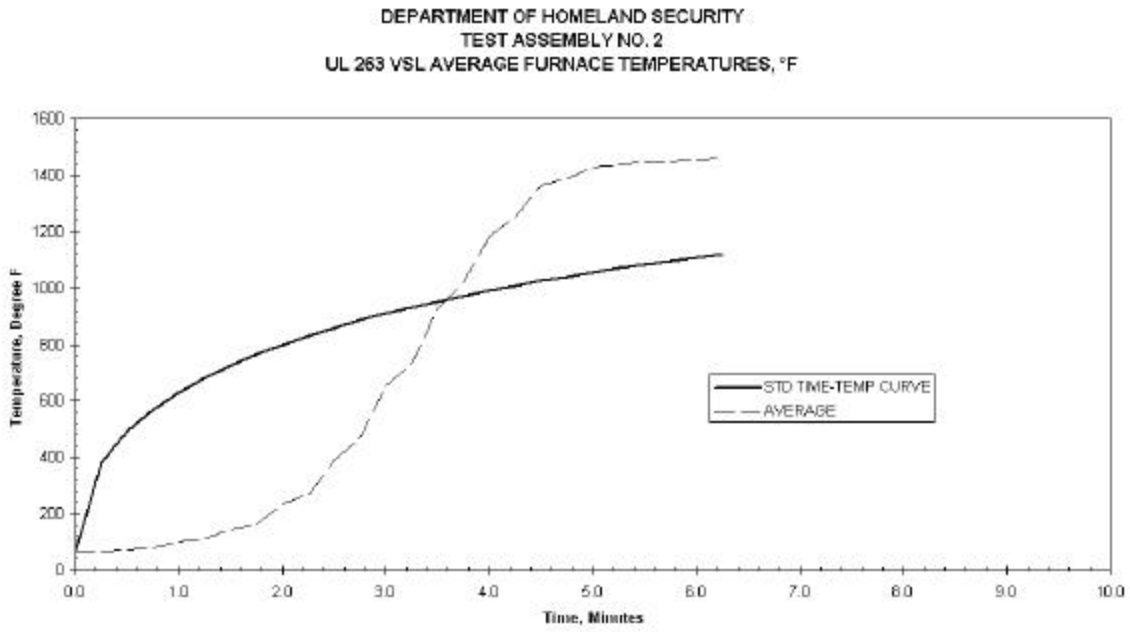

Figure 28 - Comparison of furnace thermocouple and standard time-temperature curve

Figure 29 compares the results from the thermal model (labeled 2a) with averaged thermocouple measurements from various points in the assembly. The data for assembly 2 is shown for only 6 minutes as compared to 18 minutes for assembly 1 since assembly 2 collapsed within 6 minutes. The temperatures on the underside of the floor were represented by the measurements at the bottom of the I-joist, side of the I-joist and bottom of sub-floor. All model temperatures are significantly below the thermocouple measurements and around 2 minutes, the thermocouple couple measurements from the underside of the floor assembly exceed that of the standard time-temperature curve. Since the thermal model could not predict temperatures higher than the heat source, this model needed further refinement to improve the agreement.

One shortcoming of the thermal model was the exclusion of the heat generation from wood burning. Test notes indicate that the portions of the floor charred within the first minute. Also the addition of heat generation to the thermal model would lead to higher temperatures bringing the results more in line with the test data. To incorporate the effect of wood burning, similar to assembly 1, an internal heat generation profile was assumed based on Figure 16. This heat profile was initiated within an element volume once it reaches an average temperature of 570 ^{0}F.

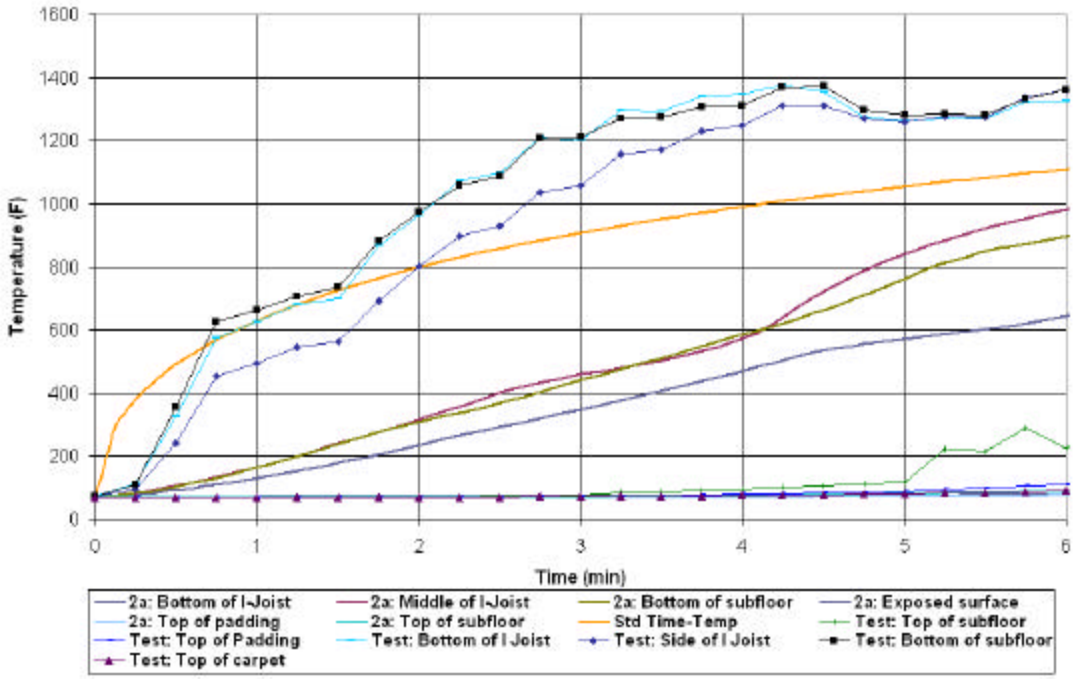

Figure 29 - Thermal results for model with standard time-temperature input

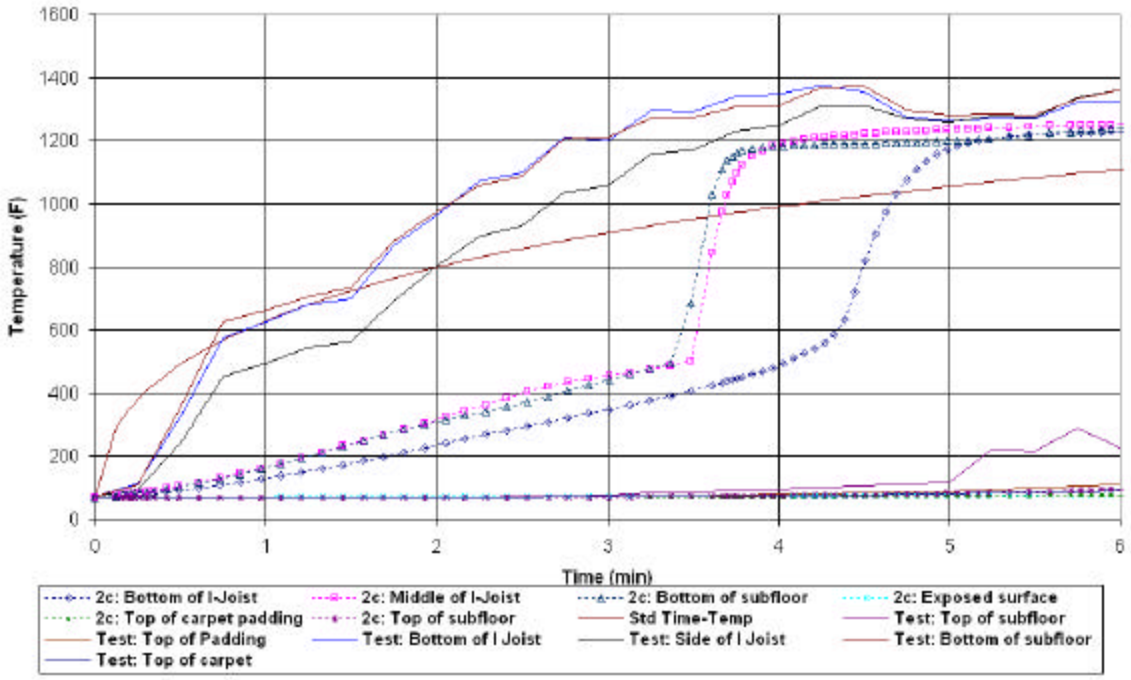

Figure 30 - Thermal results for model with heat generation and standard time-temperature input

Figure 30 show the thermal results (labeled 2c) with a heat source following the standard time-temperature curve and internal heat generation. In this case, the temperatures of the underside of the floor approach those of the test after about 3-1/2 minutes. The distinct rise in temperature for the thermal model is a direct consequence of the underside of the floor reaching 570 ^{0}F. However, the agreement in the early portion of the test is still unaffected by the inclusion of internal heat generation and suggests that the heating rate in the early stages may not be representative of the actual heating rate within the test.

A review of the test temperatures the top of the sub-floor shows a rapid increase after 5 minutes. This is likely driven by the changing heat transfer mechanism (flames and heat reaching via convection and radiation) as cracks and openings develop with the large deformations seen at this point in the test. Since these events were outside the physics of the current model, this temperature rise was not predicted.

Examining at the thermocouple measurements from the interstitial regions of the floor assembly as shown in Figure 18, much higher temperatures than either the standard time-temperature curve or the furnace thermocouples are seen. The high reading from these thermocouples was likely due to their proximity to the underside of the floor where the wood starts to burn and flames spread. It may be noted that temperatures for the interstitial thermocouples for assembly 2 are higher than assembly 1 starting from 30 seconds to about 2-1/2 minutes of test time. This suggests that assembly 2 was burning faster or generating more heat from wood burning than assembly 1.

Following the same sequence as for assembly 1, the predictions of the thermal model were generated with the heat source prescribed to follow the time-temperature data from the averaged interstitial thermocouple measurements. It was expected that these thermocouples included some of the effect of heat generation from wood burning. Internal heat generation in this thermal model was excluded.

Figure 31 shows the thermal results (labeled 2b) with heat source following the test data from the interstitial thermocouples. The gap between the test data and the thermal model temperatures was reduced in the first 2 minutes as compared to the previous two thermal models. However, the difference was still sufficiently large that it would translate adversely into the structural analysis.

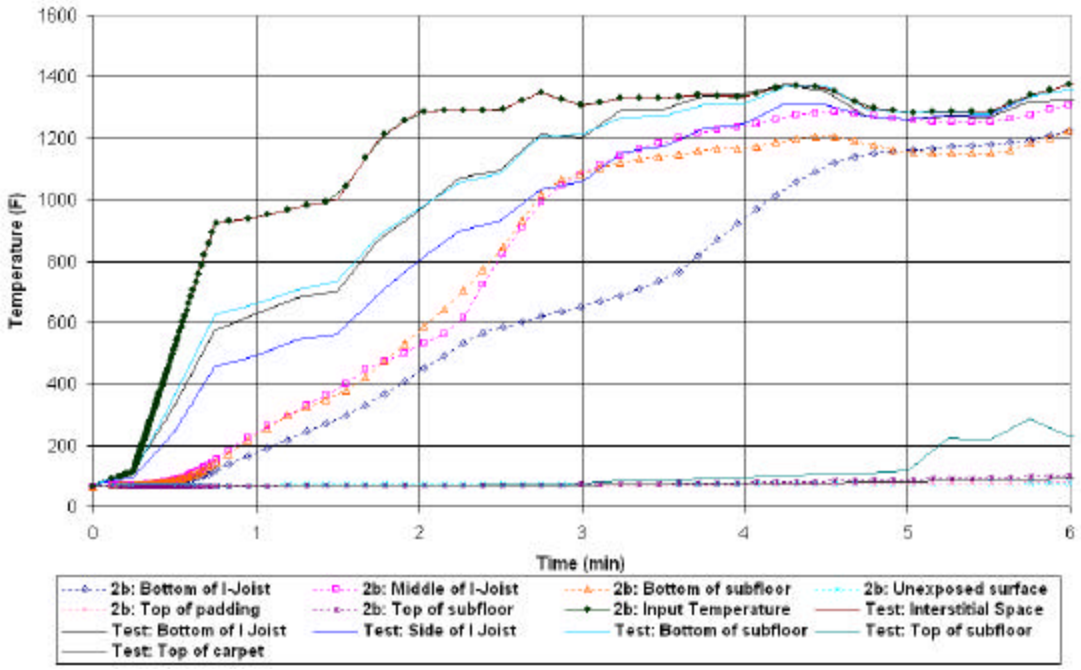

Figure 31 - Thermal results with heat input calculated based on temperatures of the interstitial thermocouples

Thus, following the analysis methodology for assembly 1, the temperatures of the underside of the floor assembly were set to follow the temperature data from the bottom of the sub-floor averaged thermocouple measurements. In addition, the elements for the I-joist were from changed from linear to second-order.

Figure 32 shows a comparison between the thermal results for the model (labeled 2f) where the entire underside of the model, except the boundaries that do not directly receive heat from the furnace, is set to the thermocouple measurements from the bottom of the sub-floor. As expected, the temperature rise in the early part of test was captured. However, as a consequence of the higher heating in the early stages as compared to the other cases, the top of the sub-floor experienced higher temperatures than seen during the test.

Figure 33 shows the temperature contours for the I-joist at approximately 3 minutes. The 3-sided heating of the top chord, almost 4-side heating of the bottom chord and the sharp gradient in the web are demonstrated. For this assembly, the burning rate has been calculated to be approximately 4 mm/min, which is much higher than the measured values of 0.6-0.8 mm/min.

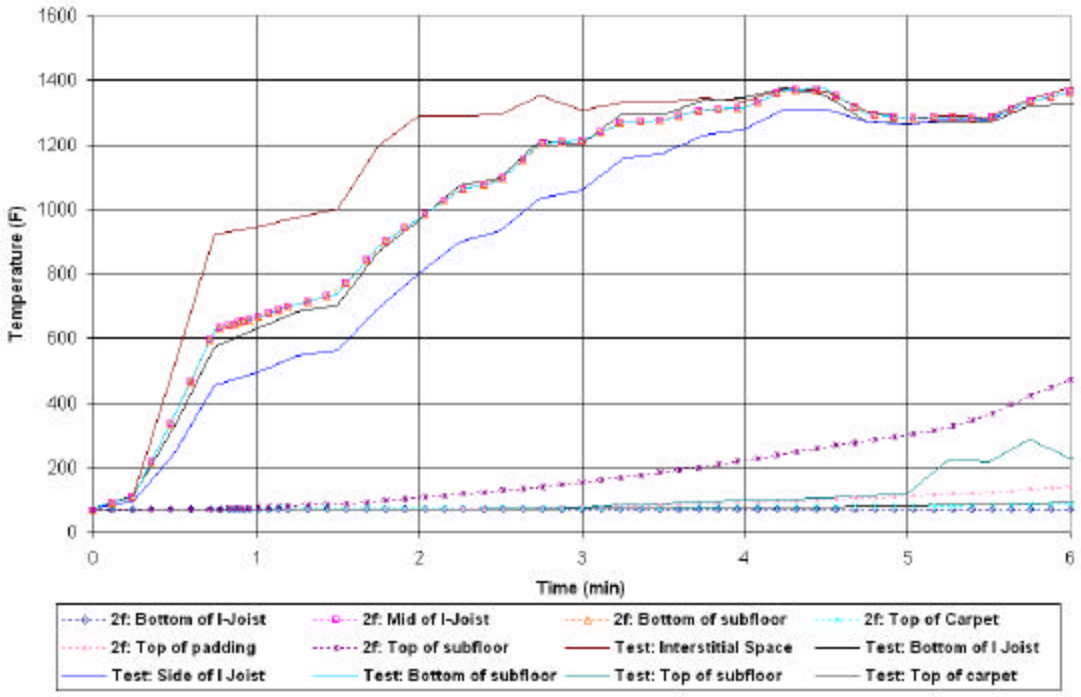

Figure 32 – Thermal results for model with prescribed underside floor assembly temperatures

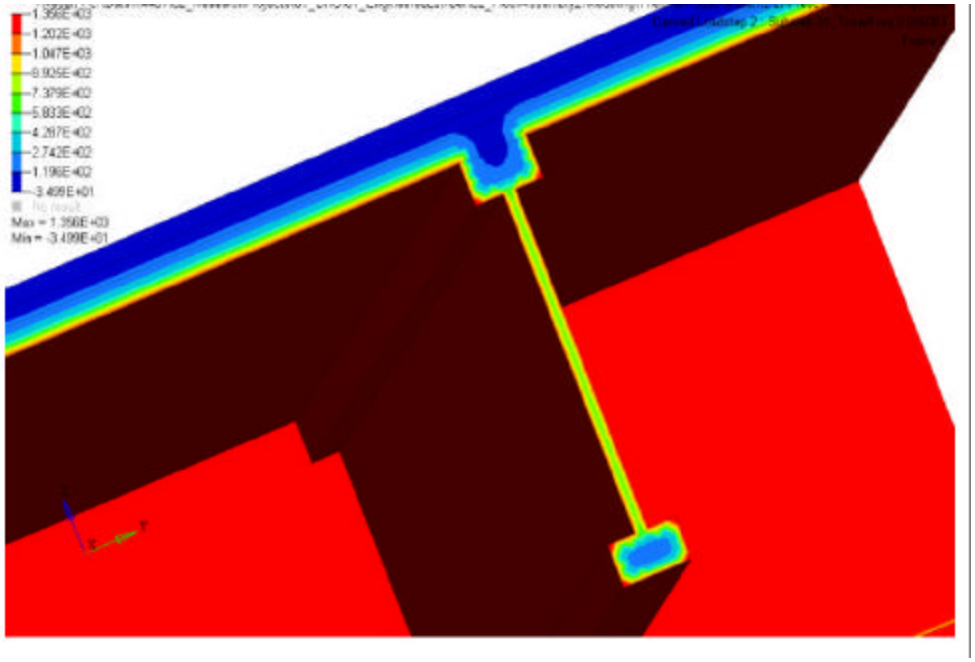

Figure 33 - Close up of temperature contours of I-joist for assembly 2 at 3 minutes

Structural FE Analysis

In addition the thermal loading, the floor assemblies supported 7 concrete blocks each providing 40 pounds per square feet (psf). The change in the loading pattern from the ASTM E119 standard was meant to simulate the more realistic non-uniform loading expected in the typical residence (See Appendix A). Two other loads weighing 300 lbs each were placed over the center of the floor representing the loading from two fire personnel carrying equipment (Figure 35). This loading configuration was detailed in the structural models for assemblies 1 and 2 as shown in Figure 34. In the test, all gravity loads were tethered by ropes to avoid damage to the furnace in event of floor collapse. The rope tether was arranged to allow for continuous contact of gravity loads for large deformations of the floors.

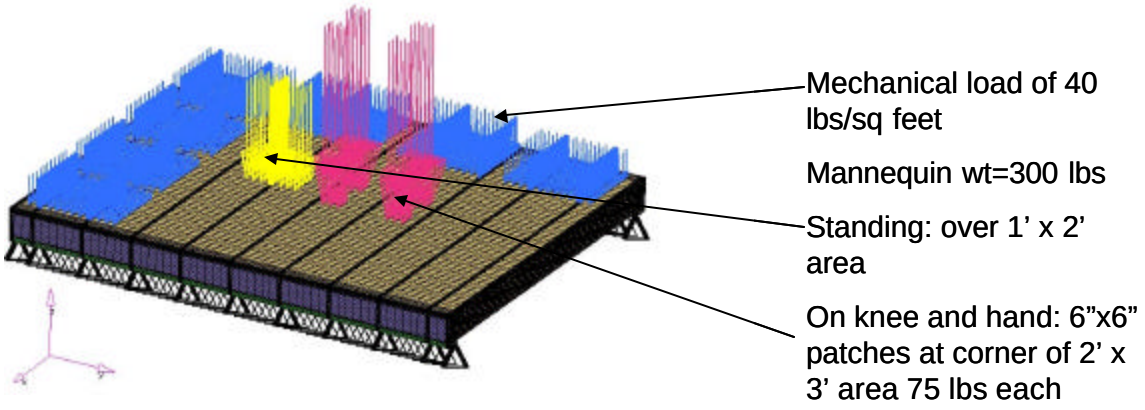

Figure 34 - Loading of structural model of assemblies 1 and 2

Besides the mechanical and thermal loadings, the structural assembly boundary conditions were defined to match closely with the test setup. In the test, two edges of the assembly, the edges not parallel to the joists, were placed upon steel angle brackets assuming no gap between the wall of the test frame and the edge of the floor assembly. The other two edges were assumed to be unconstrained. All components of the floor assembly were assumed to be in perfect contact. Details of the joining or piece-wise construction were ignored in this analysis.

One advantage of using a multi-physics platform such as ANSYS is the relative ease in transferring data from one analysis type to another. In this case, the finite element mesh for the thermal model and structural model were exactly the same. The nodal temperature data was transferred to the structural model as a load input.

Figure 35 - Picture from test showing floor loads

For the edges sitting on the angle bracket, the vertical deflection was set to zero along a line parallel to the edge at a distance of about 5 inches (Figure 36). To avoid in-plane rigid body motions and translations, the displacements of additional points of the floor were also constrained. The structural analysis had the same mesh density as the thermal analysis while using the SOLID45 element type. Since the material was assumed to be isotropic, homogeneous and elastic, the time history of deformations was not critical. The structural analysis was henceforth run as steady state for each time/temperature data set. The option for large deformations was also activated for all runs.

The key aspects of wood burning that must be captured in the structural analysis are the degradation of material properties and loss of cross-section due to charring. Two approaches exist to modeling the charring of wood. One approach as mentioned in the Survey of Research section is to assume a fixed charring rate or use the results from the thermal analysis directly to calculate the charring rate. The latter approach was taken in this analysis with the assumption that charring began at a temperature of 570 ^{0}F. When this temperature was reached in an element, an element kill option in ANSYS, which reduces the modulus to a value of 10^{-6} of original modulus, was activated. The structural analysis using the kill option did not converge. The solution did converge when using a modulus reduction factor of 10^{-3}.

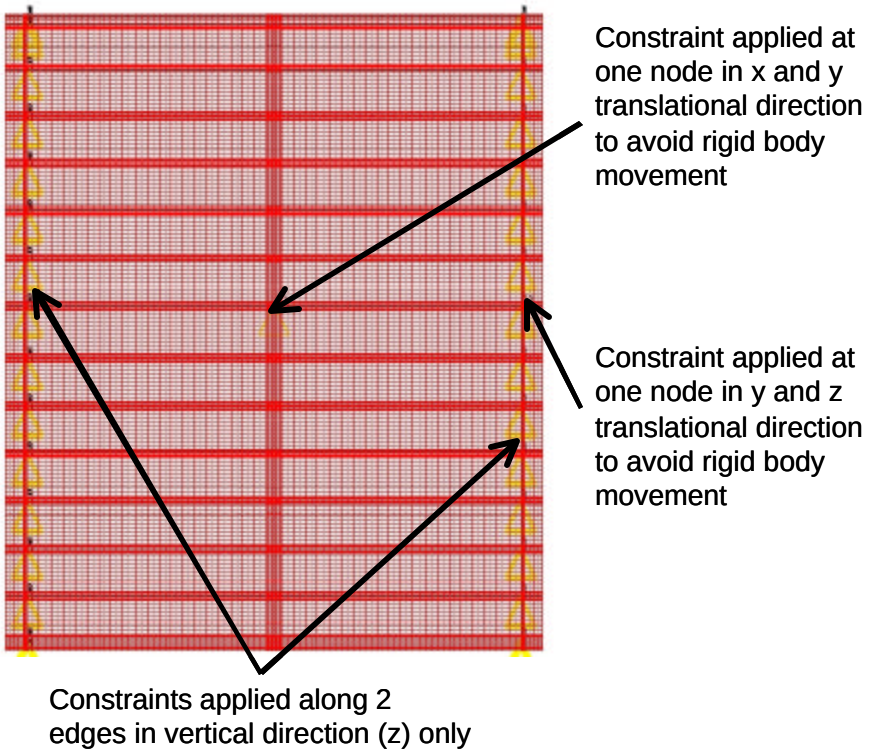

Figure 36 – Boundary conditions for structural model of floor assembly (x and y in the plane of the floor and z perpendicular to the plane of the floor)

Structural Model Details for Assembly 1

For assembly 1, the structural FE model geometry was exactly the same as the thermal model and is described in detail in Appendix A. The boundary conditions and mechanical loading were as described in the previous section. The other key input were the mechanical properties of the different components of the floor assembly as a function of temperature. These properties are listed in Table 10. The Poisson ratio was set to 0.2. The coefficient of thermal expansion was ignored for this analysis.

Structural Model Details for Assembly 2

For assembly 2, the structural FE model geometry was exactly the same as the thermal model and is detailed in Appendix A. The boundary conditions and mechanical loading were described in the previous section. The other key input is the mechanical properties of the different components of the floor assembly as a function of temperature. These properties are listed in Table 11. The Poisson ratio was set to 0.2. The coefficient of thermal expansion was ignored for this analysis. The elements for the I-joist were second order.

Table 10 - Mechanical properties for components in assembly 1

Conventional Lumber			
Modulus of Elasticity (MOE) Specimen A			
Temp C	**Temp F**	**MPa**	**PSI**
20	68	10552.44	1.530E+06
100	212	9707.40	1.408E+06
150	302	9179.25	1.331E+06
200	392	8651.10	1.255E+06
250	482	6834.26	9.912E+05
280	536	5566.70	8.073E+05
300	572	55.67	8.073E+03
1093	2000	55.67	8.073E+03
Plywood			
Modulus of Elasticity (MOE) Specimen C			
Temp C	**Temp F**	**MPa**	**PSI**
20	68	9990.00	1.449E+06
100	212	9190.00	1.333E+06
150	302	8690.00	1.260E+06
200	392	8190.00	1.188E+06
250	482	6470.00	9.383E+05
280	536	5270.00	7.643E+05
300	572	52.70	7.643E+03
1093	2000	52.70	7.643E+03

Table 11 - Mechanical properties for components in assembly 2

Joist Chord				
Modulus of elasticity Specimen B				17643
Temp C	**Temp F**	**MPa**	**PSI**	**Elasticity ratio**
20	68	17625.36	2.556E+06	0.999
100	212	16213.92	2.352E+06	0.919
150	302	15331.77	2.224E+06	0.869
200	392	14449.62	2.096E+06	0.819
250	482	11415.02	1.656E+06	0.647
280	536	9297.86	1.348E+06	0.527
300	572	92.98	1.348E+04	
1093	2000	92.98	1.348E+04	
OSB				
Modulus of Elasticity (MOE) MPa				5000
Temp C	**Temp F**	**MPa**	**PSI**	**Elasticity ratio**
20	68	4995.00	7.244E+05	0.999
100	212	4595.00	6.664E+05	0.919
150	302	4345.00	6.302E+05	0.869
200	392	4095.00	5.939E+05	0.819
250	482	3235.00	4.692E+05	0.647
280	536	2635.00	3.822E+05	0.527
300	572	26.35	3.822E+03	
1093	2000	26.35	3.822E+03	

Structural Results for Assemblies 1 and 2

Before presenting the results from the models, the deflection data from the 5 transducers placed on the top of the floor assemblies (Appendix A) are first reviewed.

Figure 37 shows that the downward (positive) deflections for assembly 1 increased gradually with transducer 3 having the highest reading until about 18 minutes into the test. At that point, the deflection rate changed dramatically indicating the onset of instability. For assembly 1, around 18:30 minutes, flaming through the floor near the mannequins were observed (Figure 39). By 18:45 minutes into the test, the mannequins did fall through the floor. By the end of the test, the floor had deflected over 15 inches.

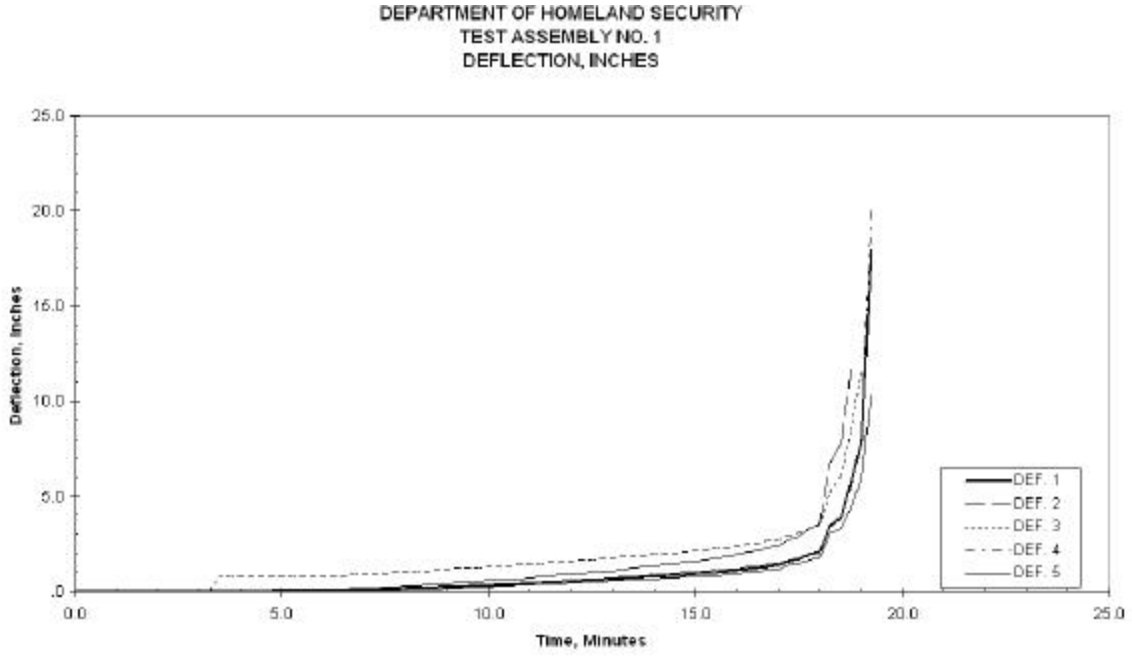

Figure 37 – Deflection test data for assembly 1

An examination of the data in the early stages of the test (Figure 38) shows that transducer 3 had a sudden jump of approximately 0.75 inches around 3 minutes.

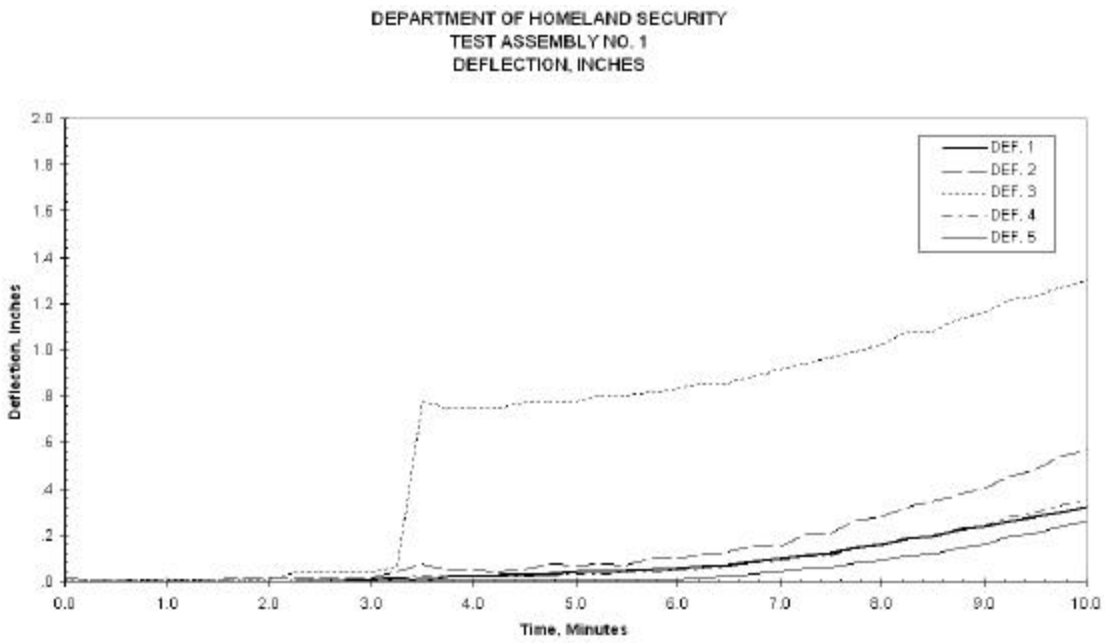

Figure 38 – Close up of deflection test data for assembly 1

Figure 39 – Picture of one instance where flaming through the floor is visible

For assembly 2, Figure 40 shows that the measured deflections developed more rapidly as compared to assembly 1. In addition, the deflection rate changed at several points in the test (Figure 41). Test observations (Table 12) had noted cracking noises, flames from top of assembly and eventual collapse by 6 minutes after start of test.

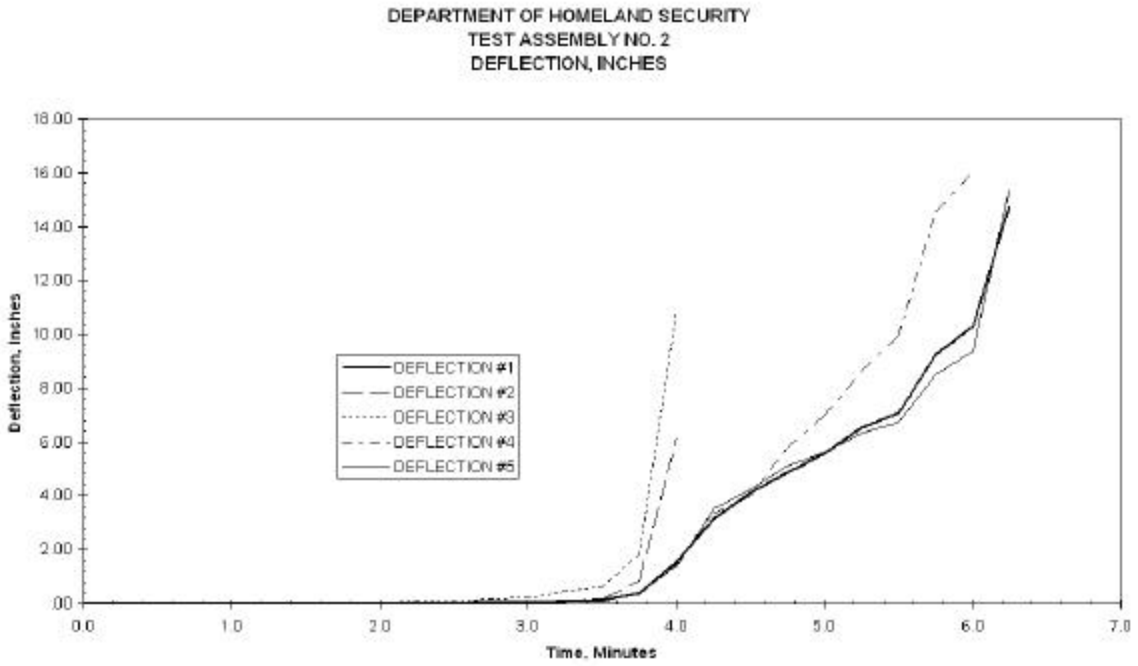

Figure 40 - Deflection test data for assembly 2

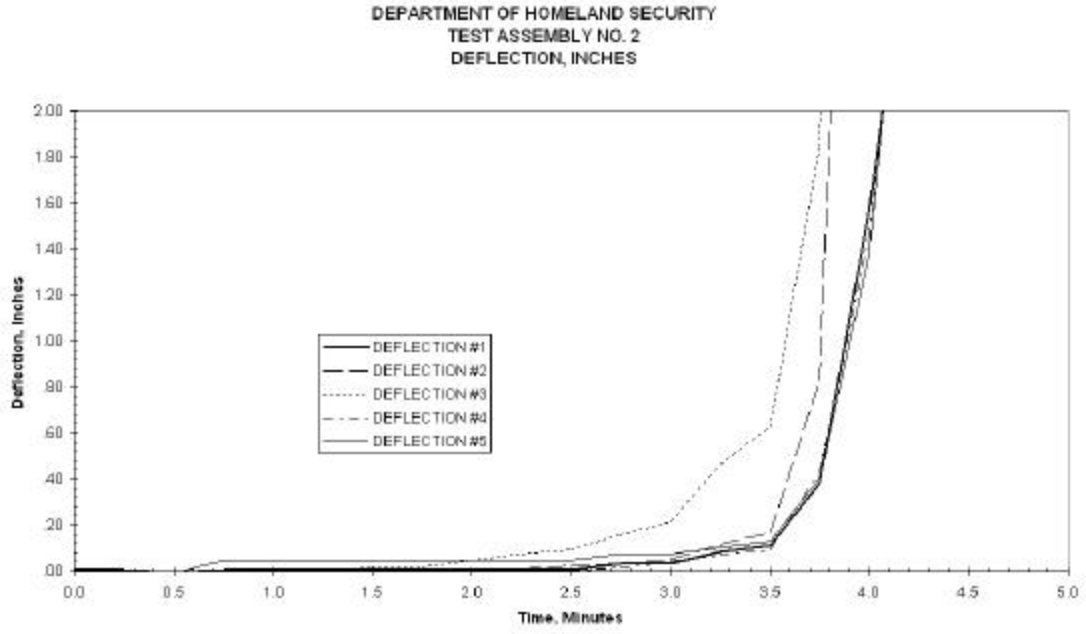

Figure 41 - Close-up of deflection test data for assembly 2

Table 12 - Observations from test for assembly 2

Test Time, Min:Sec	Exposed (E) or Unexposed (U) Surface	Observations
0:55	E	Wood members began to char.
1:00	U	No change.
1:25	E	All wood ignited.
2:00	E	All member completely engulfed in flames.
2:00	U	Smoke emitting from perimeter and smoke emitted from long plywood joints.
2:30	E	*Vibrations could be felt and the furnace was sucking air from below.*
2:35	U	*Floor vibrating up and down.*
3:15	U	*Vibration continued.*
3:30	E	*Sucking of air continued.*
4:00	U	*Vibration continued and noticeable deflection about 6 inches.*
4:30	U	*Vibration stopped.*
5:00	U	*Crackling could be heard and deflection about 1-1.5 ft.*
6:00	U	*Flame through at South West corner of assembly.*
6:03	U	*Gas off.*
6:03	E	*Floor collapsed. Gas off.*

The largest deflections at the transducer locations for the floor assemblies from the loading by the concrete blocks and mannequins at room temperature are shown in Table 13 for the test and the model. It was observed that for both floors, the model underestimated the static deflection. The models of the floors are stiffer than the test assemblies. Furthermore, it appears that the model for floor assembly 2 is stiffer than the model for assembly 1 whereas according to the test measurements floor assembly 1 is stiffer than assembly 2.

Table 13 - Initial deflection due to static loads before start of test

Test Assembly Number	Model Deflection (Inch)	Test Deflection (Inch)
1	0.06	0.13
2	0.04	0.25

Figure 42 shows the downward vertical deflections from the model for locations similar to the transducer locations from the test. For these results, the modulus of the material beyond 570^{0}F was set to a value of 0.1% of the value of the MOE at 530^{0}F to capture the cross section reduction due to charring. The model predicted that after 3 minutes the structure experienced a rather sudden increase in deflections. This jump is driven by the rapid change in modulus of the supports as a result of the abrupt

increase in heating rate of the support as seen in Figure 22. From the test data, only transducer 3 displayed a jump, though much smaller.

One source of error might be the insufficiency of the mesh for strict convergence. The modulus for the charred sections must be as close to zero as possible. For the model of assembly 1, it was not possible to obtain convergence in a reasonable time when the MOE was reduced to 0.001% of the MOE at 530^0F. The jump in the readings from transducer 3 during the test might suggest that a localized failure occurred in the floor though it is difficult to draw any conclusive remarks regarding the coincidence of the jump in the model data at the same point in time. Also, the accuracy of the predicted temperatures and heating rate from the thermal model will affect the accuracy of the structural results. In the model all supports heat up uniformly and lose stiffness uniformly[14]. However, in the test, it is likely that the heating and weakening of the supports was more non-uniform.

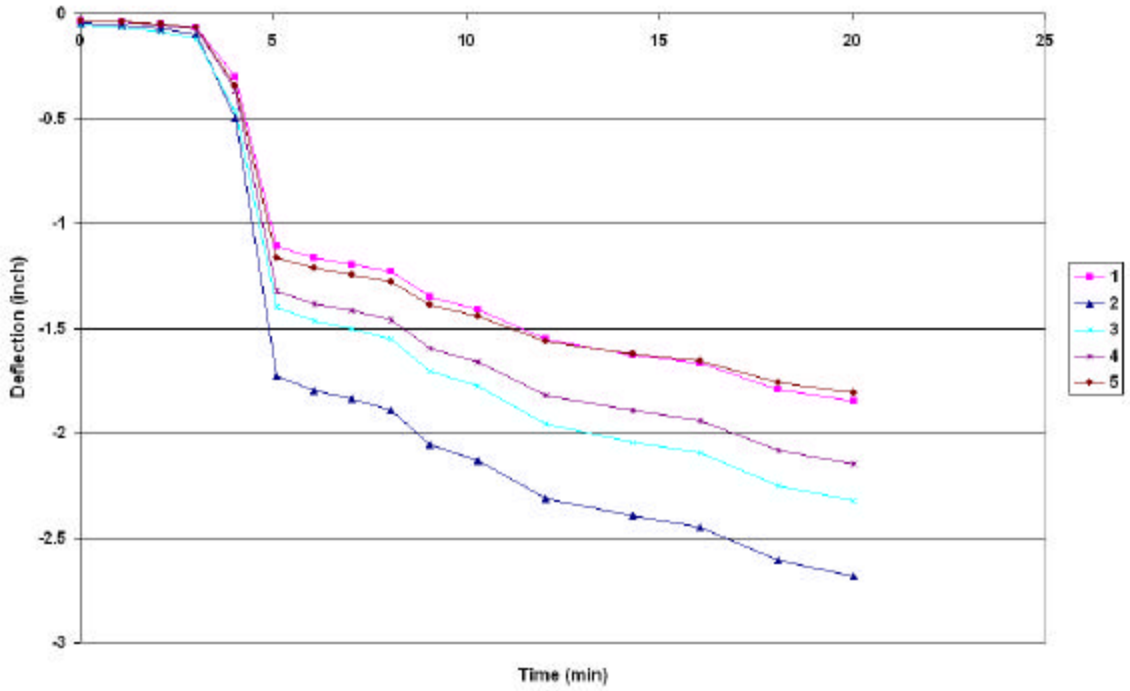

Figure 42- Structural model results for assembly 1

Figure 43 shows a comparison of the deflections for transducer 3. It was anticipated that there would be differences in the results from the model as compared to the test due to joining failures or wood cracking not accounted for in the model. These structural features may account for the significant change in the deflection rate slope

[14] Also the sudden increase may be a consequence of the low mesh density through the thickness of the support.

observed during the test. The jump seen in the data around 3-4 minutes in the test is likely due to some localized event. Now this transducer resides over a support beam so it is not clear whether this single beam might have been the first to burn through leading to the sudden loss of stiffness. The jump may also be due to settling or floor cracking near the transducer. However, in the model, the same jump is seen in all transducers indicating a global loss of stiffness. Recall that for the model, all the support beams heat uniformly and lose stiffness uniformly.

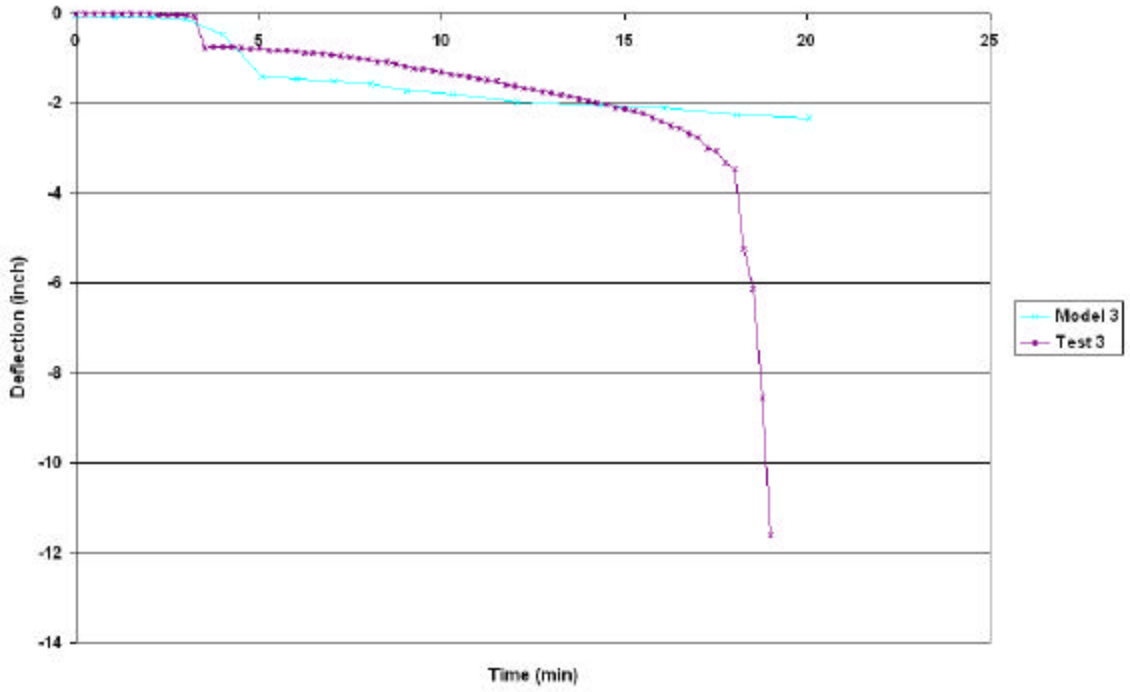

Figure 43 - Comparison of test and model deflections for transducer 3 for assembly 1

Figure 44 shows the downward (positive) deflections of structural model for assembly 2 at the same locations as the test transducers. For these results, the modulus of the material beyond 570 ^{0}F was set to a value of 0.1% of the value of the MOE at 530 ^{0}F to capture the material weakening due to charring. In this case, similar to assembly 1, a sudden jump in the downward deflections is seen. This jump occurs at an earlier time in the test as compared to assembly 1. The main reason for the sudden change in the deflections is tied to sudden heating rate and the subsequent material property degradation around 2:30 minutes into the test[15].

Figure 45 shows a comparison for transducer deflection measurements and the model results at the same location. For the test, the increase in deflection was gradual until

[15] Also the sudden increase may be a consequence of the low mesh density through the thickness of the support.

about 4 minutes when there was a steep rise in the deflection rate. For the model, there was only a sudden increase in the deflections around 2.5 minutes into the test followed by a monotonic increase in downward deflections.

The same errors sources are applicable to model for assembly 2 and so were not repeated here except for one. It was found that the deflections predicted by the model for assembly 2 were sensitive to the choice of the charred modulus than for assembly 1. This is likely due to the fact that a very thin web connects the upper and lower chords. Even with the very reduced modulus of the web, the lower chord is likely to still contribute to the load bearing capacity of the assembly. Post-test observations of the furnace floor found entire sections of the lower chord residing on the bottom. This suggests that the results for this model may still change with further reductions in the charred modulus.

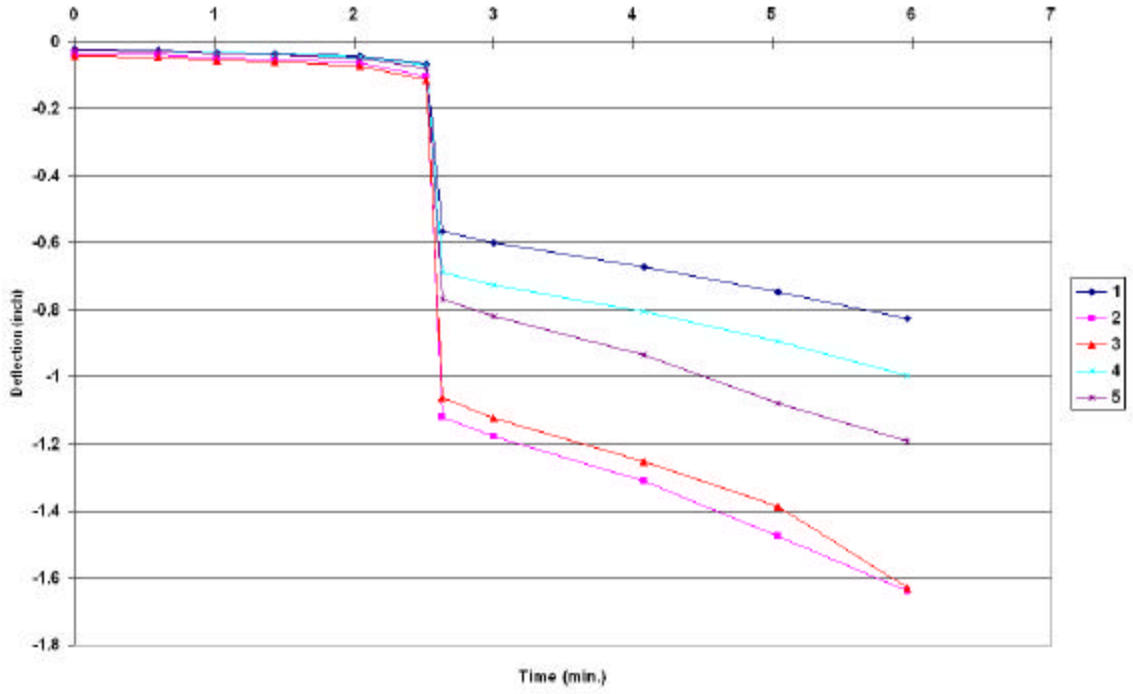

Figure 44 – Structural model results for assembly 2

The comparison of the model results for the two assemblies, as shown in Figure 46, shows that assembly 2 would exhibit the sharp deflection increase sooner with a steeper slope as compared to assembly 1. The steeper slope implies that assembly 2 loses stiffness at a faster rate than assembly 1 during heating. This might suggest that assembly 2 is weaker than assembly 1 but it is difficult at this point to assign confidence levels to the absolute deflections values. Note that the FE models for

assemblies 1 and 2 predict that the greatest deflection occurs at transducer 2 located between the two mannequins.

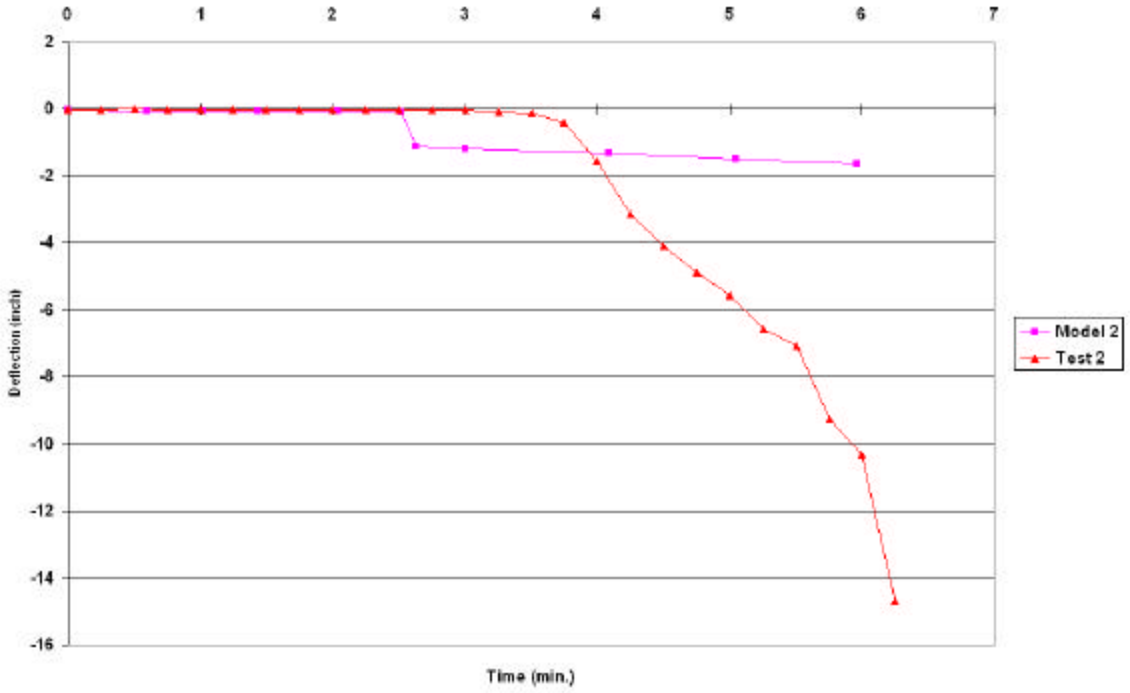

Figure 45 - Comparison of test and model deflections for transducer 2 for assembly 2

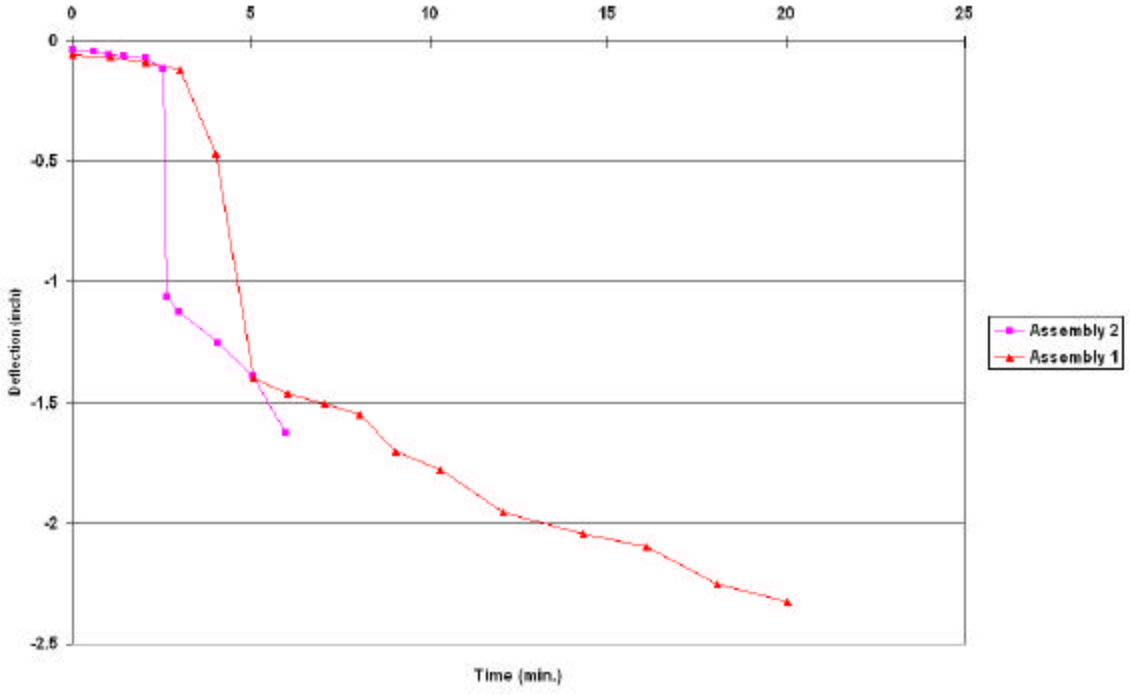

Figure 46 - Comparison of the model results for both assemblies at transducer 3

Figure 47 and Figure 48 display the deflection contours superimposed on the magnified deflected models for assembly 1 and 2. For assembly 1 only the support and edge beams are shown. For assembly 2, the entire floor assembly is displayed. The deflections for assembly 1 changed more gradually for adjacent beams giving an eccentric peak deflection due to the asymmetry of the mechanical loads. For assembly 2, there is a more abrupt difference in deflection contours between adjacent beams.

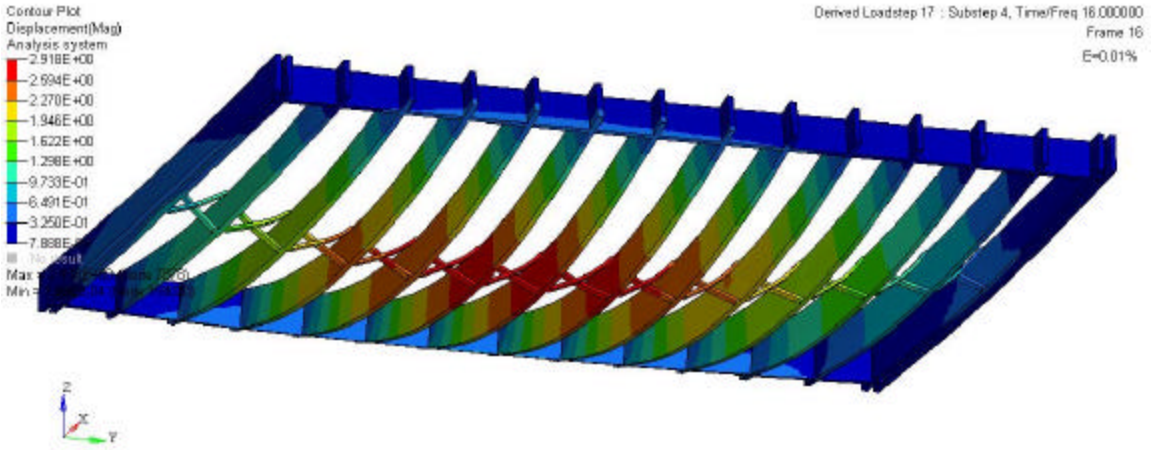

Figure 47 - Deflection contours of assembly 1 model at 20 minutes

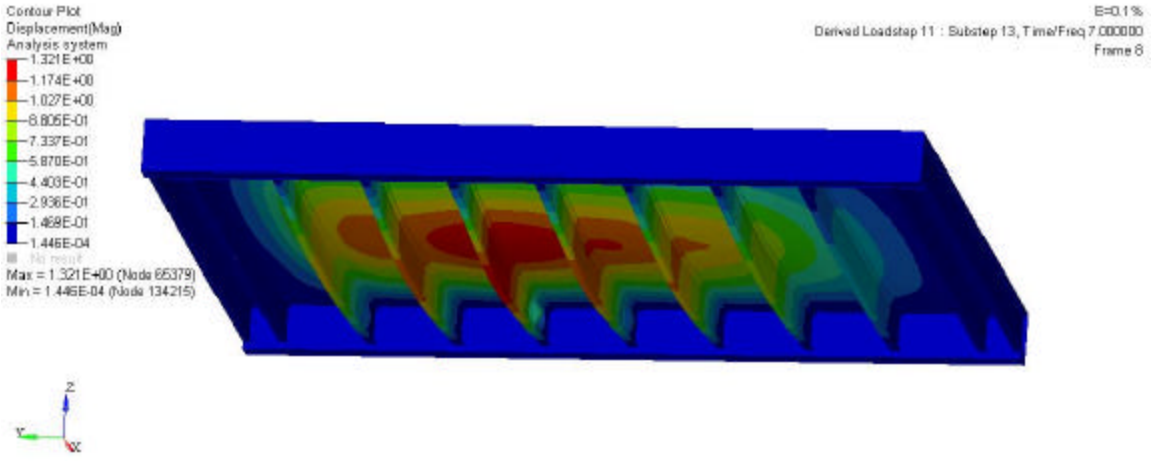

Figure 48- Deflection contours of assembly 2 model at 3 minutes

SUMMARY OF FINDINGS AND RECOMMENDATIONS

Physics-based simulations can provide remarkable insight into complex physical phenomena. The response of structures in fires qualifies as a complex system. The multitude of mechanisms that generate and transfer heat, degrade and decompose materials, weaken and destabilize components and connections requires a great deal of upfront work to validate structural fire models. Despite the tremendous strides in computational power and numerical techniques, models must be developed with assumptions that allow for tractable and reasonable run times and results. The growth of modeling will not replace testing but instead will require tests designed and carried out with validation of models in mind.

In this report, task of building and evaluating FE models of wood-based floor assemblies was described in detail. This section delineates the challenges encountered in this research and discusses potential next steps in furthering the capabilities of computational engineering tools to predict the fire performance of structures. These steps cover not only the computational challenges but also the type of test data that are available as inputs to models and as a database for model validation. It is very important to continue to evaluate and improve the capabilities of computational modeling. The progress of fire safety engineering will be strongly shaped by these tools.

Thermal Modeling

In predicting the mechanical performance of buildings subjected to fires, the prerequisite is the knowledge of the temperature distribution throughout the structure. The thermal models show great potential in predicting the thermal response of combustible structures to fires as the following areas are addressed:

- Heat source: The temperatures throughout the structure depend upon the heat source. In this case, the furnace burners provided the initial heat source prior to combustion of wood. In the furnace, thermocouples were placed to provide such a measure as is common for standard fire tests described by ASTM E119. However, as seen in Figure 28, the furnace thermocouples did not provide an accurate representation of the heat generated by the furnace burners. It is likely that the measurements of temperature by these thermocouples were affected by the smoke and soot generated by wood combustion early in the test. Tests regularly carried out on composite concrete/steel floors, which are not combustible, do not present this issue. Even floors that have some protection lead to improvements in the furnace

thermocouples matching the standard time-temperature curve as seen in Figure 49 (Assembly 4 as described in Table 1).

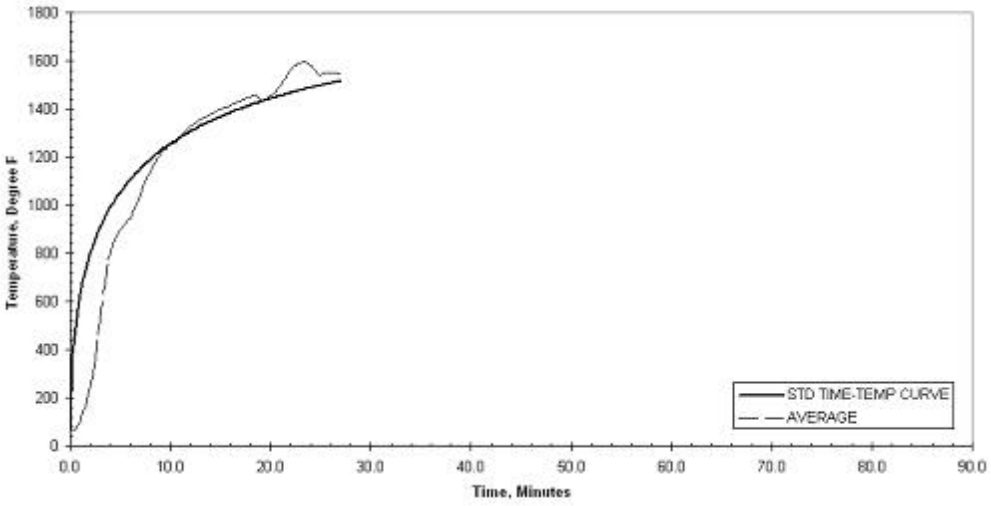

Figure 49 - Furnace thermocouple measurements from a floor assembly with gypsum protection

- Heat generation: Even with an accurate measure of the thermal flux reaching the underside of the floor assemblies, an additional source of heat exists for wood floors in high temperature environments and that is the burning of wood. At temperatures approaching 570 ^{0}F (300 ^{0}C), the combustion of wood leads to an exothermic process. The thermal results showed the noteworthy improvement that a very simple heat generation model provides and that further fine-tuning will certainly lead to better results.

- Thermal properties: For wood there are many challenges related to thermal properties such as

    1. The wide temperature range over which properties must be measured
    2. The decomposition and degradation of materials due to the high temperatures seen in fires such as charring
    3. The measure of 'effective' properties that account for multi-mode heat transfer and moisture diffusion within the wood
    4. The anisotropic, heterogeneous and porous nature of wood

A measure of the properties of charred wood is very critical as it is expected to provide an insulative effect on heat flux. For both thermal models, when the temperature of the underside was prescribed, the calculated burning rate was

much higher than that measured on test samples. This was likely due to the inaccuracy in the charring properties. All these items suggest that testing methodologies for wood samples must be well defined and documented and that as many samples as possible must be tested. Also one advantage of not prescribing the charring rate in the thermal models is that the charring parameter now provides another means of assessing the thermal model output.

- Finite Element Meshing: Finite element methods rely on discretization of a continuous model to achieve a large set of algebraic equations that can be solved numerically. It is known that that quality of the mesh and the mesh density can affect the solution convergence. Generally, in areas where a response parameter shows a large degree of variability, a very fine mesh is required. The drawback of any increase in the number and density of the elements within a model is the increase in run times. In this study, due to project limitations, this exercise was not conducted. It is a critical component of any follow up work.

- Radiation: In the thermal models, the only source of radiation was the heat source representing the furnace burners. However, in the actual assembly, it is likely that as the underside of the floor was burning, generating a great deal of heat, some of that heat would radiate to nearby surfaces. This effect should be considered in future models.

- Instrumentation: For these floor assemblies, it was difficult to validate the models with the available measurements at the underside of the floor and the top of the floor. The exposed side of the floor did not heat up much during these tests except for when the floor was approaching failure. It was difficult to assess the accuracy of the model and its inputs such as material properties. In fire tests of complex structures, measurements throughout a component (and any connections), especially along the thickness would provide much needed additional points in assessing the performance of the thermal models. The challenges with measuring the furnace burner output must also be addressed as noted in the heat source discussion.

- Design of 'Targeted' Tests: To help the progress on validating and applying computational modeling tools to structures in fires, quite often tests need to be designed with this consideration in mind. Fire standard tests, which are carried out regularly, can provide a wealth of data with some relatively simple modifications. These changes mainly involve additional instrumentation during the construction of the test specimen.

Structural Modeling

Once a thermal model is validated, its results can be transferred to the structural model. Since the software selected for this analysis was ANSYS multi-physics FE program, the issues associated with data transfer from one analysis to another was well established. This may not be the case in other instances where different programs are involved. In addition, the issues related to the relative mesh density of one analysis versus another analysis must be considered. For structural analysis, the prediction of failure, where components break after weakening due to high temperatures and charring is very challenging. The actual failure mode will vary depending upon the construction, connections, heat loading and location, etc.

For this investigation, the structural response of two unprotected wood floor assemblies was modeled. Both failed dramatically in short times displaying very severe deflections prior to failure. Test photos and videos captured the appearance of flames through the floors prior to the collapse. The models were developed with assumptions that limited the scope of applicability to the early stages of the test much before the final collapse of the structure. It is recommended that further research work focus on the following areas to improve the predictions of computational modeling tools:

- Mechanical properties: The challenges listed for the thermal properties are applicable to the mechanical properties. More measurements are needed on the mechanical properties to develop a better understanding of the anisotropic, heterogeneous, and porous nature of wood. Furthermore, constitutive relations that capture plasticity and creep may be necessary depending upon the application. As these models for the fire growth stage develop, fire safety concerns will extend beyond the heating period of structures and will focus on assessing the stability of structures during the cooling period. Material properties that are measured based on such cycling will be necessary.

- Charring Rate: The main effect of charring on wood structures is the reduction in cross section available to carry the load. One approach to assessing the structural performance in fire is to assume a charring rate once the surface of the wood is ignited. In this study, the option to determine the temperature distribution was followed in an attempt to account for the varying properties of char, and then establish a temperature criterion to reduce the modulus of an element that exceeds this temperature to extremely small values. However, convergence difficulties were encountered with values of modulus reduced beyond 0.01% of the pre-char modulus. To lower

the modulus further it is likely that the mesh density must be increased. As mentioned in the summary for the thermal results, it is important to conduct a sensitivity analysis for the mesh density.

- Construction details: For wood, the joining methods such as adhesives, tongue and groove connections, etc. will eventually affect the structural performance of the wood components as the deflections grow. Small-scale tests that focus on characterizing the properties of wood connections are critical.

- Coefficient of Thermal Expansion: Shrinkage in wood especially at temperatures higher than 200 ^{0}F is important as free water evaporates. The thermal expansion of wood is much higher than concrete or steel and its influence on the structural response should be examined.

- Design of 'Targeted' Tests: To help the progress on validating and applying computational modeling tools to structures in fires, quite often tests need to be designed with this consideration in mind. Fire standard tests, which are carried out regularly, can provide a wealth of data with some relatively simple modifications. These changes mainly involve the addition of instrumentation during the construction of the test specimen.

- Instrumentation: For these floor assemblies, it was difficult to validate the models with the relatively few measurements provided on the top of the floor. Transducers that can measure acceleration, strain and deflection measurements are recommended. The number and placement of transducers will depend upon the test configuration.

- Post-Failure Analyses: For the structural failures such as these it is important to document the failure site as much as possible in order to gain insight into the possible mode of failure. In structural analyses, some idea of the anticipated failure is necessary to ensure that the proper physics are part of the model.

Floor Assembly 1 vs. 2

The main goal of the overall project was to assess the stability of building components, specifically floors, in a fire environment comparing legacy materials with engineered wood products. The prevalence of engineered wood lumber has led to concerns regarding the safety of occupants and fire personnel. The relatively high stiffness to weight ratio provides opportunities for using lightweight constructions

and thinner sectional dimensions. For the modeling portion of the project, two unprotected floor assemblies, one supported with standard timber and the other supported by engineered lumber were the focus of this study. The tests conducted in the first part of the project and in another recent study [54] show the relatively quick instability that can be seen in unprotected engineered lumber floors. These unprotected engineered lumber floors represent the type of construction present in basement of houses.

In this study, the FE models were not strictly validated against test data and so it is necessary to be cautious in drawing conclusions from the data in assessing the fire performance of the floor assemblies. The main issue was that the I-joist web for floor assembly 2 was only 3/8 inch. This very thin cross section is expected to burn through quickly.

Since the structural models still require further refinement to achieve acceptable agreement with the test data, quantitative assessments cannot be formed. Instead, the assessment is limited to a comparison of the qualitative features of the deflections over time as shown in Figure 46. An examination of the slope of the deflection-time curve subsequent to the initial drop reveals that the effective stiffness of assembly 2 degraded at a much faster rate than assembly 1. It is anticipated that this trend will hold even after the improvements cited above.

Once some of the issues with meshing and properties of char are resolved, sensitivity studies using the model can be carried out with confidence - using the same heat source – to assess the effect of various types of loads, dimensional and geometric changes.

REFERENCES

[1] Drysdale, D., *An Introduction to Fire Dynamics*, Wiley & Sons, 2005.

[2] Gronli, M. and Melaaen, M., Mathematical Model for Wood Pyrolysis – Comparison of Experimental Measurements with Model Predictions, *Energy & Fuels*, No. 14, 2000, pp. 791-800.

[3] Winady, J. and Rowell, R., Chapter 11: Chemistry of Wood Strength, in *Handbook of Wood Chemistry and Wood Composites*, CRC Press LLC, 2005.

[4] Babrauskas, V., Ignition of Wood: A Review of State of the Art, in *Interflam 2001*, Interscience Communications Ltd., 2001.

[5] Moghtaderi, B., The state-of-the-art in pyrolysis modeling of lignocellulosic fuels, *Fire and Materials*, 30, 2006, pp. 1-34.

[6] Janssens, M., Modeling of the thermal degradation of structural wood members exposed to fire, *Fire and Materials*, 28, 2004, pp. 199-207.

[7] Babrauskas, V., Charring rate of wood as a tool for fire investigations, *Fire Safety Journal*, 40, 2005, pp. 528-554.

[8] Friquin, K.L., A Review of Models for Calculation of the Charring Rate of Solid Wood Structural Elements and Glue-Laminated Beams/Columns, in *Proceedings of the Fifth International Conference on Structures in Fires*, 2008.

[9] White, R., *Charring Rates of Different Wood Species*, Ph.D. Thesis, University of Wisconsin, 1988.

[10] Eriksson, J., et al., Finite-Element Analysis of Coupled Nonlinear Heat and Moisture Transfer in Wood, *Numerical Heat Transfer, Part A*, 50, 2006, pp. 851-864.

[11] Hunt, J.F., and Gu, H., Finite Element Analysis of Two Dimensional, Anistropic Heat Transfer in Wood, *Proceedings of International ANSYS Conference*, 2004.

[12] Park, W.C., *A Study of Pyrolysis of Charring Materials and its Application to Fire Safety and Biomass Utilization*, Ph.D. dissertation, University of Michigan, 2008.

[13] Yuen, R., et al., The Influence of Moisture on the Combustion of Wood, *Numerical Heat Transfer, Part A*, 2000, pp. 257-280.

[14] Adl-Zarrabi, B., et al, Using the TPS method for determining the thermal properties of concrete and wood at elevated temperatures, *Fire and Materials*, 20, 2006, pp. 359-369.

[15] Thunman, H., and Leckner, B., Thermal conductivity of wood – models for different stages of combustion, *Biomass & Bioenergy*, 23, 2002, pp. 47-54.

[16] Konig, J., Effective thermal actions and thermal properties of timber members in natural fires, Fire and Materials, 30, 2006, pp. 51-63.

[17] Viskanta, R. and Menguc, M., Radiation Heat Transfer in Combustion Systems, *Progress in Energy Combustion Science*, 13, 1987, pp. 97-160.

[18] Ghojel, J.I., A new approach to modeling heat transfer in compartment fires, *Fire Safety Journal*, 31, 1998, pp. 227-237.

[19] Clancy, P., Probability of Failure with Time for Wood Framed Walls in Real Fire, *Journal of Fire Protection Engineering*, 12, 2002, pp. 197-223.

[20] TenWolde, A. et al, Thermal Properties of Wood and Wood Panel Products for Use in Buildings, ORNL/sub/87-21697/1, Oak Ridge National Laboratory Report, 1988.

[21] ASTM E1355, Standard Guide for Evaluating the Predictive Capability of Deterministic Fire Models, ASTM Subcommittee E05.33, 2005.

[22] Sultan, M., and Kodur, V., The Effects of Subfloor and Insulation Type and Thickness on the Fire Resistance of Small-scale Floor assemblies, *Fire and Materials*, 24, 2000, pp. 131-141.

[23] Richardson, L., Thoughts and Observations on Fire-endurance Tests of Wood-frame Assemblies Protected by Gypsum Board, *Fire and Materials*, 25, 2001, pp. 223-239.

[24] Park, JS, and Lee JJ, Fire Resistance of Light-framed Wood Floors Exposed to Real and Standard Fire, *Journal of Fire Sciences*, 22, 2004, pp. 449-471.

[25] Benichou, N., and Sultan, M., Fire Resistance Performance of Lightweight Wood-Framed Assemblies, *Fire Technology*, 36, 2000, pp. 184-219.

[26] ASTM E119, Standard Test Methods for Fire Tests of Building Construction and Materials, ASTM Subcommittee E05.11, 2008.

[27] Tabaddor, M., et al, Thermo-mechanical Analysis of Fire Doors Subjected to a Fire Endurance Test, *Journal of Fire Protection Engineering*, 19, 2009, *to be published*.

[28] Kodur, V.K.R., Harmathy, T.Z., "Properties of Building materials", (in press) *SFPE Handbook of Fire Protection Engineering*, 4th edition, P.J.DiNenno, National Fire Protection Association, 2008, pp. 42.

[29] Benichou, N. and Sultan M., "Fire resistance of lightweight wood-framed assemblies: State of the art report," M.A. IRC-IR-776, NRCC Canada, 1999.

[30] Lie, T.T., (Editor), *Structural Fire Protection*, American Society of Civil Engineers, Manuals and Reports on Engineering Practice No.78, 1992.

[31] Eurocode 5, Design of Timber Structures, Part 1-2: General –Structural fire design, European committee for standardization (CEN), Brussels, Belgium, 1995.

[32] Tabiei, A. and Wu, J., Three-dimensional nonlinear orthotropic finite element material model for wood, *Composite Structures*, 50, 2000, pp. 143-149.

[33] Smith, I, et al, Failure Mechanism in wood-based materials: A review of discrete, continuum, and hybrid finite-element representations, *Holzforschung*, 61, 2007, pp. 352-359.

[34] Vasic, S. et al, Finite element techniques and models for wood fracture mechanics, *Wood Science Technology*, 39, 2005, pp. 3-17.

[35] Jauslin, C. et al, Finite-Element Analysis of Wood Joints, *Journal of Materials in Civil Engineering*, 7, 1995, pp. 50-58.

[36] Guan, Z.W., and, Zhu, E.C., Nonlinear Finite Element Modeling of Crack Behavior in Oriented Strand Board Webbed Wood I-Beams with Openings, *Journal of Structural Engineering*, 130, 2004, pp. 1562-1569.

[37] Mirianon, F., et al, A method to model wood by using ABAQUS finite element software, Part 1. Constitutive model and computation details, VTT Technical Research Centre of Finland, VTT Publications 687, 2008.

[38] Serrano, E. and Enquist, B., Contact-free measurement and non-linear finite element analyses of strain distribution along wood adhesive bonds, *Holzforschung*, 59, 2005, pp. 641-646.

[38] Clancy, P., and Jong, F., The Influence of Creep on the Failure of Wood-framed Walls in Fire, *Journal of Fire Protection Engineering*, 13, 2003, pp. 221-250.

[39] Young, S. and Clancy, P., Compression Mechanical Properties of Wood at Temperatures Simulating Fire Conditions, *Fire and Materials*, 25, 2001, pp. 83-93.

[40] Fredlund, B., A Model for Heat and Mass Transfer in Timber Structures During Fire, A Theoretical, Numerical and Experimental Study, Department of Fire Safety Engineering, Institute of Science and Technology, Lund University, Sweden, 1988.

[41] Konig, J., Structural fire design according to Eurocode 5 – design rules and their background, *Fire and Materials*, 29, 2005, pp. 147-163.

[42] Thomas, G.C., Fire Resistance of Light Timber Framed Walls and Floors, Fire Engineering Research Report 97/7, School of Engineering, University of Canterbury, NZ, May 1997.

[43] Malhotra H.L., *Design of Fire-Resisting Structures*, Surrey University Press, London, England, 1982.

[44] Schaffer, E.L., Charring Rate of Selected Woods- Transverse to Grain, FPL 69, US Department of Agriculture, Forest Service, Forest Products Laboratory, 1967.

[45] Wood Handbook 1999: Wood as an Engineering Material, Gen.Tech.Rep. FPL-GTR-113. Madison, WI: U.S. Department of Agriculture, Forest Service, Forest Products Laboratory.463 p.

[46] Knudson, RM, and Schniewind, AP, Performance of structural wood members exposed to fire, *Forest Products Journal*, 25, 1975, pp. 23-32.

[47] Wardle, T.M., Fire Resistance of Heavy Timber Construction, Information Series No. 53, New Zealand Forest Services, Wellington, NZ, 1966.

[48] Tenning, K., Glued Laminated Timber Beams: Fire Tests and Experience in Practice, in Symposium No. 3 Fire and Structural Use of Timber in Buildings (London, 1967), HMSO, London, pp. 1-6.

[49] Odeen,K., Fire Resistance of Glued Laminated Timber Structures, in Symposium No. 3 Fire and Structural Use of Timber in Buildings (London, 1967), HMSO, London, pp. 7-15.

[50] Issa, C., and Kmeid, Z., Advanced wood engineering: glulam beams, *Construction and Building Materials*, 19, 2005, pp. 99-106.

[51] Rogowski, B.F.W., Charring of Timber in Fire Tests, Symposium No.3 Fire and Structural Use of Timber in Buildings (London, 1967), HMSO, London, pp. 52-59.

[52] Richardson, L., Failure of Floor Assemblies Constructed with Timber Joists, Wood Trusses or I-Joists During Fire Resistance Tests, *interFLAM 2004*, Scotland.

[53] ANSYS Release 11.0, Theory Reference for ANSYS and ANSYS Workbench, ANSYS Inc., January 2007.

[54] Su, J.Z., et al, Fire Performance of Houses, Phase I Study of Unprotected Floor assemblies in Basement Fire Scenarios, Summary Report, IRC-RR-252, Institute for Research in Construction, December 15, 2008.

[55] AS 1720.4, Timber Structures, Part 4: Fire resistance for structural adequacy of timber members, Standards Australia, 2006.

[56] Handbook of Fire Protection Engineering, DiNenno, P. (Editor-in-Chief), Society of Fire Protection Engineers, Third Edition, 2002.

.

Appendix A

Details of Floor Assemblies

In this section, details on the construction design for the floor assemblies, list of materials, and the location and type of transducers installed for the tests are provided. These details are given for floor assemblies 1 and 2. In addition to the instruments installed on and near the floor assembly, a set of 16 furnace thermocouples were spaced symmetrically throughout the furnace in rows of four.

Assembly No. 1:

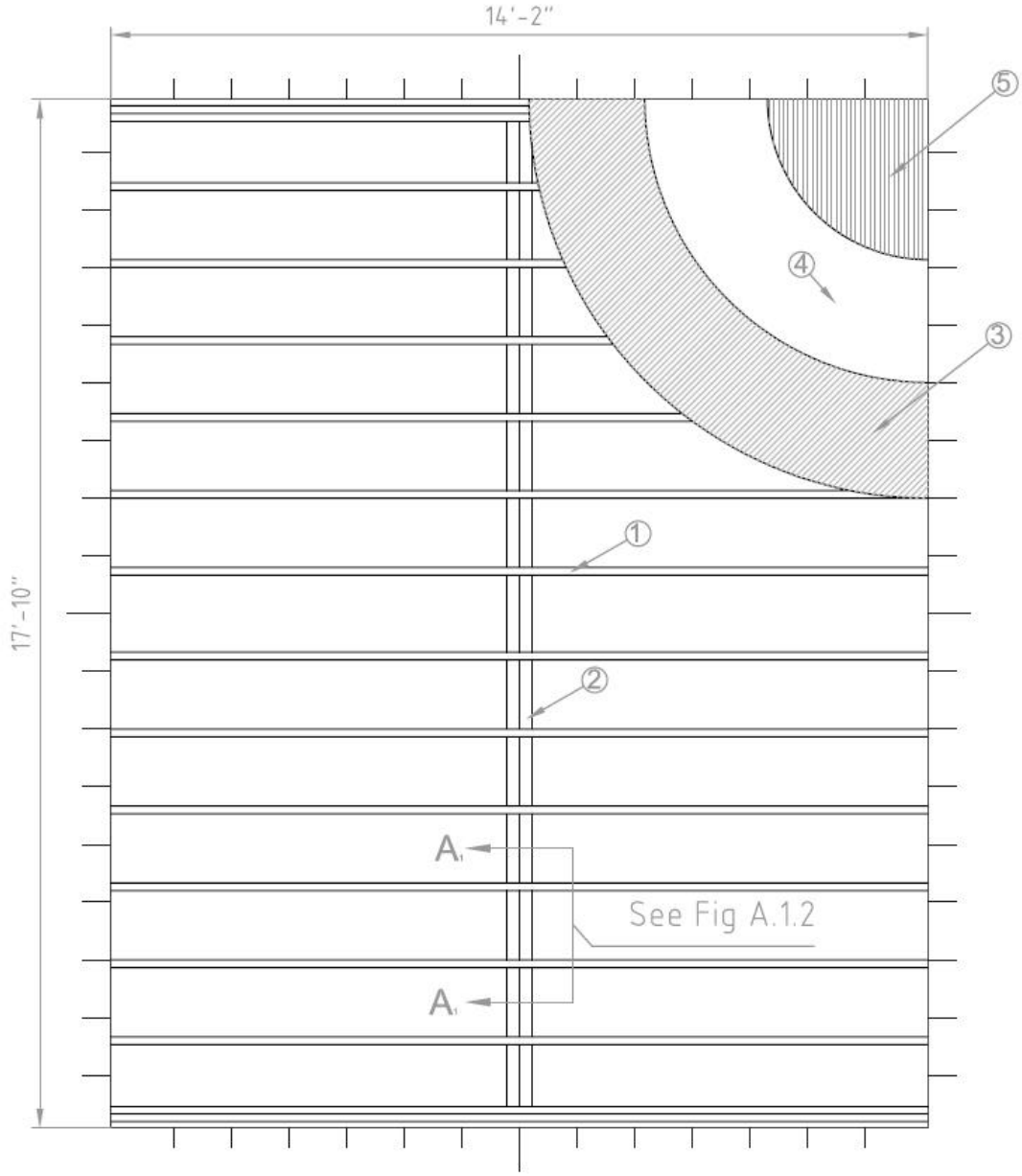

Figure A.1 Construction Layout

Assembly No. 1

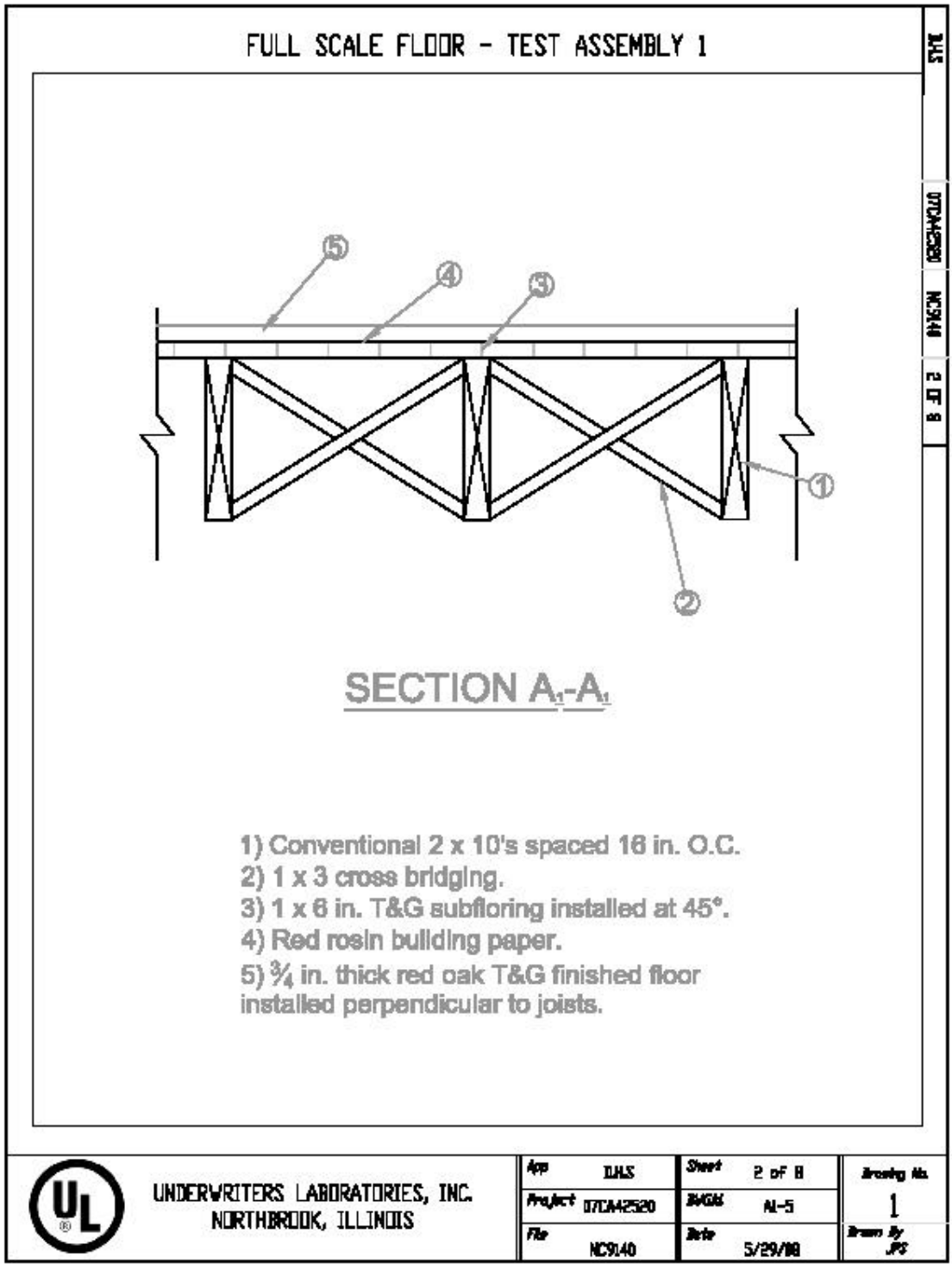

Figure A.2 Construction Layout Section A_1-A_1

Assembly No. 1

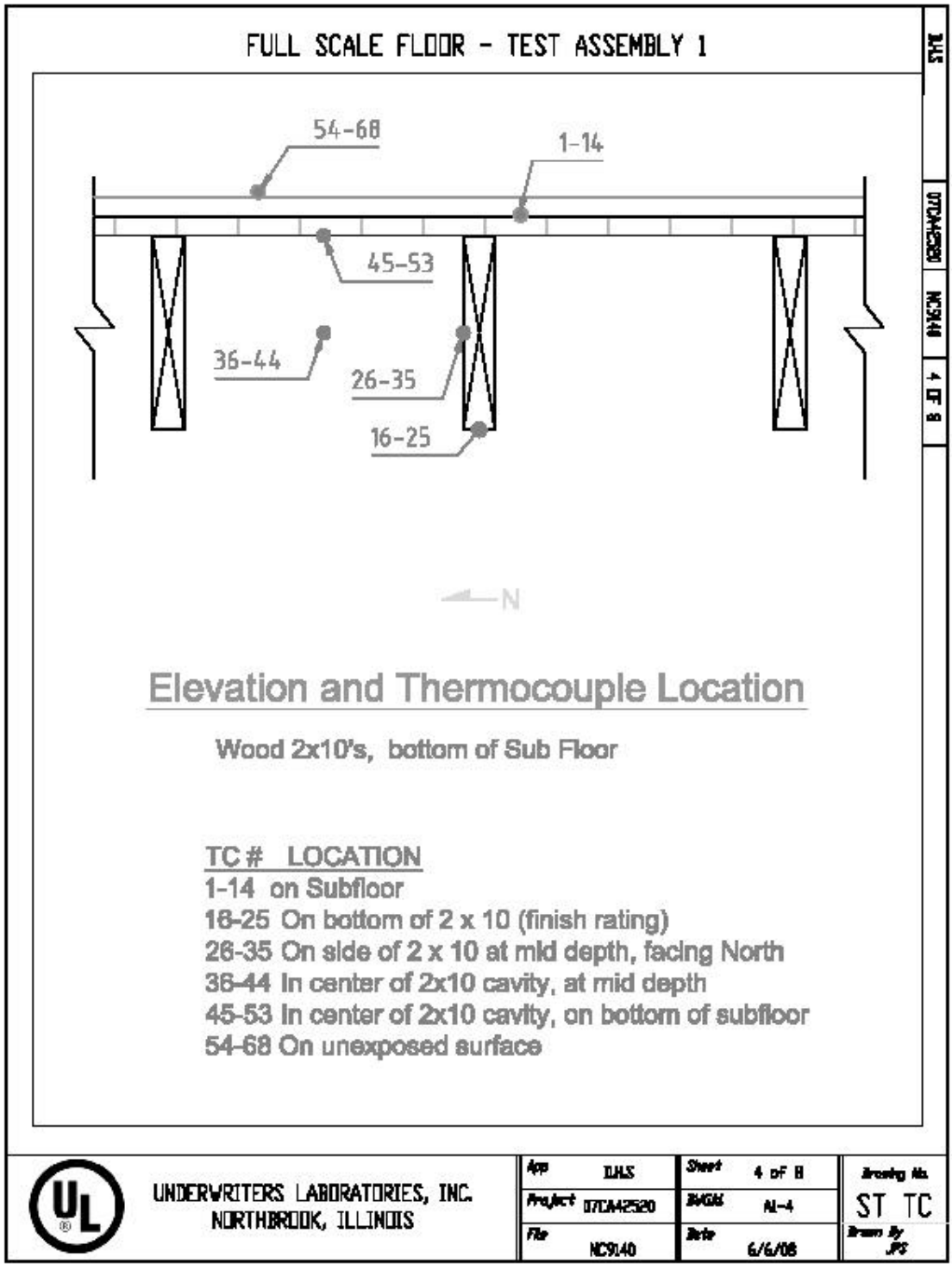

Figure A.3 Thermocouple Locations - Elevation

Assembly No. 1

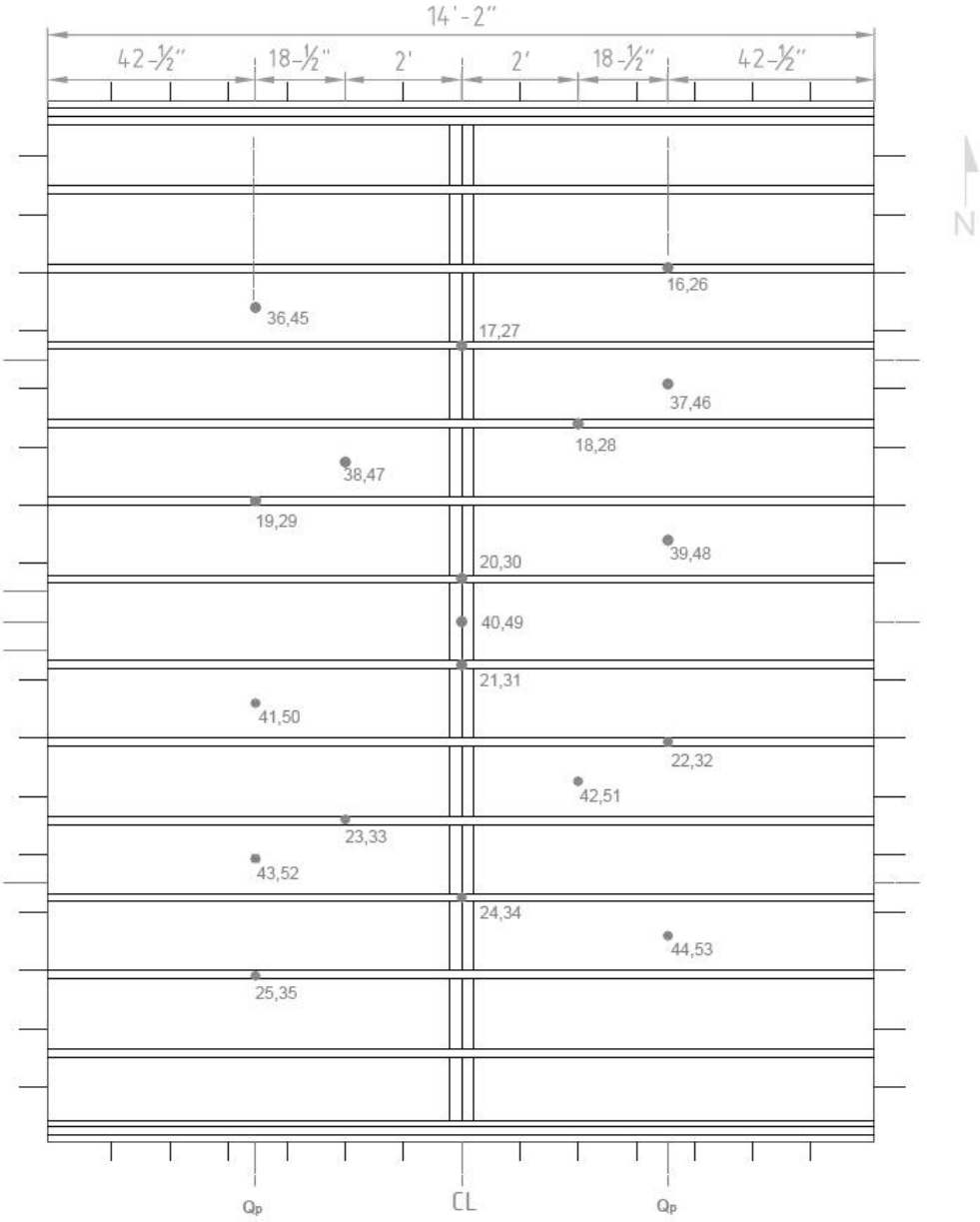

Figure A.4 – Thermocouple Locations on Wood Members

Assembly No. 1

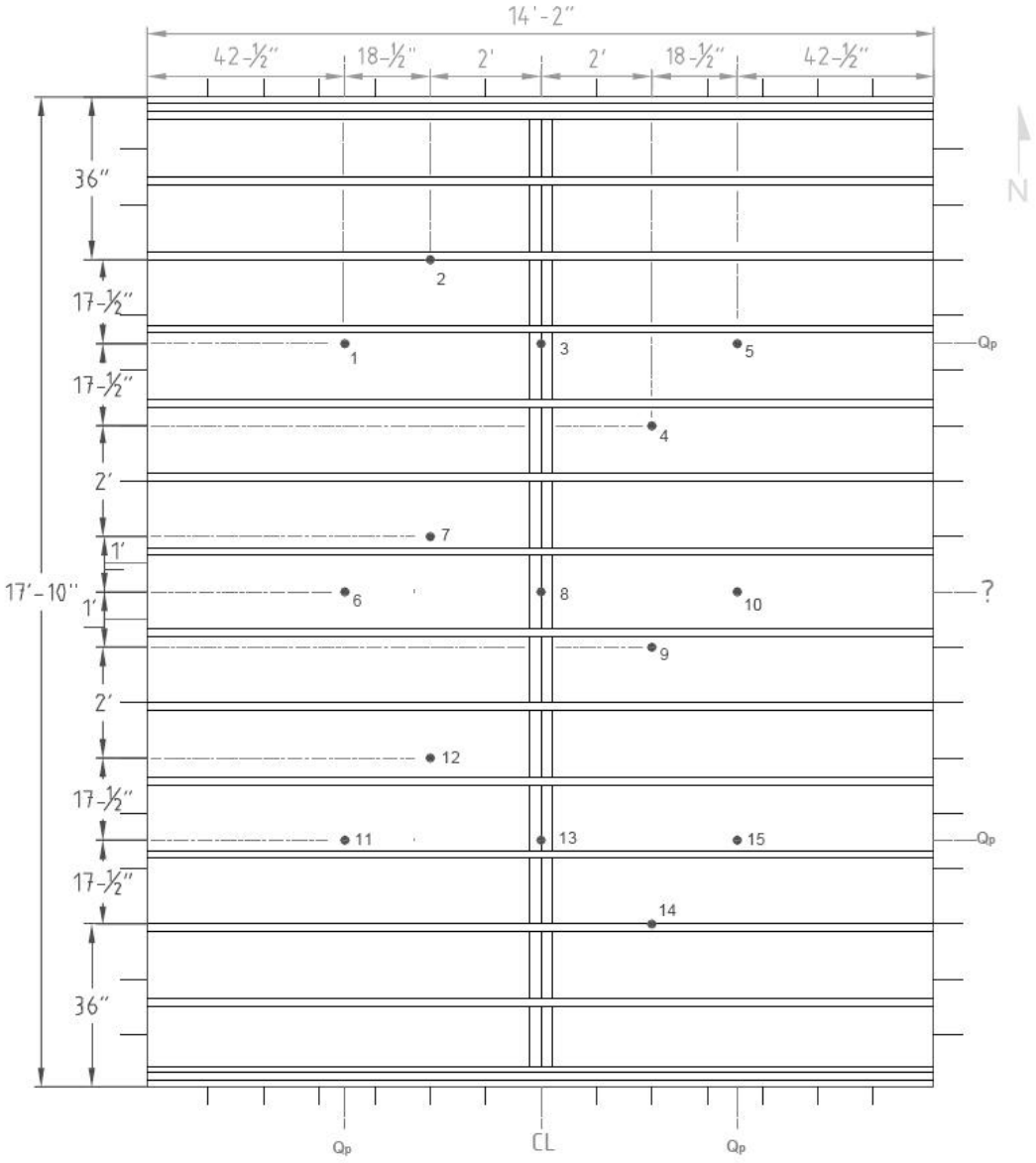

Figure A.5 – Thermocouple Locations on Sub-floor

Assembly No. 1

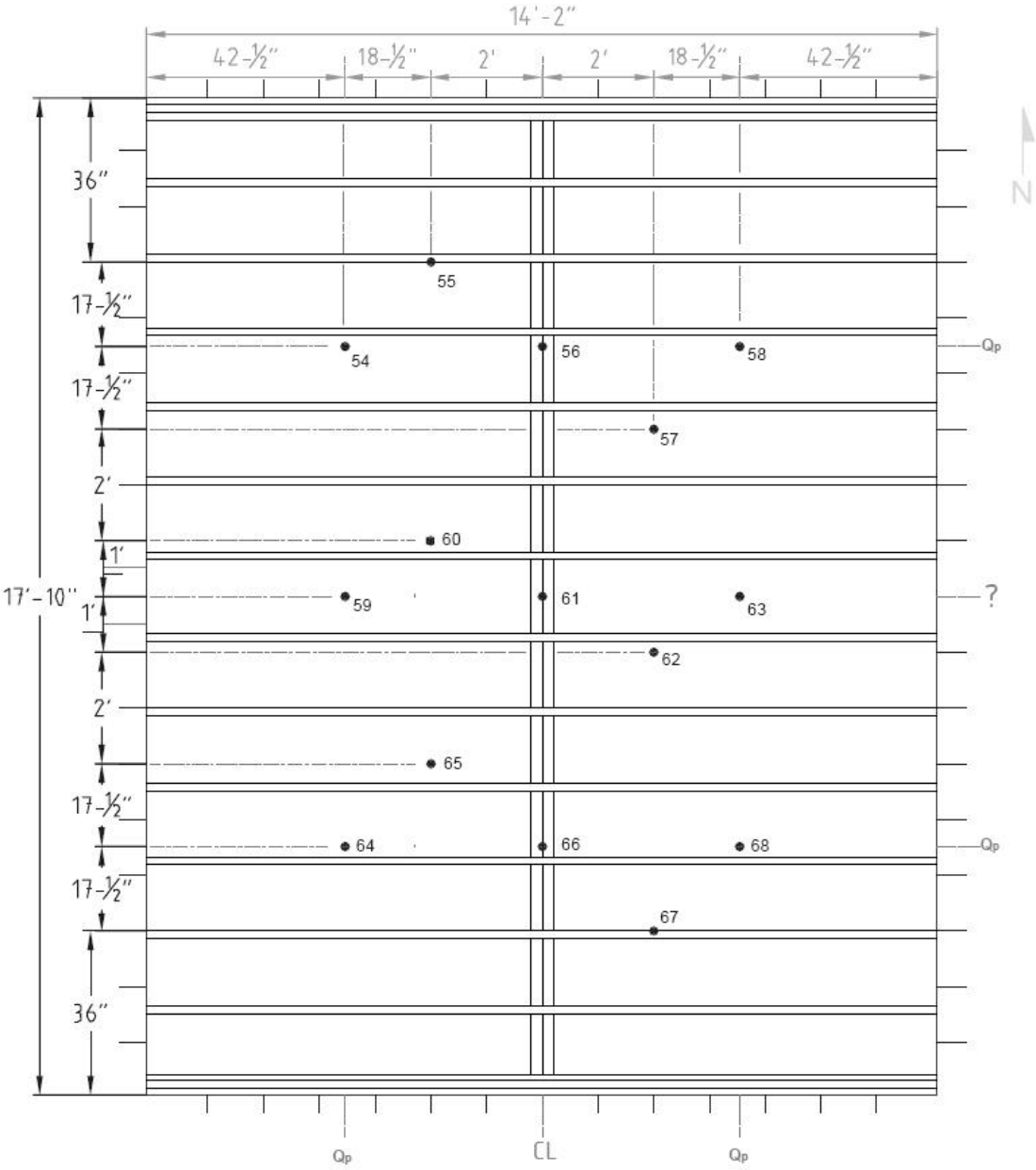

Figure A.6 – Thermocouple Locations on Unexposed Surface for assembly 1

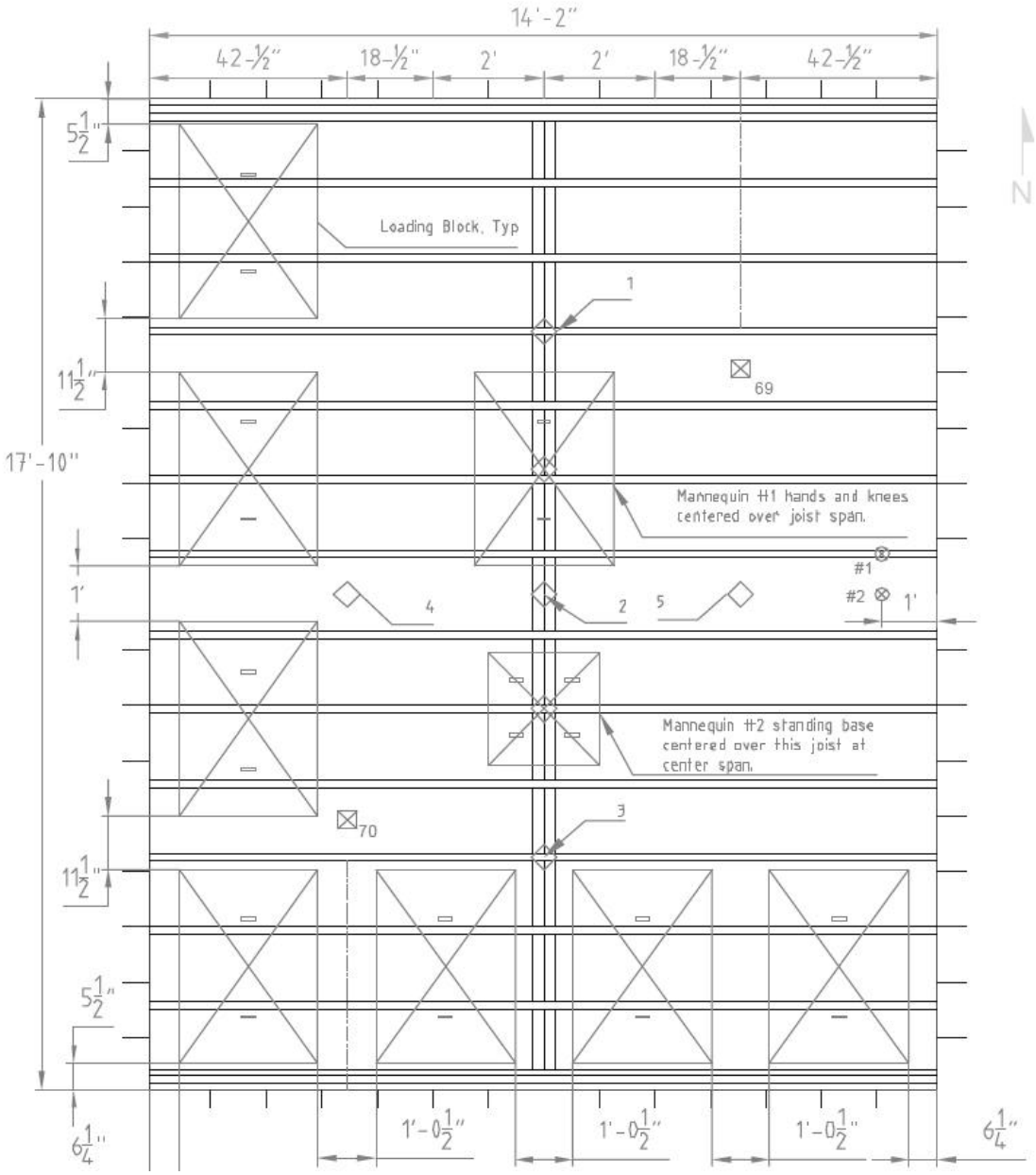

Figure A.7 – Loading and Instrumentation Layout (See Figure A.8) for assembly 1

Assembly No. 1

Figure A.8 – Loading and Instrumentation Key

Assembly No. 2

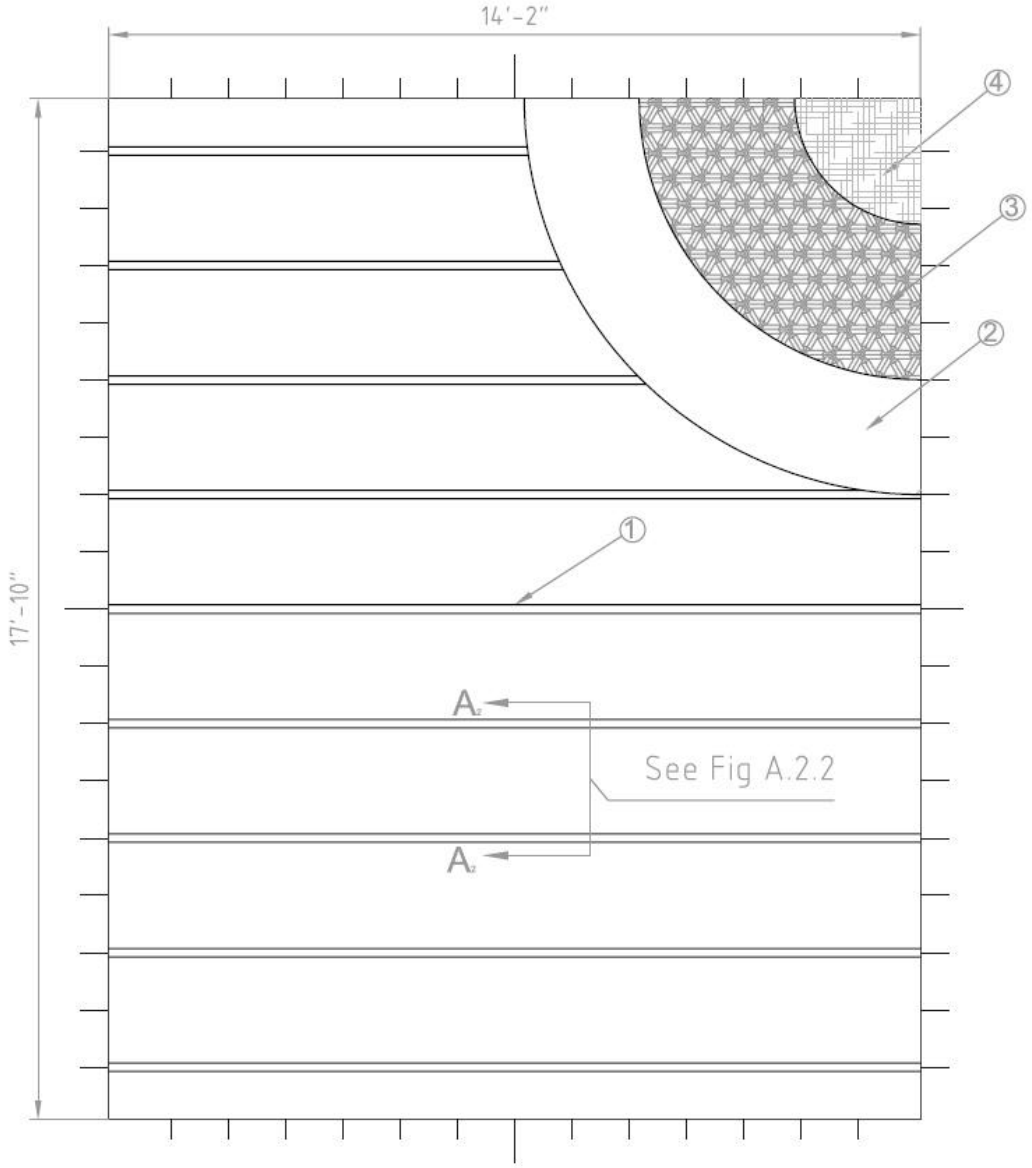

Figure A.9 – Construction Layout

Assembly No. 2

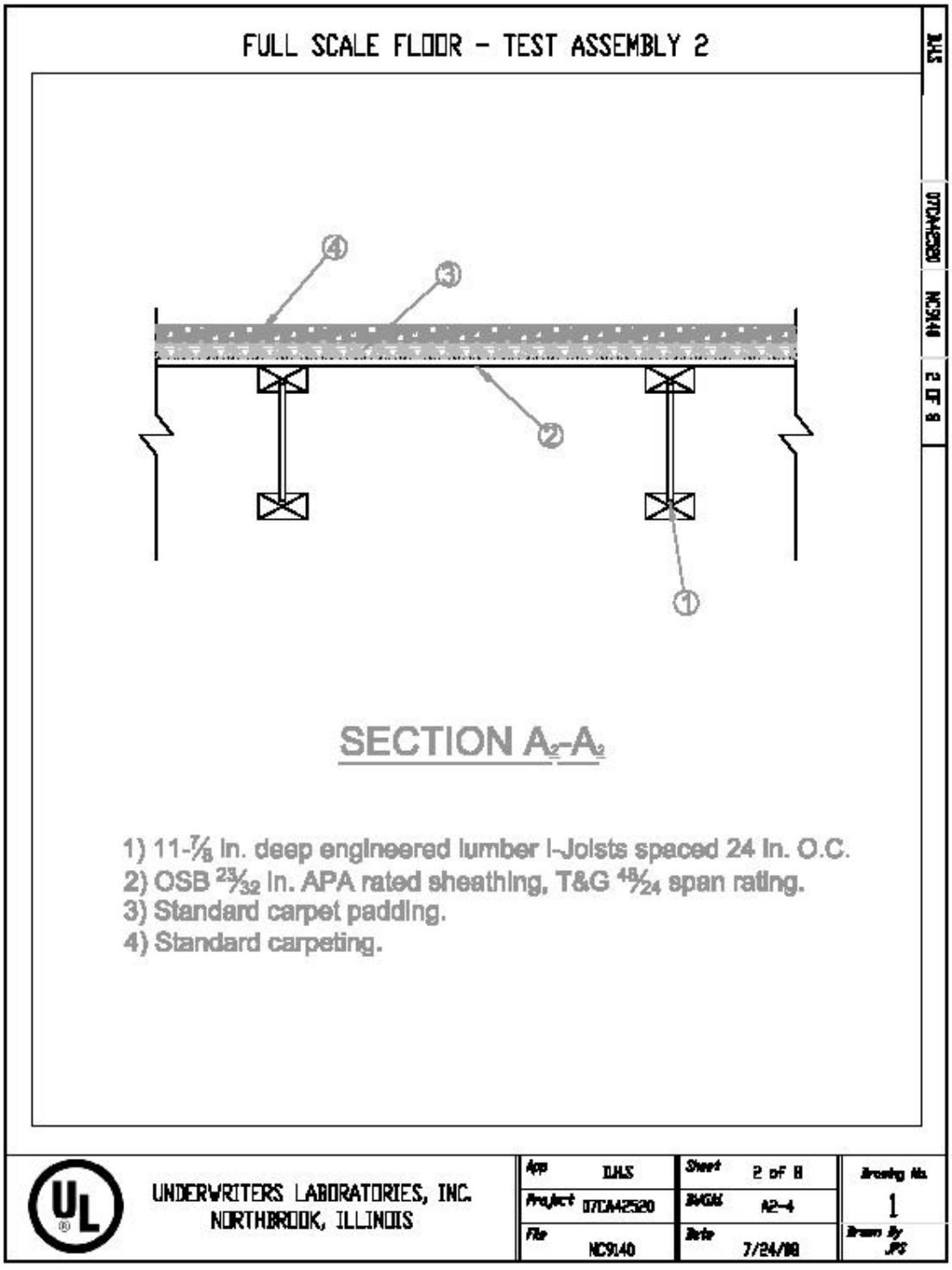

Figure A.10 – Construction Layout Section A2-A2

Assembly No. 2

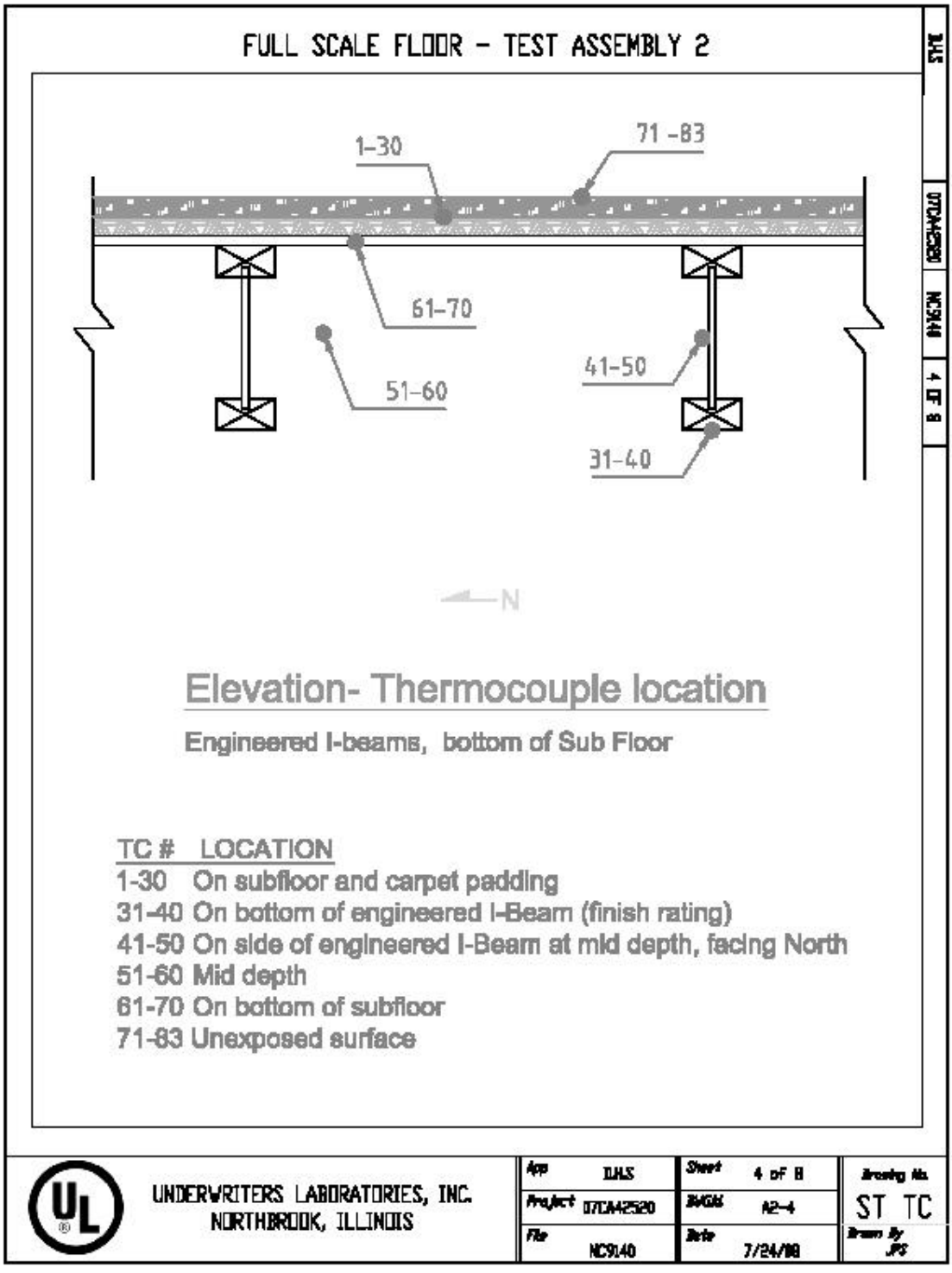

Figure A.11 – Thermocouple Locations - Elevation

Assembly No. 2

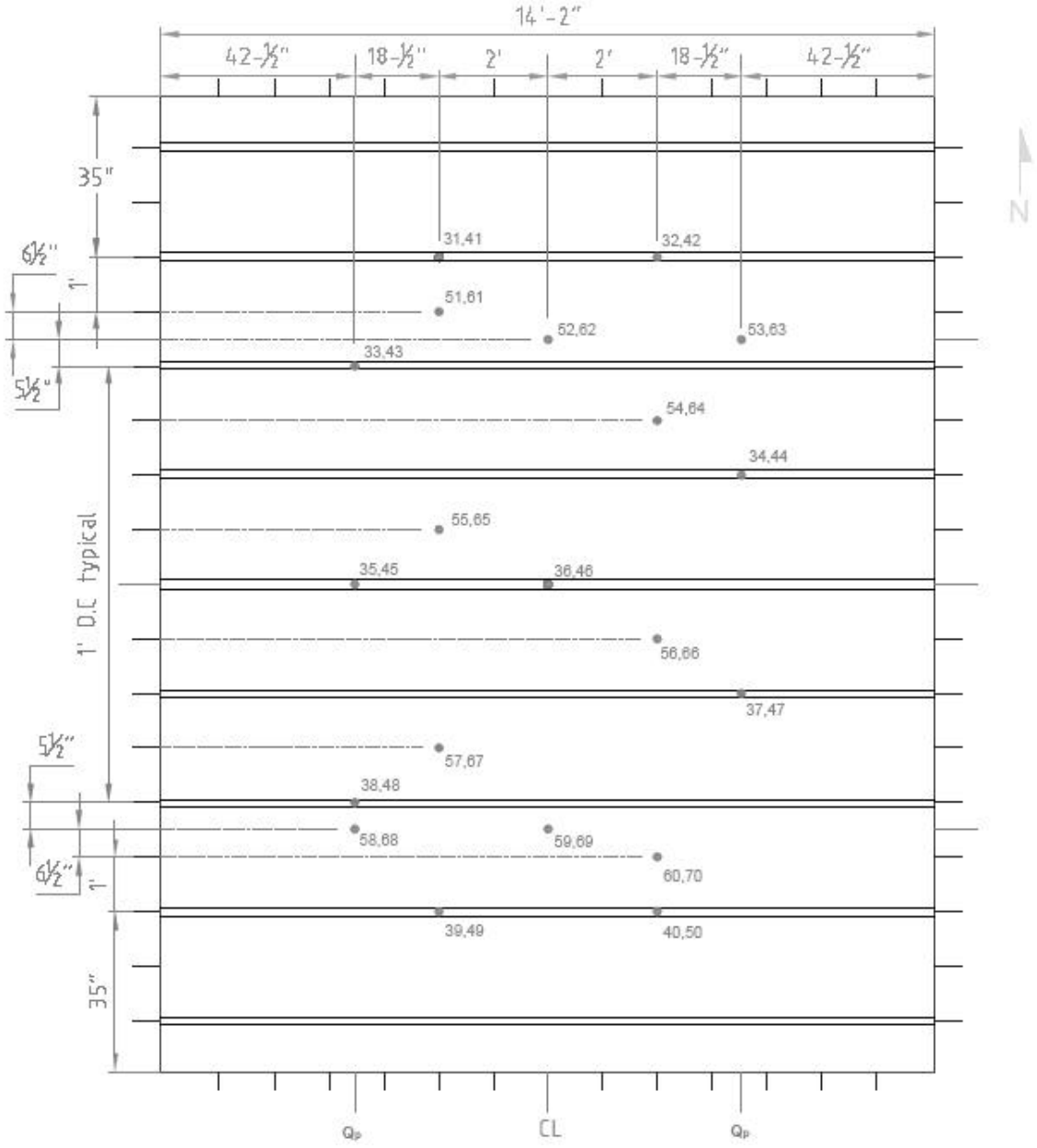

Figure A.12 – Thermocouple Locations on Wood Members

Assembly No. 2

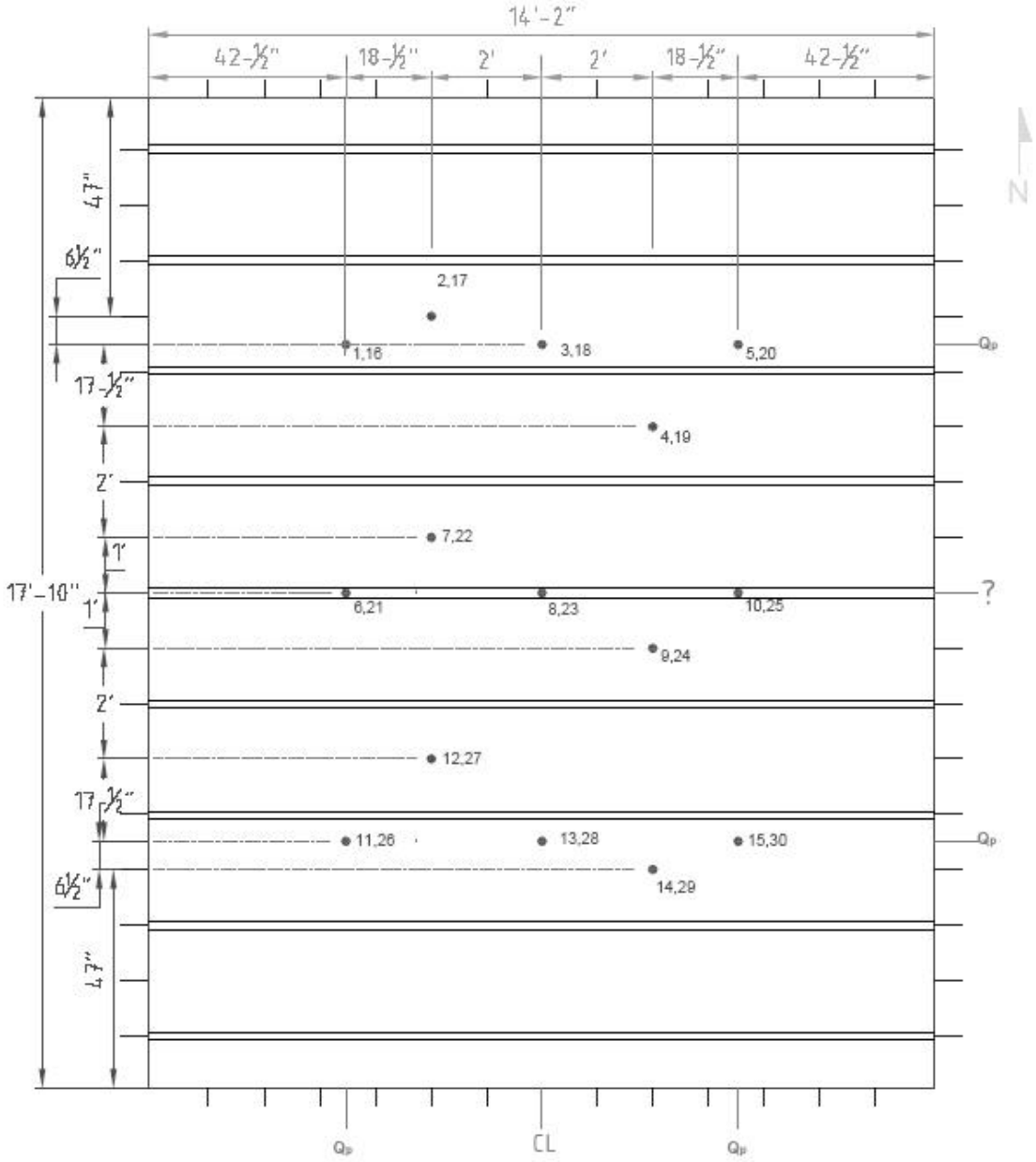

Figure A.13 – Thermocouple Locations on Sub-floor and Carpet Padding

Assembly No. 2

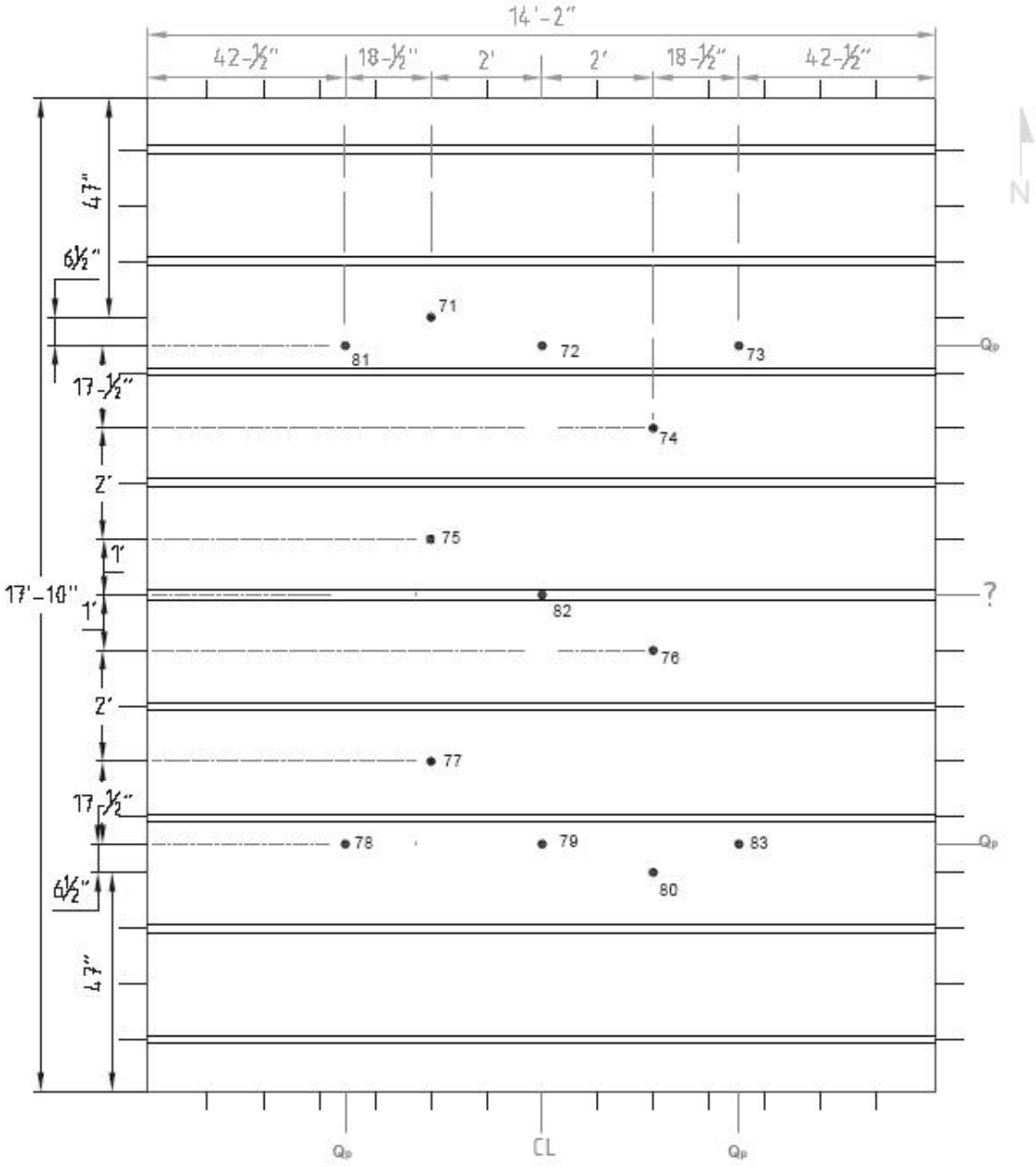

Figure A.14 – Thermocouple Locations on Unexposed Surface

Assembly No. 2

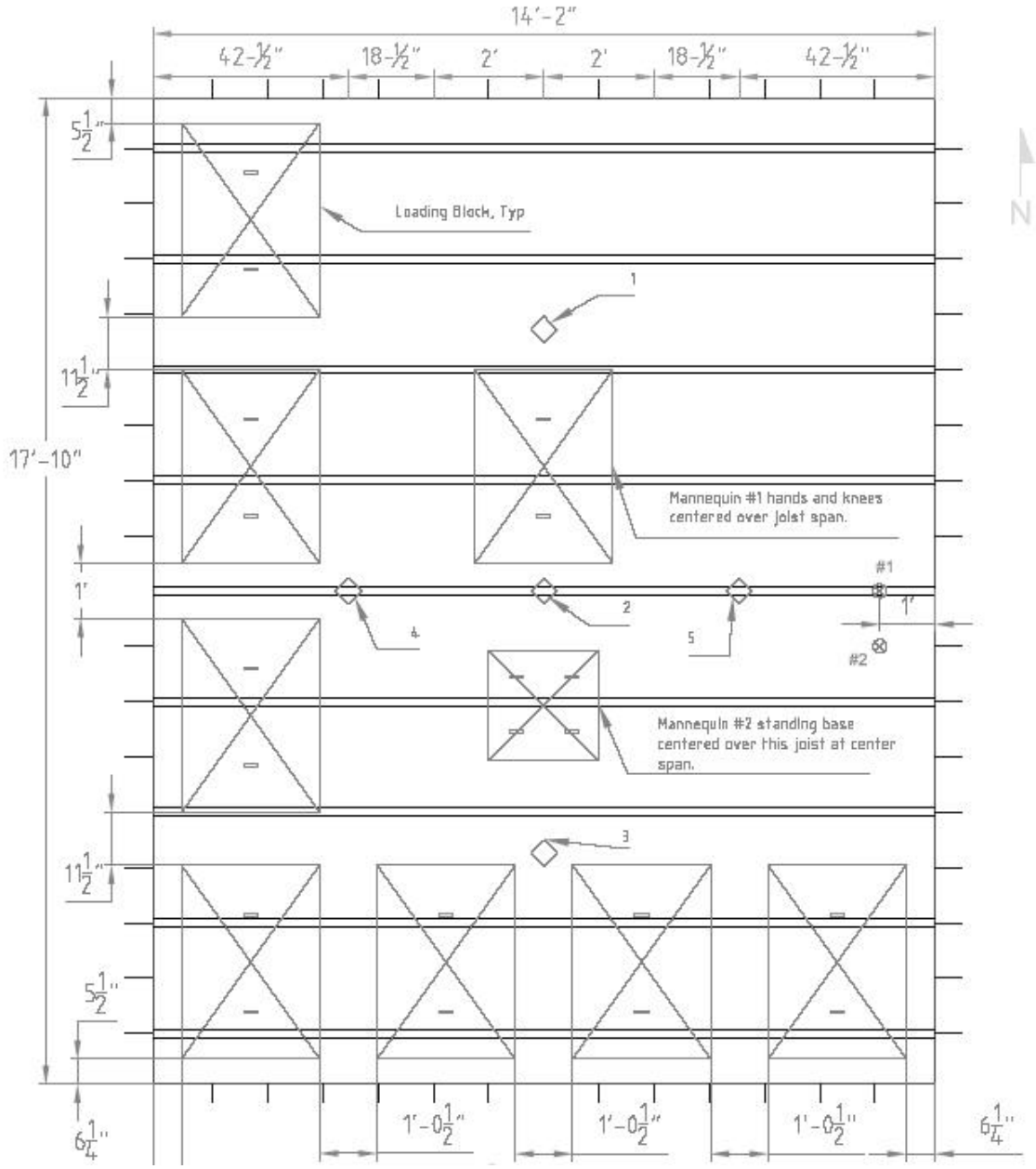

Figure A.15 – Loading and Instrumentation Layout (See Figure A.16)

Assembly No. 2

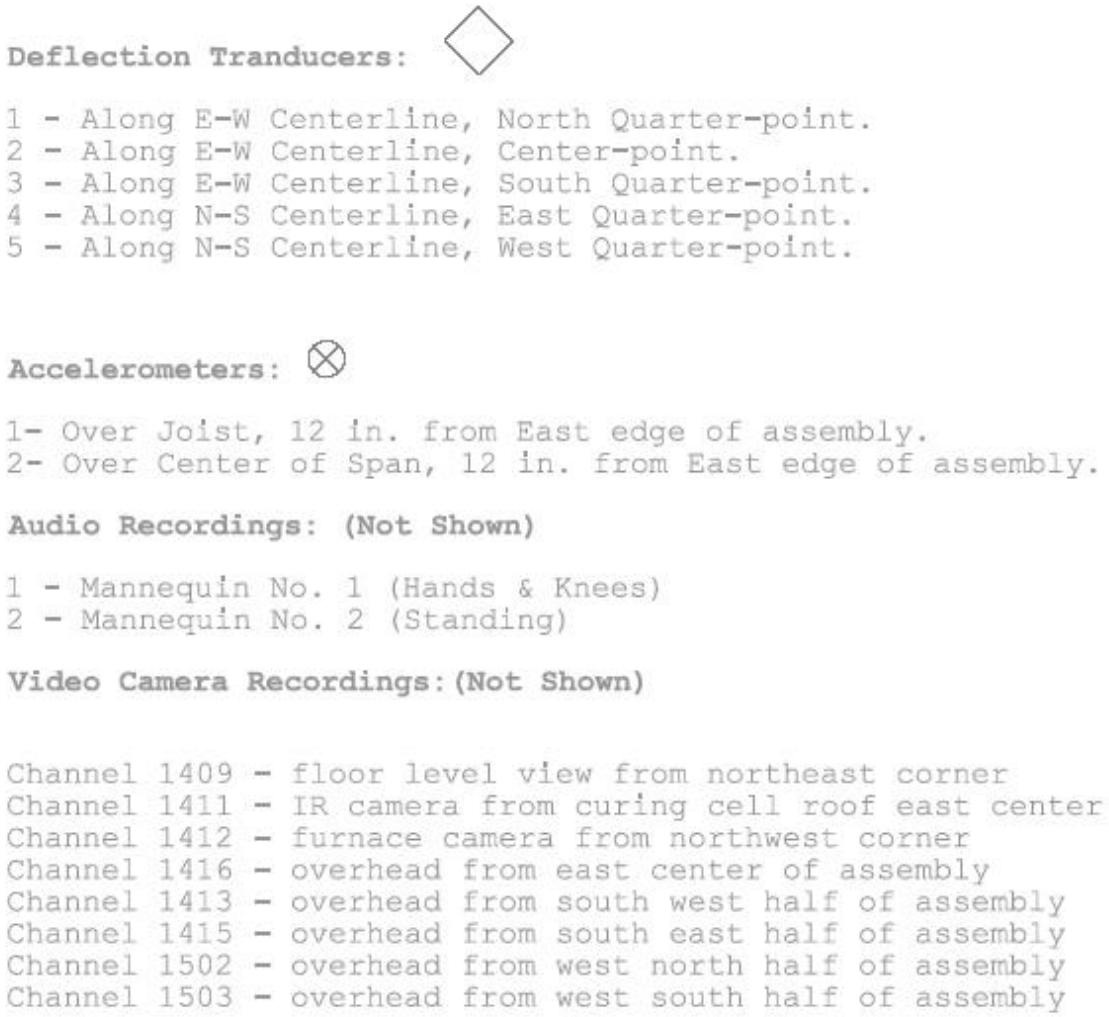

Figure A.16 – Loading and Instrumentation Key

Appendix B

Test Wood Sample Details

Specimen A - Conventional wood (Floor Assembly # 1)

	Length (in)	Width (in)	Thickness (in)	Weight (lbs)	Volume (in^3)	Density (lb/ft^3)
A1	48	9?	1½	8.88	657	23.37
A2	48	9?	1½	11.73	657	30.85
A3	48	9?	1½	11.42	657	30.04
A4	48	9?	1½	11.62	657	30.56
A5	48	9?	1½	11.44	657	30.09

Specimen B - Engineered lumber joist with OSB web (Floor Assembly # 2)

	1 (in)	2 (in)	3 (in)	4 (in)	5 (in)	Length (in)	Weight (lbs)	Volume (in^3)	Density (lb/ft^3)
B1	11?	?	2	1.1875	9½	48	9.79	399	42.39
B2	11?	?	2	1.1875	9½	48	10.27	399	44.49
B3	11?	?	2	1.1875	9½	48	10.32	399	44.68
B4	11?	?	2	1.1875	9½	48	10.03	399	43.44
B5	11?	?	2	1.1875	9½	48	10.43	399	45.16

Specimen C - Conventional T&G wood (Sub floor in Floor Assembly # 1)

	1 (in)	2 (in)	3 (in)	4 (in)	Weight (lbs)	Volume (in^3)	Density (lb/ft^3)
C1	5?	¾	¼	48	3.66	198	31.94
C2	5?	¾	¼	48	3.22	198	28.09
C3	5?	¾	¼	48	3.62	198	31.55

Specimen D - OSB sheeting (Sub floor in Floor Assembly # 2)

	Length (in)	Width (in)	Thickness (in)	Weight (lbs)	Volume (in^3)	Density (lb/ft^3)
D1	48	48	¾	35.45	1728	35.45
D2	48	48	¾	35.69	1728	35.69

Appendix C

Summary of Strength Testing on Wood Specimen

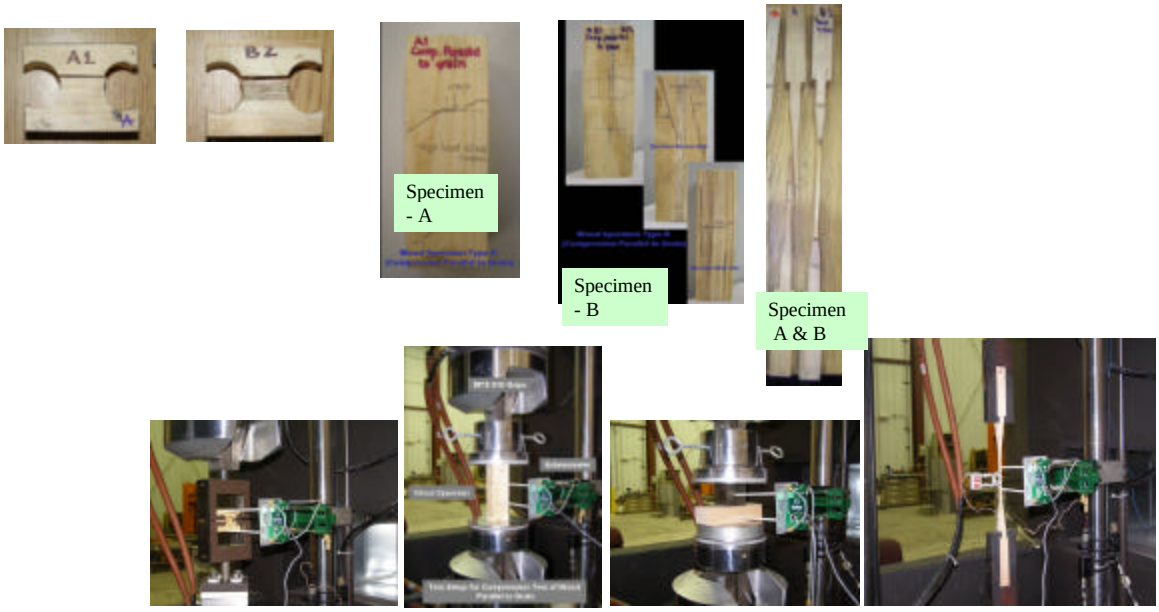

Figure C.1: Illustrations of test set-up for testing wood specimens
Top: Different wood specimens for compression and tension tests
Bottom: (a) Tension perpendicular to the grain (b) Compression parallel to the grain (c) Tension parallel to the grain (d) compression perpendicular to the grain

Table 14 – Strength properties of wood

Test Mode	Grain orientation	Specimen type	Room temp °C	100°C	200°C
			MPa	MPa	MPa
Tension	Parallel	A	64.58	44.97	26.46
		B	49.07	26.46	24.10
	Perpendicular	A	3.23	0.99	1.42
		B	1.42	0.87	0.48
Compression	Parallel	A	54.31	53.12	44.78
		B	46.68	42.18	31.61
	Perpendicular*	A	8.10	13.14	13.59
		B	18.41	14.83	14.07

* Compression test terminated when he deformation in the specimen was approx 2.5mm

Appendix D[16]

Material Property Tests on Wood Specimens

D1. Objective

To conduct material characterization tests on wood (and OSB) to generate high temperature thermal and mechanical properties for use in fire resistance modeling of floor assemblies.

D2. Background

Key parameters that are needed as input data for thermal FE models are the high temperature material properties of wood. The three types of wood that are under consideration for floor assemblies are conventional wood joists, engineered lumber joists, T&G wood. In addition tests on OSB were also conducted since OSB is used in sub-flooring in one of the floor assemblies.

The thermal properties of wood that are important for fire resistance modeling are specific heat, density, thermal conductivity and thermal diffusivity. The mechanical properties of wood that are of relevant for fire resistance evaluation are strength and modulus of elasticity. In addition, charring, which occurs under fire conditions, influences the fire performance of wood assemblies. All these properties vary with temperature and the composition and type of wood.

There is limited information in the literature on the high temperature properties of wood and also on procedures for undertaking many of the tests. Further, these properties vary significantly among different species of wood and also on the test conditions of the specimen, such as moisture content and age. The characterization tests were carried out on three types of wood and also on OSB specimens.

D3. Thermal Property Tests

D3.1 General

The thermal properties of four types of wood, supplied by UL, were measured at various temperatures in 20-250°C range. The wood specimens were exposed to a target temperature until the temperatures stabilized and then measurements were

[16] Final Report on Material Property Tests on Wood Specimens, Dr. Kodur, MSU, November 26, 2008.

done 30 minutes after the temperature stability was attained. The measurements were carried out at room temperature and also at 100, 150, 200 and 250°C. The measured thermal properties were density, thermal conductivity, specific heat, thermal diffusivity, and thermal expansion. The four types of wood considered in this project are designated as A, B, C, and D. Specimen A is conventional wood used as joists in floor assembly 1, while Specimen B is engineered lumber used in floor assembly 2. Specimen C is T&G wood panel used, as sub flooring in assembly 1, and Specimen D is OSB sheeting used as sub-flooring in floor assembly 2. Dimensions of the four specimens are provided in Appendix B.

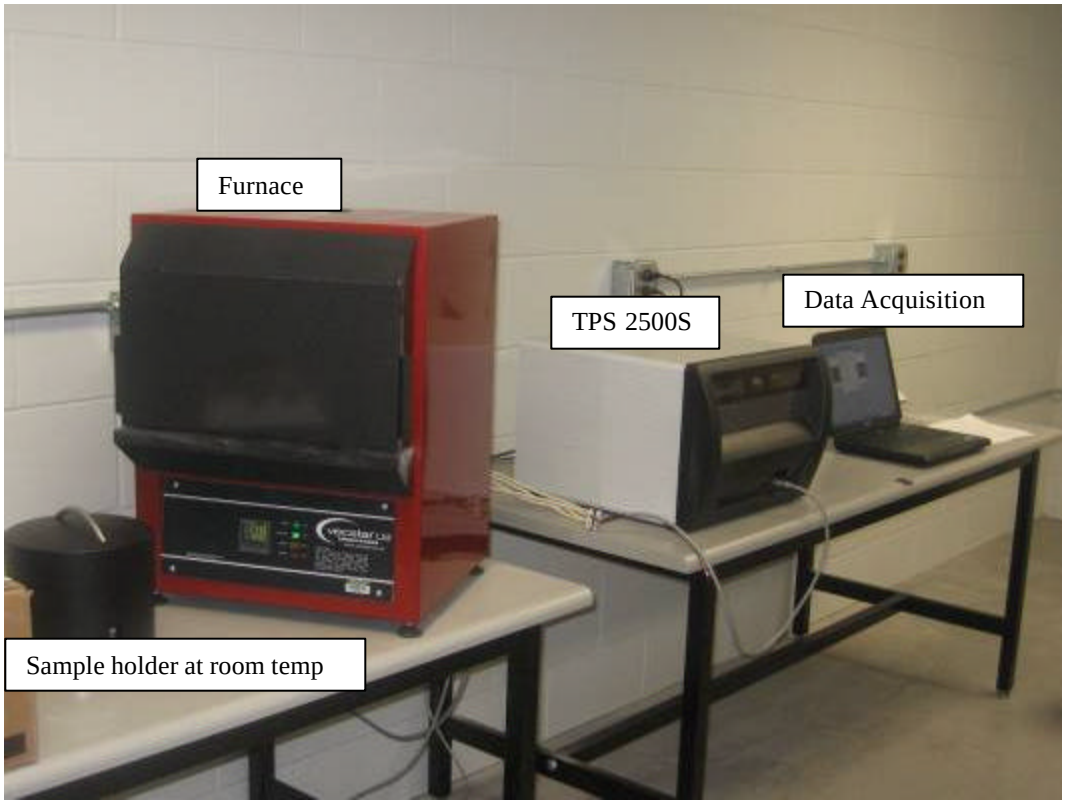

Figure D1 - Hot disk equipment setup for measurement of thermal properties

D3.2 Test Setup

The specific heat, thermal conductivity and thermal diffusivity properties were measured using "Hot Disk TPS 2500S" thermal constants analyzer equipment. Figure D1 shows the "Hot Disk" equipment set up. This equipment was connected to a furnace in which the specimens were exposed to desired high temperature. The thermal properties were then measured using a high temperature mica sensor placed

inside the test specimens connected to Hot Disk. This state-of-the-art equipment utilizes the transient plane source (TPS) technique to measure the thermal properties of materials. Figure D2 shows the time-temperature graph followed during measurement of thermal properties.

The thermal expansion property was measured using thermo-mechanical analysis (TMA) apparatus. The TMA measured dimensional changes of sample under conditions of controlled temperature. It utilized a movable-core linear variable differential transducer (LVDT), which generated an output signal directly proportional to the sample dimension change. Figure D3 shows the test set up for measuring the dimensional changes in wood specimens. The density was measured using conventional hot oven.

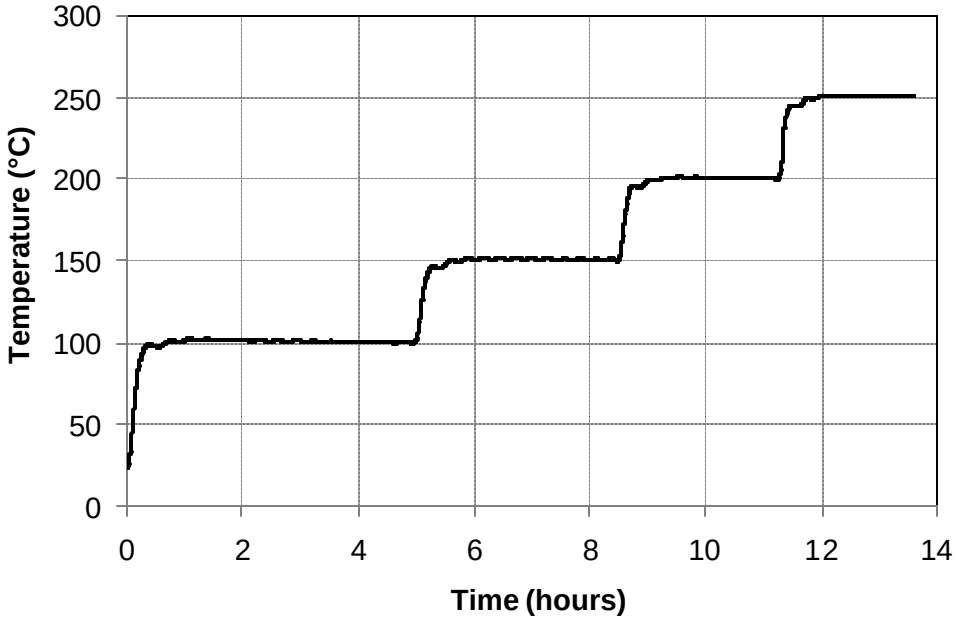

Figure D2 - Time-temperature graph showing stability of temperature attained during 'hot disk' measurement

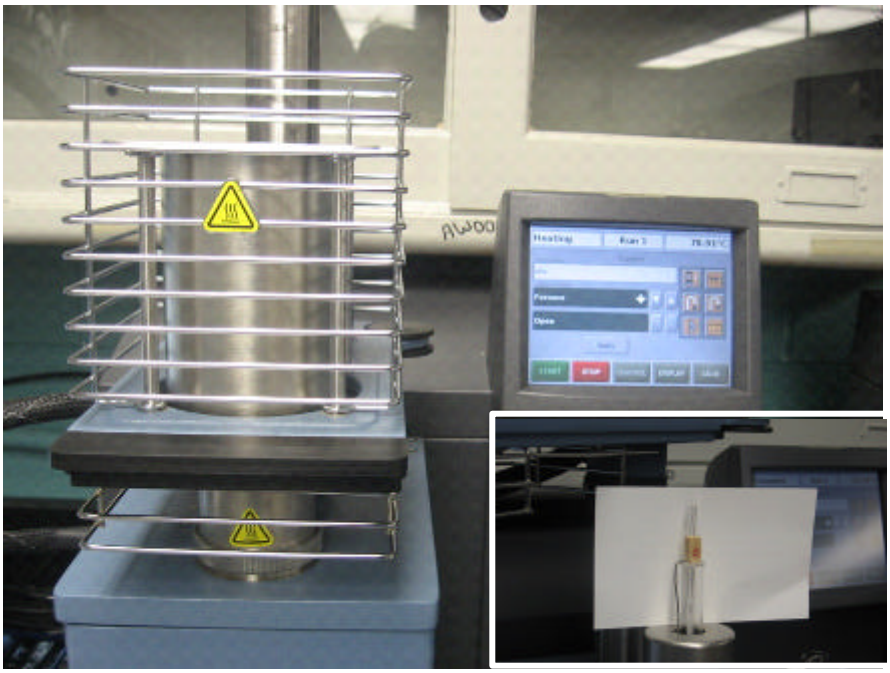

Figure D3 - TMA set up for measurement of dimensional changes

D3.3 Specimen Preparation

For property measurements using Hot Disk apparatus a sample size of 2×2×1 inches was prepared for a 20 mm diameter high temperature Hot-Disk sensor. Test specimens A and B were prepared by cutting samples from conventional wood and engineered lumber to required size. However, T&G wood and OSB (C&D) from floor assemblies were ¾ in thick, so extra thickness was added by supplementing a vein of same wood or OSB to make specimen C and D thickness to be 1 inch. This was necessary to keep the specimens in Hot Disk sample holder. However, probing depth was kept within the ¾ inch so that the joint would not affect the properties.

For thermal expansion property measurements, a wood sample of 3/8×3/8×3/4 inches, as shown in the inset of Figure D3 was prepared.

For density measurement samples were prepared based on the available thickness of the specimens. Test specimen A was 2.75×2.75×1.5 inches. Specimen B had web and chord parts; so two samples, one from the web and the other from the chord were cut. The specimen B web was of 3×3×0.438 inches while the flange of specimen B was 2×3×1.25 inches. For both specimens C and D a size of 3×2.25×0.75 inches was cut.

D3.4 Test Procedure

The prepared test samples were mounted on the high temperature sample holder assembly and placed in the furnace. The properties were first measured at ambient temperature and then these samples were subjected to other target temperatures in

100 to 250°C range. The thermal properties were recorded through the TPS 2500S equipment with proper measuring parameters applied through requisite software. For getting full set of measurements in 20 to 250°C range, a time period of 13 to 14 hours was needed as illustrated in Figure D2. This included the time required to reach a desired temperature and an additional 30 minutes for temperature stability to be attained. Figure D4 shows a monitor displaying data recorded after a test was complete and also with the insert in the figure illustrating the test specimen in the furnace. Figure D5 shows the charred wood sample (Specimen B) that was removed from the furnace at the end of the test.

For density measurement, first the weight of the sample was measured at room temperature. Then the sample was subjected to temperatures of 100°C, 150°C, 200°C and 250°C using the conventional hot oven. Most of the wood specimens, with the exception of specimen C charred at a temperature of 250°C. After subjecting the wood samples to high temperatures for about 2 hours, the samples were taken out and allowed to cool to room temperature. Then the weight of the samples was measured and density values were calculated.

The temperature increase for thermal expansion depends on the ramp set by the user in a particular test. For the wood samples, the selected ramp (heating rate) was 5°C per minute. After placing the sample with the probe into the TMA furnace, the test was controlled by software that recorded the dimensional change with increasing temperature.

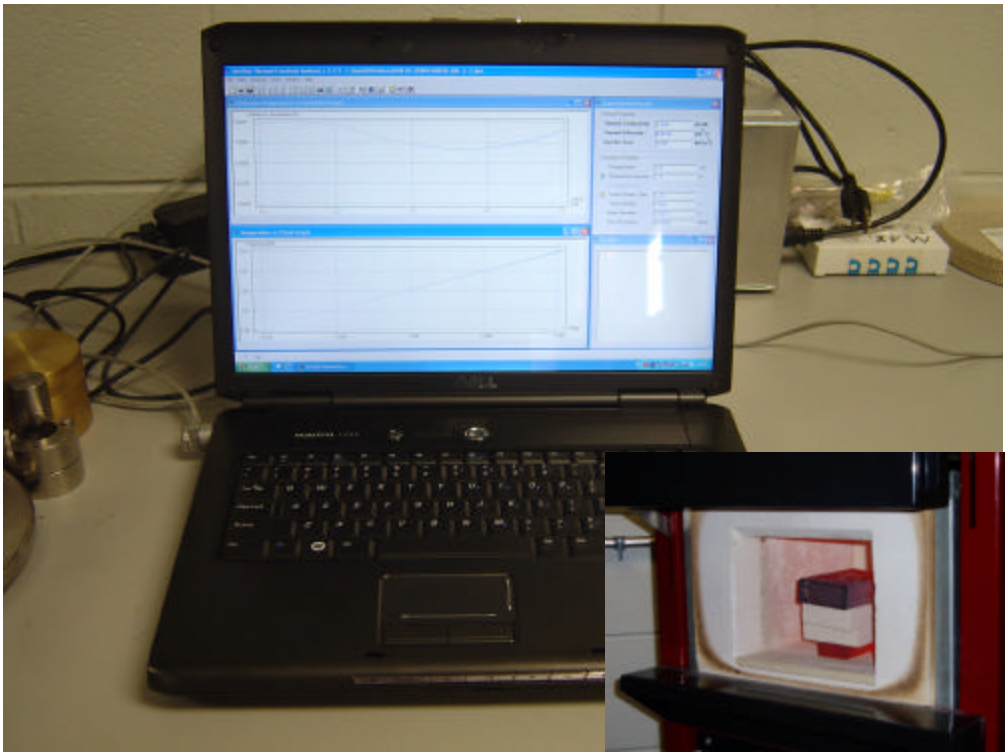

Figure D4 - Measured data with parametric graphs on monitor and specimens inside the furnace

Figure D5 - Charred wood from engineered lumber (Type B) after completion of thermal properties experiment

D3.5 Results and Observations

a. Thermal Conductivity, Specific Heat, Thermal Diffusivity and Density

The measured thermal conductivity (k), specific heat (Cp), thermal diffusivity and density values for four UL wood samples are tabulated in Tables D1 to D4 at various temperatures. These properties are also plotted in Figures D6 to D9. The differences in values of thermal conductivity, specific heat, thermal diffusivity and density can be attributed to different types of wood. The propagation of heat in these wood samples was considered to result from differences in density, moisture content, and grain orientation. The following observations are based on the general trends in the recorded data:

- The thermal properties for all wood types are within the range reported by other researchers in the literature [1, 2].
- As expected the thermal conductivity of specimen B (engineered lumber) was higher due to compressed plies in binding material.
- Thermal conductivity and density generally decreased with temperature in all specimens.
- OSB samples (specimen D) charred at much lower temperatures than other wood samples. Thus its properties could not be measured at temperatures of 150ºC and higher.
- The specific heat in specimen C was much higher than other wood samples and this might be probably due to presence of thick wood gum layers.
- The thermal diffusivity decreased with temperature for all specimens (see Figure D8). The decrease was more gradual in specimens A and B, as compared to specimens C and D. For specimen C, the decreased in thermal diffusivity was only up to a temperature of 100ºC and it remained constant beyond that temperature.

Table D1 – Recorded thermal conductivity values at various temperatures for UL wood samples

Specimen A		Specimen B		Specimen C		Specimen D	
Temp (ºC)	Thermal conductivity - (k) (W/mK)	Temp (ºC)	Thermal conductivity - (k) (W/mK)	Temp (ºC)	Thermal conductivity - (k) (W/mK)	Temp (ºC)	Thermal conductivity - (k) (W/mK)
22	0.265217	22	0.637404	22	0.26384	22	0.310073
100	0.257264	100	0.490633	100	0.15158	70	0.411321
150	0.217768	150	0.384995	150	0.068942	100	0.281312
200	0.213585	200	0.152164	200	0.081787	150	*
250	0.207038	250	0.092537	250	0.079729	200	*

- Data could not be recorded due to charring at these temperatures

Table D2 - Recorded specific heat values at various temperatures for UL wood samples

Specimen A		Specimen B		Specimen C		Specimen D	
Temp (°C)	Specific heat - (Cp) MJ/m³K	Temp (°C)	Specific heat - (Cp) MJ/m3K	Temp (°C)	Specific heat - (Cp) MJ/m3K	Temp (°C)	Specific heat - (Cp) MJ/m3K
22	0.78743	22	1.496831	22	0.480805	22	1.186567
100	0.803298	100	2.319671	100	13.45949	70	1.450774
150	0.954995	150	2.304956	150	8.884578	100	2.391506
200	0.874629	200	7.717064	200	7.495219	150	*
250	0.890001	250	1.684688	250	3.289634	200	*

* Data could not be recorded due to charring at these temperatures

Table D3 - Recorded thermal diffusivity values at various temperatures for UL wood samples

Specimen A		Specimen B		Specimen C		Specimen D	
Temp (°C)	Thermal diffusivity mm²/Sec	Temp (°C)	Thermal diffusivity mm²/Sec	Temp (°C)	Thermal diffusivity mm²/Sec	Temp (°C)	Thermal diffusivity mm²/Sec
22	0.336814	22	0.425835	22	0.548747	22	0.261319
100	0.32026	100	0.21151	100	0.011262	70	0.283518
150	0.22803	150	0.167029	150	0.00776	100	0.11763
200	0.244201	200	0.019718	200	0.010912	150	*
250	0.232627	250	0.054928	250	0.024237	200	*

* Data could not be recorded due to charring at these temperatures

Table D4 - Recorded density values at various temperatures for UL wood samples

	Temp (°C) = 100 °C		Temp (°C) = 150 °C		Temp (°C) = 200 °C		Temp (°C) = 250 °C	
	Density – (?) (kg/m³)		Density – (?) (kg/m³)		Density – (?) (kg/m³)		Density – (?) (kg/m³)	
	Before test	After test	Before test	After test	Before test	After test	Before test	After test
Specimen A	512.667	491.686	485.026	450.672	433.087	388.091	460.651	*
Specimen B web	615.274	587.378	613.725	578.079	580.042	533.754	603.186	*
Specimen B flange	679.397	651.736	636.455	586.732	656.059	594.393	633.833	*
Specimen C	455.644	425.508	485.779	442.385	519.379	466.493	488.190	326.816
Specimen D	607.525	583.116	614.757	575.883	613.854	564.131	580.404	*

* Data could not be recorded due to charring at these temperatures

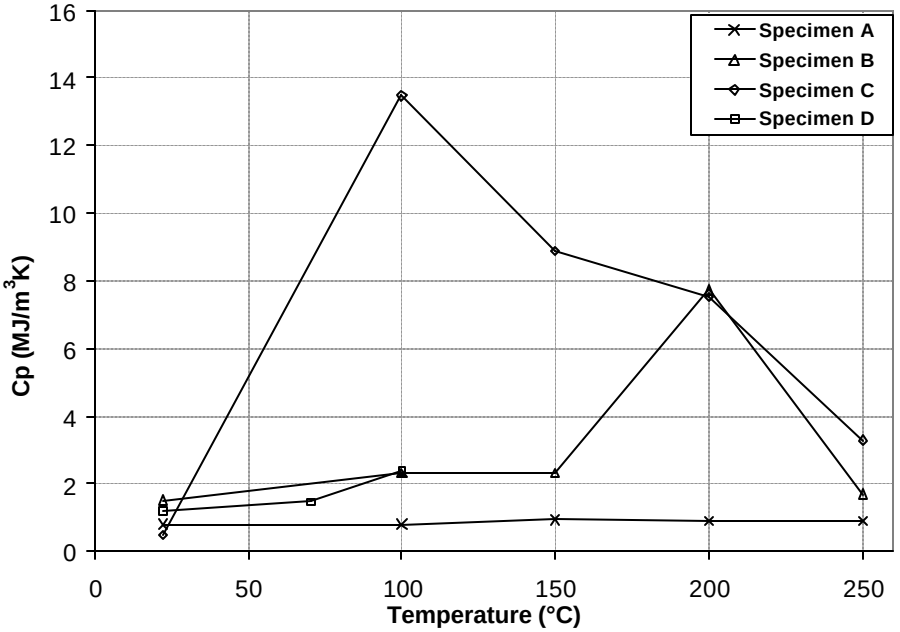

Figure D6 - Measured specific heat as a function of temperature

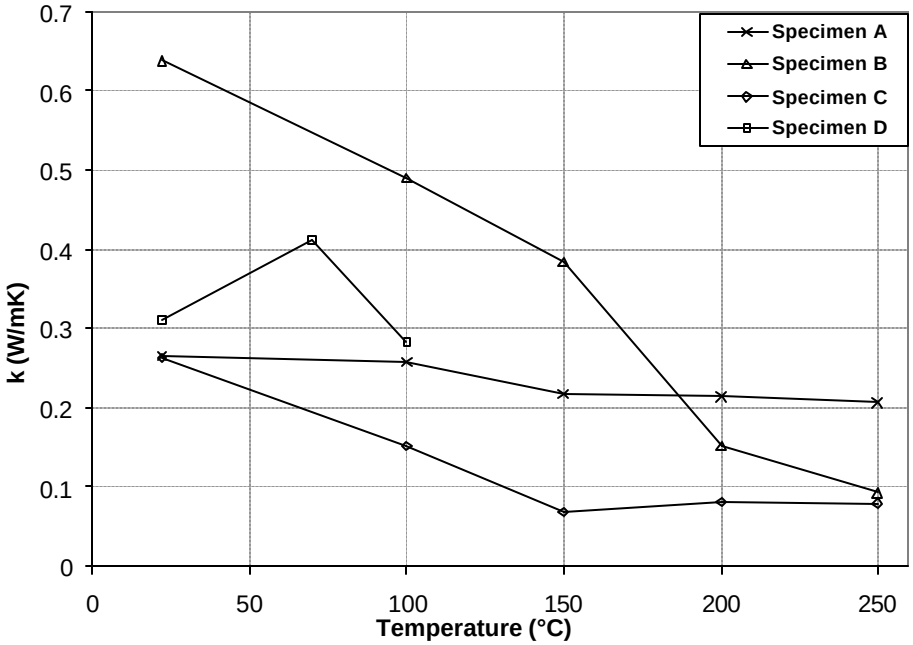

Figure D7 - Measured thermal conductivity as a function of temperature

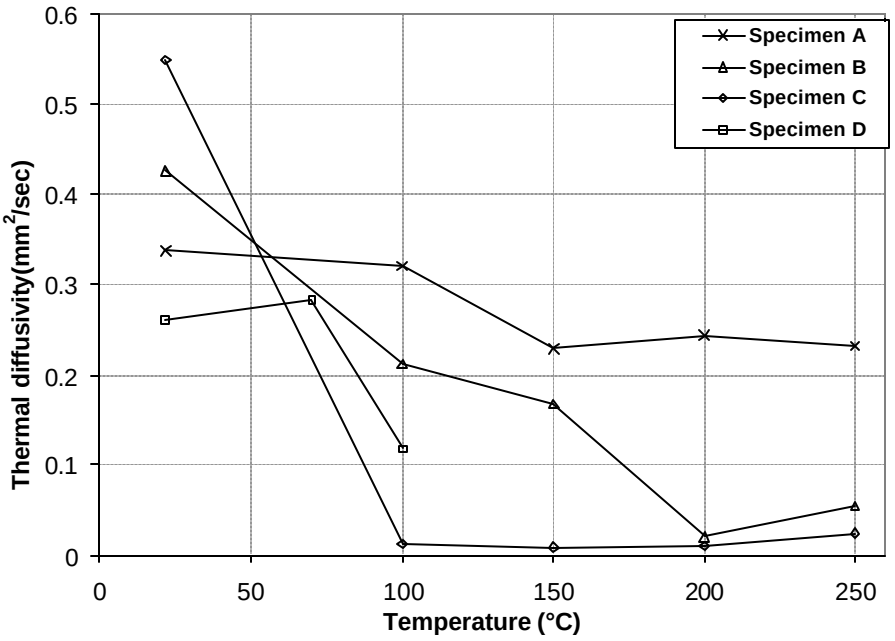

Figure D8 - Measured thermal diffusivity as a function of temperature

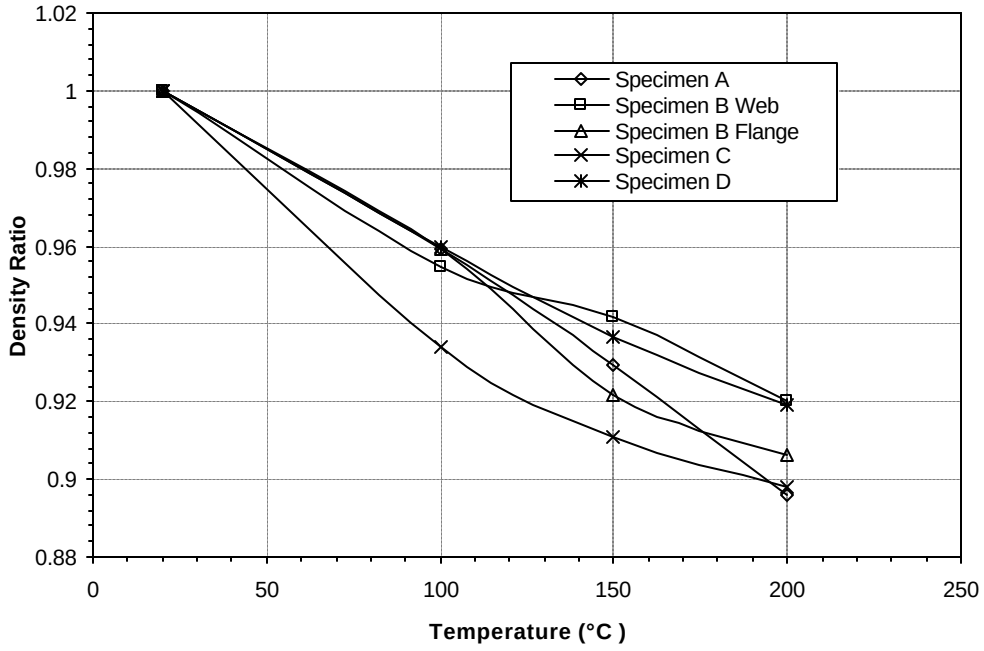

Figure D9 - Measured density ratio as a function of temperature

b. Thermal Expansion

Figure D10 shows dimensional change in the wood samples as a function of temperature obtained from the TMA apparatus. The values of coefficient of thermal expansion for specimens A and B are tabulated in Table D5. These values were calculated from change in dimension to the original dimension of the samples. Only specimens A and B were tested for coefficient of thermal expansion due to limited resource in this project. Generally wood expands up to initial temperatures of about 70°C, and then shrinks in 70-250°C range with different values of coefficient of thermal expansion [2]. As expected the thermal expansion of specimens A and B was within the range of values published in the literature. The coefficient of thermal expansion was different for the two samples used in the test. The major shrinkage was attributed to loss of moisture content in the wood and, later, to the charring. It was observed from these results that:

- For specimen A there was not much expansion at the lower temperature, the wood shrinks monotonically to 250°C.
- Specimen B displayed expansion at the lower temperatures and then it shrinks with different expansion coefficients in temperature range of 160 to 250°C respectively.

Table D5 – Measured values of coefficient of thermal expansion as a function of temperature

	Coefficient of thermal expansion (µm/m.°C)		
Wood sample	**Temperature range 15-24°C**	**Temperature range 24-160°C**	**Temperature range 160-250°C**
Specimen A	3.885	-22.68	1.718
Specimen B	26.18	-218	-64.88

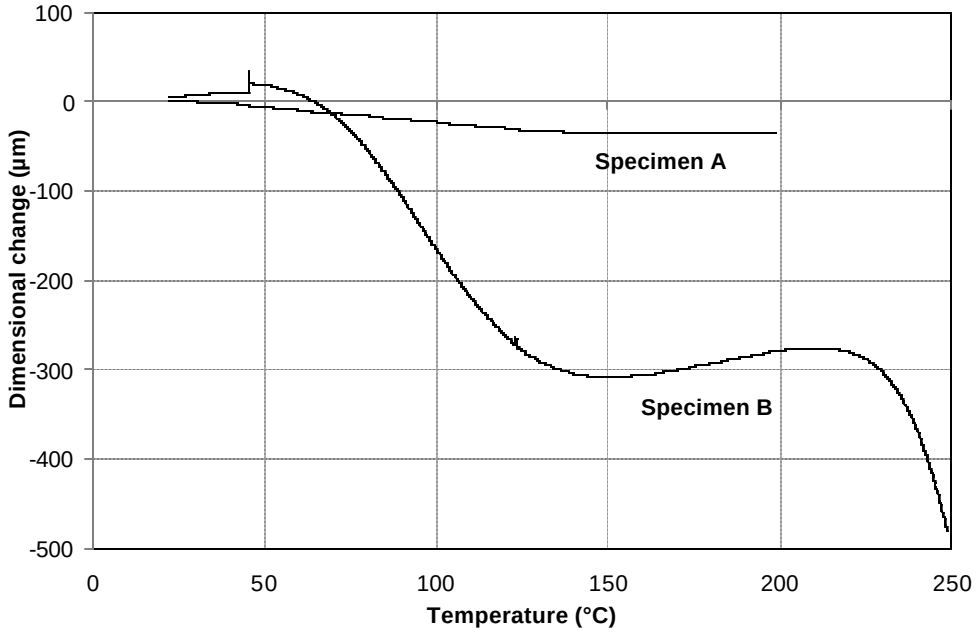

Figure D 10 - Dimensional change as a function of temperature

D4 Mechanical Property Tests

D4.1 General

In order to evaluate high temperature strength properties, tests were conducted on two types of wood (Specimens A and B) at room temperature, and at 100°C and 200°C. Both compression and tension tests were conducted in two grain orientations namely:

- Compressive strength loaded parallel to the grain
- Compressive strength loaded perpendicular to the grain
- Tensile strength loaded parallel to the grain
- Tensile strength loaded perpendicular to the grain.

D4.2 Test Specimens

Test specimens A and B for four different tests were prepared as specified in ASTM standard [D143-94, 2006]. However, specimen sizes for tests, except for the case of tension tests parallel to grain, were slightly different than that specified in ASTM standard. This was primarily because of the fact that the wood members used in the floor assemblies are of lesser thickness than that specified in ASTM. The test specimens used for the tension tests were as shown in Figures D11.

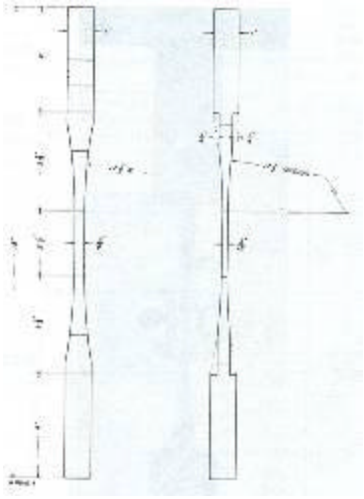

(a) *Tension parallel to grain*

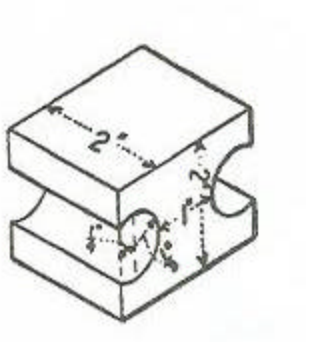

(b) *Tension perpendicular to grain*

Figure D11 - Test specimen for tension tests

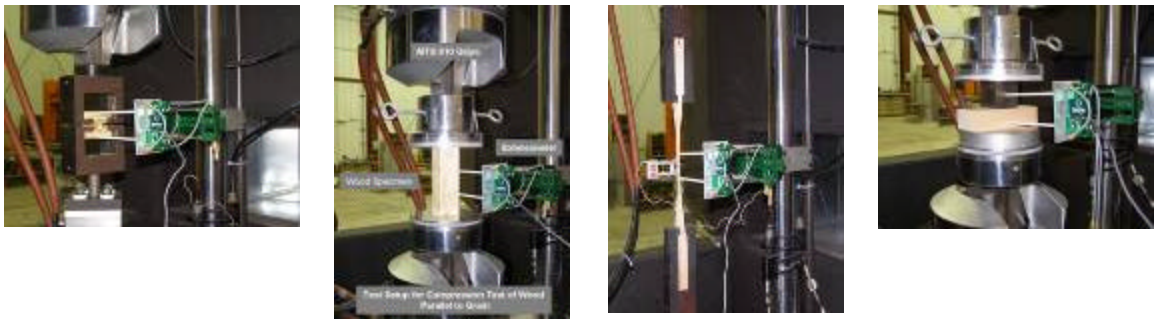

(a) (b) (c) (d)

Figure D12 - Test setup for testing wood specimens (a) Tension perpendicular to the grain (b) Compression parallel to the grain (c) compression perpendicular to the grain (d) Tension parallel to the grain

D4.3 Test Set-up

The mechanical properties were determined using a MTS machine. Special grips, which could hold specimens at elevated temperatures, without compromising the operating temperature restrictions for MTS hydraulic grips, were designed (Figure D12). For high temperature testing, all specimens were pre-heated to a desired temperature in a special oven for at least one hour and then the specimens were held at constant temperature till stability was attained (Figure D13). The heated samples were wrapped in a heat insulating cloth and prepared for testing in less than 2 minutes to avoid any considerable heat loss.

D4.4 Test Procedure

The insulated specimens were loaded in increments as specified in ASTM [D143-94, 2006]. All specimens, except the ones with compression perpendicular to the grain were tested till failure was attained. The tests were carried out at ambient temperature, 100°C, and 200°C. Attempts were made to undertake various tests at 250°C; however, wood started charring and thus the tests could not be carried out (Figure D14). The recorded (applied) load at failure and the deformation of the specimens were used to calculate the mechanical properties of wood samples (Table D6).

Figure D 13 - Heating the specimen in oven

Figure D 14 - Wood charring at 250°C

D4.5 Observations and Results

The following observations are based on the general trends in the recorded data:

- The measured strength properties of specimen A & B were within the range of values reported in the literature.
- The tension and compression strength of both specimens (A&B) decreased with temperature. In tension tests (both parallel and perpendicular to grain), the specimen behaved in a brittle fashion compared to room temperature tests. This can be attributed to more compactness in wood fibers, which after heating attains sudden failure at low strains.
- The computed elastic modulus of Specimen B (engineered lumber) was relatively high due to orientation of compressed plies (to optimize the properties) in a specific direction.
- The wood started to char at a temperature range of 250°C. Therefore, the strength properties deteriorated considerably at and beyond this temperature.
- The mechanical properties reported in Table D6 are based on a single test on each specimen. Thus caution should be used in using this data, since there can be significant variability in properties of wood. Additional tests are

recommended on each specimen type to get more reliable properties at specified temperature.

Table D6: Mechanical Properties of Conventional and Engineered Wood

Test Mode	Grain Orientation	Specimen Type	Room Temp °C	100°C	200°C
			MPa	MPa	MPa
Tension	Parallel	A	64.5	44.9	26.4
		B	49.0	26.4	24.1
	Perpendicular	A	3.2	0.9	1.4
		B	1.4	0.8	0.4
Compression	Parallel	A	54.3	53.1	44.7
		B	46.6	42.1	31.6
	Perpendicular*	A	8.1	13.1	13.5
		B	18.4	14.8	14.0

* Compression test terminated when the deformation in the specimen was approximately 2.5mm

D5. Charring Tests

D5.1 General

Charring tests were carried out on three types of wood (Specimens A, B and C) and OSB (Specimen D) samples. These tests were conducted in newly build fire test furnace at MSU. A special platform was constructed inside the furnace chamber to undertake charring test.

D5.2 Test Setup

The test setup consisted of a temporary shelf constructed inside a MSU intermediate-scale furnace. An access door allowing the removal of samples at the appropriate time was also provided. The shelf had a layer of 5/8" Type X drywall on the bottom, a layer of ¾ plywood on top of that, two layers of 5/8 OSB with another layer of 5/8" Type X drywall on top of that. The platform was supported by 2 4X6's, which were also covered on all exposed sides with 5/8" Type X drywall. All drywall was attached with 1-5/8 drywall screws on 8" patterns with the screw heads covered with joint compound. The platform extended 30 inches into the furnace and was 48 inches wide.

D5.3 Specimen Preparation:

In order to have appreciable charring data it was necessary to layer the specimens to increase the mass to surface area ratio. For this, each of the specimens was cut into several pieces of the same size. The pieces were then fastened together using Elmer's wood glue, and pressure was applied to the joint for 8 hours while the glue dried. The final size of the specimens was as follows:

- Specimen A (Conventional wood): 2x10's: 8" long by 4" wide by 3" thick (2-1.5" layers)
- Specimen B: Engineered joist: 8" long
- Specimen C: T&G wood subfloor: 6" long by 4.875" wide by 2.25" thick (3-0.75" layers)
- Specimen D: OSB subflooring: 8" long by 8" wide by 1.5" thick (2-0.75" layers)

D5.4 Time Temperature Profile

The target time temperature profile was ASTM E-119. ASTM E-119 as well as the actual time temperature profile attained in testing is shown in Figure D15 below. At the end of the 40 minutes testing period the area difference between the test and the ASTM profiles was 0.10%, well within the acceptance limit in ASTM Standard.

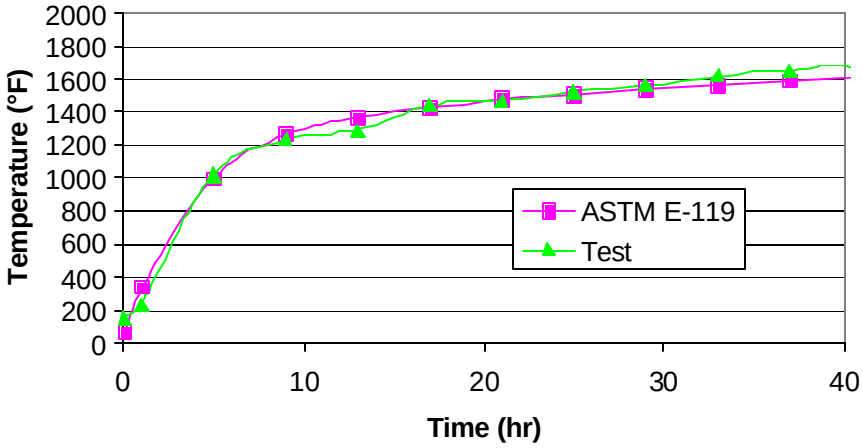

Figure D15 – Furnace temperatures

D5.5 Test Procedure

After the standard ignition process the combustion process was run for the pre-determined amount of time. When it was time to remove the samples the door was removed and one of each of the samples was removed from the furnace and placed

onto a metal tray. The tray was then taken outside and a gentle hose stream was applied to the specimens to extinguish the fire. This was done at each of the times for which data was to be collected.

D5.6 Charring measurements

To measure the char depth the specimens were cross-sectioned in the middle and the residual wood (OSB) thickness was measured. The measured value was subtracted from the total thickness to determine the char depth. In situations where the glue failed to hold the specimen together, due to combustion of the top layer of wood either the specimen was discarded, or the charring on the side of the specimen was measured.

D5.7 Observations and Results

The following are observations made during testing; they are organized by specimen type.

Specimen A: Ignition occurred after approximately 5 minuets of fire exposure. All of the samples maintained integrity through 30 minutes of fire exposure. Samples removed from the fire after 40 minutes of fire exposure were completely burned and no charring measurements could be made.

Specimen B: Ignition occurred in the web after approximately 3 minutes with the flanges not igniting until after 5 minutes. Before the first samples could be removed at 10 minutes, the webs were completely consumed and only the flange remained. After 20 minutes of fire exposure, the samples were completely consumed and no charring information could be obtained from the samples.

Specimen C: Again ignition occurred after approximately 5 minutes of fire exposure. The samples retained integrity through 20 minutes of fire exposure, after which point the bond between the layers of wood deteriorated to the point were no further information could be gathered from samples removed from the fire after more than 20 minutes of exposure.

Specimen D: Ignition occurred after approximately 3 minutes of fire exposure. While burning, the entire surface of the OSB burned evenly with bubbles forming on the surface and quickly collapsing as the glue boiled within the wood.

D5.8 Charring Rates

Table D7 below shows the depth of char and Table D8 shows the charring rates from the samples.

Table D7: Char depth (mm)

Time (min)	Specimen A 2x10	Specimen B Engineered Lumber	Specimen C T&G wood subflooring	Specimen D OSB subflooring
10	7.366	8.382	8.128	7.239
20	13.3096		15.875	13.6398
30	18.288			

Table D8: Char rate (mm/min)

Time (min)	Specimen A 2x10	Specimen B Engineered Lumber	Specimen C T&G wood subflooring	Specimen D OSB subflooring
0-10	0.7366	0.8382	0.8128	0.7239
10-20	0.59436		0.7747	0.64008
20-30	0.49784			

D6. Summary

This report presents information on high temperature thermal, mechanical and charring property tests on wood and OSB samples. Thermal properties include thermal conductivity, specific heat, density, thermal expansion, and thermal diffusivity of wood. Mechanical properties include tensile strength, compressive strength and modulus of elasticity parallel to the grain as they significantly influence the behavior of wood members in structures. In addition charring tests were also conducted. The summary of the test data is presented in this report. Due care should be taken when using these properties in fire resistance modeling of wood floor assemblies because the tests have been conducted on a limited number of samples and also since the properties of wood vary within species and between species.

References

1. ASTM, “Standard Methods of Fire Test of Building Construction and Materials”, Test Method E119-01, American Society for Testing and Materials, West Conshohocken, PA., 2007.

2. ASTM D143-94, 'Standard Test Methods for Small Clear Specimens of Timber', West Conshohocken, PA, 2006.
3. Bénichou, N. et al, "Thermal Properties of Wood, Gypsum and Insulation at Elevated Temperatures," IRC Internal Report No. 710, National Research Council of Canada, Ottawa, Canada, 2001.
4. Kodur, V.K.R., Harmathy, T.Z., "Properties of Building Materials," *SFPE Handbook of Fire Protection Engineering*, 4th edition, Chapter 10, pp 167-195, 2008.
5. UL 263, Fire Tests of Building Construction and Materials, Underwriters Laboratories, Northbrook, IL, 2003.
6. Wood Handbook, Wood as an Engineering Material, Gen.Tech.Rep. FPL-GTR-113. Madison, WI: U.S. Department of Agriculture, Forest Service, Forest Products Laboratory.463 p, 1999.